

Course Notes on Electric Drives

By
Prof. V. T. Ranganathan



Department of Electrical Engineering
Indian Institute of Science
Bangalore - 560 012
India

April 2004

Chapter 1

Control of DC Drives

The Direct Current machine have been dominating the field of adjustable speed drives for over a century; they are still the most common choice if a controlled electric drive operating over a wide speed range is specified. This is due to there excellent operational properties and control characteristics; the only essential disadvantage is the mechanical commutator which restricts the power and the speed of the motor, increases the inertia and the axial length of and requires the periodic maintenance.

In the Figure ?? a schematic cross section of a DC machine is shown, containing the fixed stator S and the cylindrical rotor, called armature A . While rotor and pole shoes are always laminated to reduce the iron losses caused by the varying magnetic field, the rest of the stator is laminated only in larger machines, when the motor is required to operate with rapidly varying torque and speed are when a static power converter with highly distorted voltages and currents is employed as the power supply. The main poles MP are fitted with the field windings, carrying the field current i_e which drives the main flux ϕ_e through the stator and rotor. A closed armature winding is placed in the axial slots of the rotor and connected to the commutator bars; it is supplied through the brushes and the commutator with the armature current i_a . This creates a distributed ampere-turns (m.m.f.) wave, fixed in space and oriented in the direction of the quadrature axis, orthogonal to the main field axis, so that maximum torque for a given armature current is produced.

In view of large air-gap in the quadrature direction the resulting armature flux ϕ_a is much smaller than the main flux ϕ_e . It can be reduced even further by placing compensating windings CW in axial slots on the pole shoes and connecting them in series with the armature. Their opposing ampere-turns all but cancel the quadrature field excited by the armature and remove the undesired armature reaction, which otherwise tends to distort the even distribution of the main field under the poles along the circumference of the rotor. Compensating windings are common only on larger machines or converter-fed motors for heavy duty applications such as traction or steel mill drives. Compensated DC machines can withstand higher overload than uncompensated machine; also the armature current may

rise much faster and larger current harmonics are acceptable without detrimental effects on commutation, i.e. sparking of brushes. This is of particular importance if the machine is supplied by a static converter.

The commutating poles CP , placed between the main poles and also carrying the armature current, have the task of locally modifying the field in the neutral zone, to achieve rapid and spark free commutation. This is done by inducing a suitable voltage in the armature coil temporarily shorted by the brushes.

Chapter 2

Overview of AC Drives : Types and Applications

Adjustable speed electric drives are a feature of practically every type of industry. In earlier days, such drives were realized by combining several electrical machines. An example of this is the Ward-Leonard drive. With the advent of power semiconductor devices, however, these earlier systems have been replaced by motors controlled by static power converters. The block diagram of such a drive is shown in Figure 2.1.

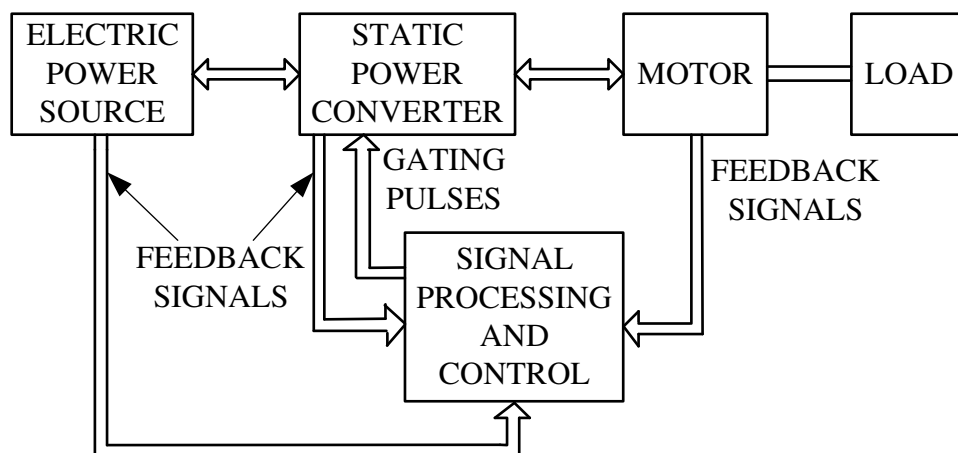


Figure 2.1: General Block Diagram of a converter controlled electric motor drive

Historically, the silicon controlled rectifier (SCR) was the first semiconductor device to become commercially available. As a result, the first converter controlled drive to find widespread application in the industry was the DC motor drive fed by a line commutated converter. The outstanding features of this type of drive are the simplicity of the power converter circuit and straightforward control, even for high performance applications such as servo drives and rolling mill drives. Drives up to the megawatt range have been satisfactorily performing in industry and have in fact become the standard against which the performance

Table 2.1: Status of Power Devices for AC Motor Drives

Device	Maximum voltage and current ratings available	Comments	Drive rating for which suitable
MOSFETs	500V upto 100A	Easy to drive; conduction losses high; High switching frequencies up to 20kHz	upto 10kVA
BJTs	1000V, upto 600A in Darlington connection	Base drive not simple ; low conduction losses in case of single device; switching frequencis up to 5kHz	upto 100kVA
IGBTs	1000V, upto 300A likely to go up 600A	Easy to drive; conduction losses lower than for MOSFETs; switching frequency up to 10-15 kHz; recent technology - prices likely to decrease	upto 50kVA likely to go up up to 100kVA
GTOs	2500V, 2000A	Gate drive complicated; better surge ratings than above switches, switching frequency up to 1kHz	Large drives up to thousands of horse power
SCRs	4000V, 3000A	Gating simple; rugged, turn-off difficult; preferred for line/ load commutated inverters	Very large drives in the MW range

of future drive types are to be judged.

However, it is well recognized that dc motors have a number of limitations:

- Their power rating is limited at high speeds due to commutation.
- The commutator and brushes require maintenance.
- DC motors are not suitable for the hazardous environments such as mines, chemical plants etc.
- The power to weight ratio of DC motor is not good as that for AC moors, especially the induction motor.

Table 2.2: AC Drives Types, Ratings and Applications

Machine Type	Converter type					
	Forced commutated				Naturally commutated	
	Voltage source		Current source		Line commutated	
	MOSFET/ BJT/IGBT	SCR/ /GTO	SCR/GTO self commtated	SCR Machine commutated	Inverter	Cyclocon verters
Permanent magnet synchronous motors	Low power drives(10 kW) with good dynamic performance(sevos)	Upto 1MW High power density (aircraft applications)				
Reluctance motors	Upto 100kW	Upto 100kW				
Squirrel cage induction motors	Upto 100kW high speed, very good dynamic performance (spindle and servodrives)	Upto 2MW good dynamic performance	Upto 4MW High speed			High power (10MW) low speed very good dynamic performance
Doubly-fed slip-ring induction motors					High power (20MW) sub synchronous operation	
Wound field synchronous motors			High power (20MW) High speed			High power low speed; Very good dynamic characteristics

There has, therefore, been a continuous effort to develop variable speed drives incorporating AC motors. A variety of power devices, power converter configurations, motor types and control techniques have emerged over last two decades, resulting in the availability of a wide variety of AC motor drives suitable for different applications.

A number of gate turn-off power switches, such as the Bipolar Junction Transistor (BJT), the power MOSFET, Insulated Gate Bipolar Transistor(IGBT), and the Gate Turn-off Thyristor(GTO) are now available for building power converters for feeding AC motor drives. Over the years ratings have been continuously improved. These devices, together with the SCR, offer a wide choice of power switches for AC motor drives. Their ratings and the power range over which each device is suitable are summarized in Table 2.1.

Of the devices listed, the BJT, the MOSFET and the IGBT are used for constructing voltage source type inverters. GTOs have been used in voltage source as well as current source type inverters, while SCRs are used in line or load commutated inverters. The various types of converter configurations available for use in AC drives are indicated in table 2.2:

In addition to the different types of converters, various motor types are also available. The major machines types are

- squirrel cage induction motors
- wound rotor induction motors
- permanent magnet synchronous motor
- wound field synchronous motors
- reluctance motor

Thus it would appear that a large number of motor-converter combinations are possible. However it is recognized by now that certain converter/machine combinations are preferable for certain classes/ratings of drives. This is summarized in Table 2.2.

In the present course, attention is focussed on AC motor drives operated from voltage source type of inverters. In particular, drives incorporating squirrel cage induction motor, permanent magnet synchronous motor and switched reluctance motors are considered. A large number of commonly used AC motor drives fall in this category, although the other drive types are also no less importance in their respective applications.

2.1 References

- 1) Leonard.W., "Electrical Drives: Universal Energy Converters", Siemens Review 4/89, pp.32-36.
- 2) Habock. A., "Electrical Drives in Process Automation", Siemens Review 4/89,pp.36-37.

Fig 1 :General block diagram of a converter controlled electrical motor drive.

Chapter 3

BJTs and GTO's Characteristics and Drive Considerations

3.1 BIPOLAR JUNCTION TRANSISTOR (BJT)

The BJT is a three terminal device whose volt-ampere characteristics are shown on Fig. 2.1.

The power electronic applications the transistor is used as a switch (ON state in the

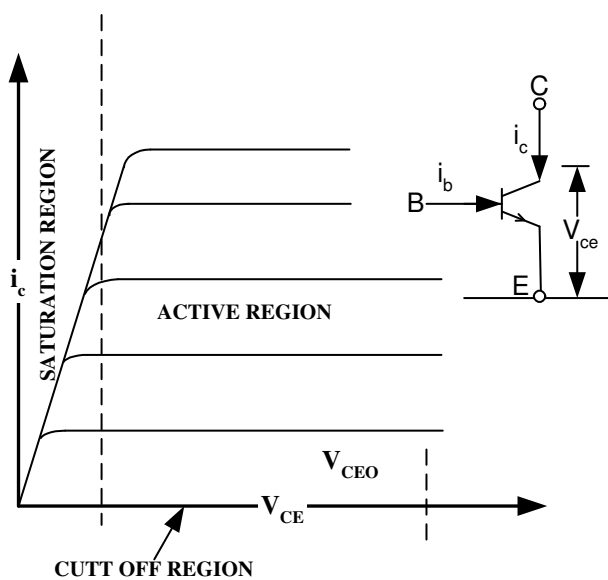


Figure 3.1: Volt-Ampere characteristics of BJT

saturation region, or OFF state in the cut-off region). When used as a switch the device losses are low. The large signal, low frequency model of the BJT is shown in fig. 2.2. The condition for the device to operate in the saturation region is that both the diodes D_{BE} and

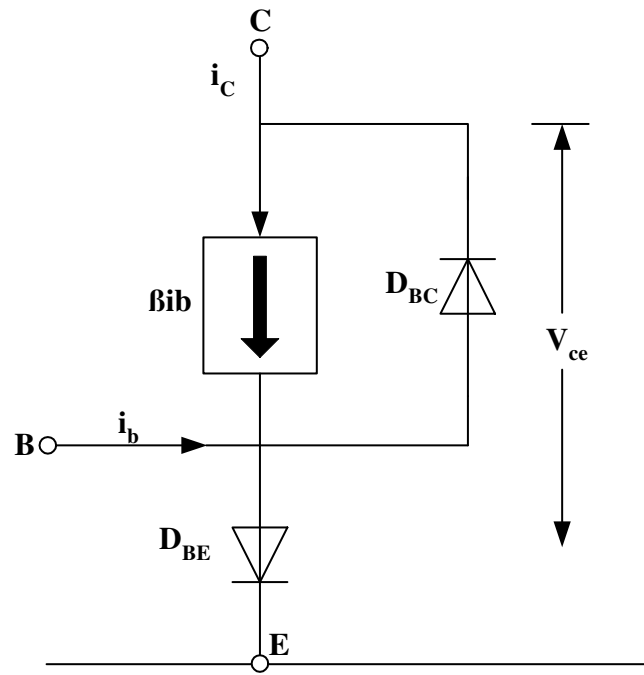


Figure 3.2: Large Signal Low Frequency Model of (BJT)

D_{BC} are conducting. or

$$\beta I_B > I_C \geq I_B > I_C / \beta$$

where β is the common emitter current gain of the device.

When the BJT is used as a switch, the following points are to be noted.

- 1) $I_{OFF} \approx 0$; $V_{OFF} \neq 0$
 $0 < V_{CE} < V_{CEO}$
- 2) $V_{ON} \approx 0$; $I_{ON} \neq 0$
 $0 < I_C < I_{CM}$
- 3) $P_{ON} \approx V_{ON} i_C$; $P_{OFF} = V_{CE} I_{OFF}$

4) The losses in the device cause heating of the junction. Suitable heatsink has to be provided to handle the device losses.

5) To turn on and turn off the device a control current has to be provided through the base emitter junction (Drive circuit).

6) The process of switching ON or OFF require a finite time.

$$t_{ON} = t_d + t_r; t_d = \text{delaytime}$$

$$t_r = \text{risetime}$$

$$t_{OFF} = t_s + t_f; t_s = \text{storagetime}$$

$$t_f = \text{falltime}$$

7) The BJT is a unidirectional device capable of blocking forward voltage ($V_{CE} > 0$) or passing forward current ($I_C > 0$).

8) The operation of the BJT has to be restricted within the safe operating area(SOA) of the v-i characteristics (in steady state and during transients) of the device.

3.1.1 SWITCHING CHARACTERISTICS (BJT)

The switching process of the BJT is shown in fig. 2.3.

TURN ON process: As soon as the base drive is established.

- 1) The base starts getting charged.
- 2) After a delay of " t_d ", the collector junction stop blocking.
- 3) In a time " t_r ", the collector-emitter voltage drops (almost) linearly to $V_{CE}(\text{sat})$.

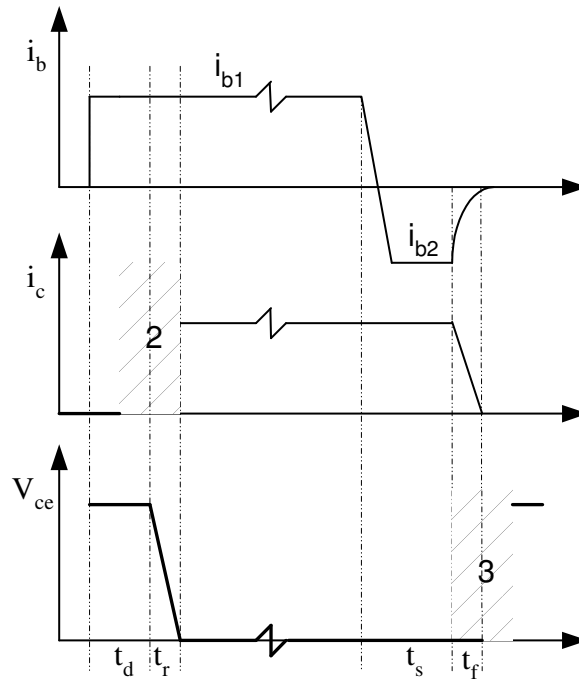


Figure 3.3: Switching Process Of BJT

4) The collector current starts getting established from the instant collector-emitter voltage starts falling. The relation ship of collector current with time during this transient is decided

by the external circuit. The collector current in the hatched region (2) of fig. 2.3 is under the control of external circuit.

TURN OFF process : To turn off the transistor, the forward base drive is removed and a negative base drive is established. When a negative base drive is established,

1) The junctions (base-emitter and base collector) remains forward biased for a duration " t_s ". During this storage time " t_s ", i_C continues to flow and V_{CE} remains low. This is the time taken to remove the stored charge in the junction, so that junction may stop conducting. The storage time increases with the IB1 decreases with the IB2.

2) After the storage time, in a small time " t_f ", collector current falls (almost) linearly to zero. During the fall time " t_f ", collector emitter voltage V_{CE} decided by the external circuit. In the hatched region (3) of fig. 2.3, the collector-emitter voltage is under the control of external circuit.

3.1.2 SWITCHING LOSSES (BJT)

It may be seen from the switching process, that the device losses are low during the transient intervals of " t_d " and " t_s ". The switching losses occur during the " t_r " and " t_f ". Collector current during " t_r " and the device voltage during " t_f " are decided by the external circuit. This feature is used to control the switching losses in any application.

3.1.3 TYPICAL DRIVE CIRCUITS (BJT)

Figure 2.4 and 2.5 show two typical isolated drive circuits suitable for operation up to 5 kHz and 20 kHz respectively. The control input is an active low signal capable of sinking about 15mA.

3.2 GATE TURN OFF THYRISTOR (GTO)

The GTO combines the features of a thyristor and a power a transistor (BJT). The operation of the GTO is seen from the classical two transistor model shown in fig. 2.6. To turn off the device a reverse current I_R is drawn out of the gate.

$$I_{C1}/I_R = \alpha_1/(\alpha_1 + \alpha_2 - 1)$$

α_1 and α_2 are the common base current gains of the two transistors in the model. In order to obtain a large turn-off gain, the device is made with suitable values of α_1 and α_2 . During turn ON and turn OFF, the GTO behaves like a power transistor and during conduction, when the anode current is greater than the latching current, it behaves like a thyristor.

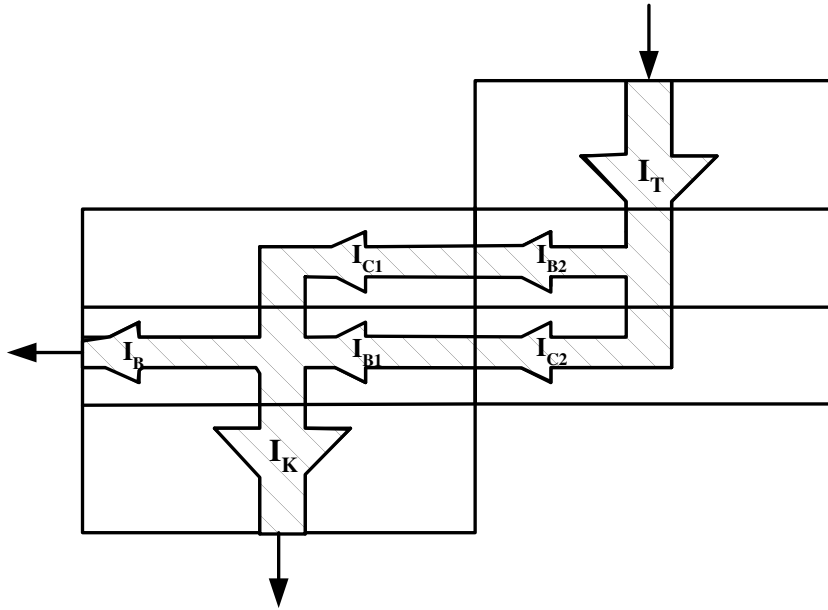


Figure 3.6: Classical Two Transistor Model Of GTO

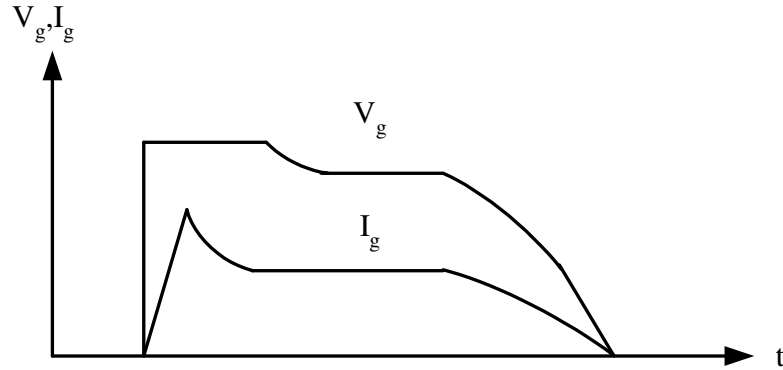


Figure 3.7: Classical Two Transistor Model Of GTO

- Higher turn off losses
- Lower conduction losses
- Higher surge capabilities
- Higher turn off time

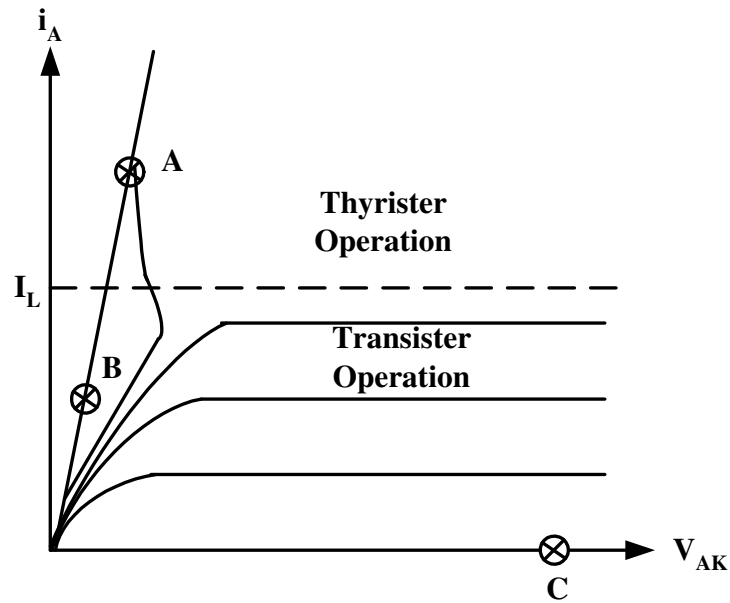


Figure 3.8: Forward Characteristics of GTO

The symmetrical version is better suited for high frequency applications. The asymmetrical version is better suited for the low frequency applications.

3.2.4 CONTROLLABILITY

The current a GTO can pass or interrupt is well in excess of its average rating. For example,

	GFT20B (Hitachi)	BTW59 (Philips)
$I_T(\text{RMS})$	7A	15A
I_{TQRM}	20A	50A

Table 3.1:

I_{TQRM} is the repetitive quenchable anode current. It is roughly 3 times the RMS current rating.

The condition for the switching off large anode currents is the limit on the applied dv/dt . The higher the current that must be switched off, the lower is the allowable reapplied dv/dt . Also for a given allowable reapplied dv/dt , and junction temperature T_J , the level of anode

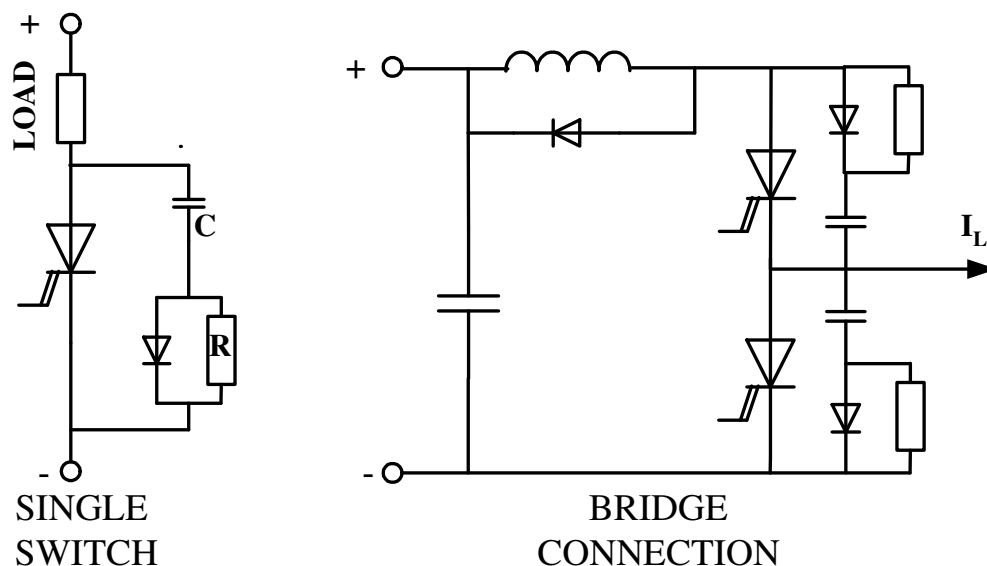


Figure 3.9: Typical Snubbers For GTO's

current that can be successfully switched off increasing the negative bias applied to the gate. It is necessary that this negative bias is applied of as low an impedance as possible. The consequence of this condition is that the inductances in the turn-off loop has to be minimized; electrolytic capacitors have to be decoupled with the paper capacitors with low ESR.

In order to minimize the reapplied dv/dt , the GTO circuits always use snubbers. Typical snubber add ones are shown in Fig. 2.9. In the bridge circuits, the snubbers are effective only if there is a decoupling inductor in the line. Any inductance in the snubber loop adversely affects the controllable anode current.

3.2.5 SAFE OPERATING AREA(SOA)

The GTO is either ON or OFF and hence does not suffer from forward biased active region of operation. During switch OFF, GTO goes through the active region. The SOA under the reverse biased condition is a rectangle. The height of the rectangle (I_{TC} = controllable anode current) depends on the reapplied dv/dt .

3.2.6 TURN ON

During turn on, care must be taken such that adequate gate drive is available whenever the anode current is below the latching level. If the anode current is slightly above latching level, a steep trailing edge of the gate pulse may also cause unlatching. The gate drive must therefore be present till the anode current crosses latching current. Further the fall time of

the gate pulse must be prolonged.

3.2.7 SWITCH ON LOSSES

To minimize the switch on losses, the gate must be overdriven rapidly (2 to 5 $I_{GT}, 1\mu s$), till the anode current reaches about 2 to 5 times latching current. Turn on discharge of the snubber capacitors in to the device has to be taken in to account especially snubber has no resistors. The continuous drive is preferred as it lowers the forward drop and conduction losses.

3.2.8 TURN OFF

Figure 2.10 shows the typical turn-off waveform. Prior to turn-off, the GTO is conducting the load current. To turn off the GTO, a negative current with specified di_g/dt is injected into the gate. When the negative current reaches the I_{GRM} (or I_{GQ}), the GTO anode current starts falling rapidly nearly (linearly) to zero in time t_f . The snubber capacitor charges with the diverted current from GTO. As the negative current is established, the anode current

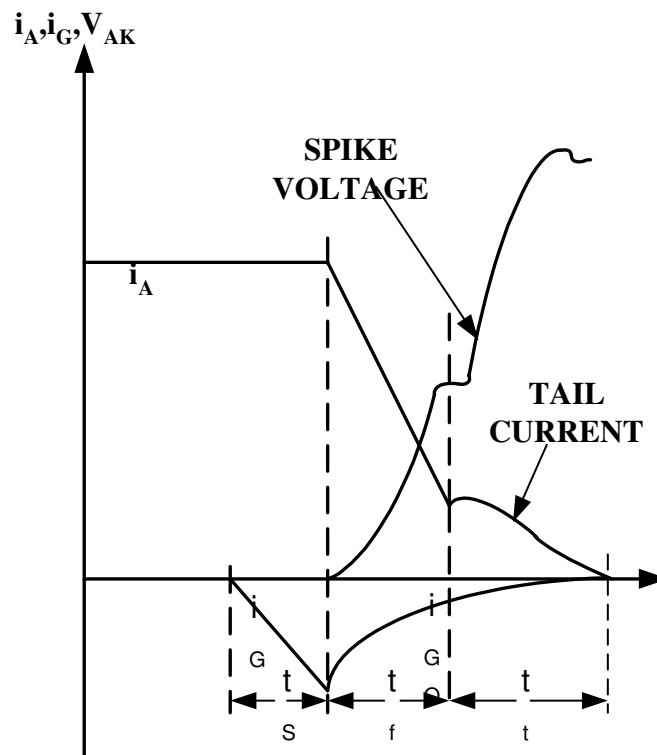


Figure 3.10: Typical Turn Off Waveform of GTO

start after falling a delay. This delay t_s is the storage delay. After the storage delay t_s , the

anode current falls steeply to a tail current value I_{TLP} (tail current is equal in magnitude to I_{GQ}) in the fall time t_f . The fall time t_f is about $1\mu\text{s}$. The anode current is bypassed to the snubber resulting in the build up of anode voltage. The anode voltage exhibits a spike on account of the parasitic inductance of the snubber circuit. A large spike is harmful as it causes high dissipation during turn-off. The snubber circuit leakage inductance therefore has to be minimized. After the spike voltage, the anode voltage builds up (with high dv/t). The rate of rise of anode voltage causes the displacement current called the tail current. Further there is an over voltage across the snubber as the device recovers. The tail current duration and the overshoot in voltage can be decreased by using large C_S . High C_S will result in large turn on losses. The snubber capacitance used for GTO are typically higher than for an SCR. The switching losses are higher for GTO and the switching frequency is limited to about 1 kHz.

3.2.9 GATE DRIVE CIRCUIT

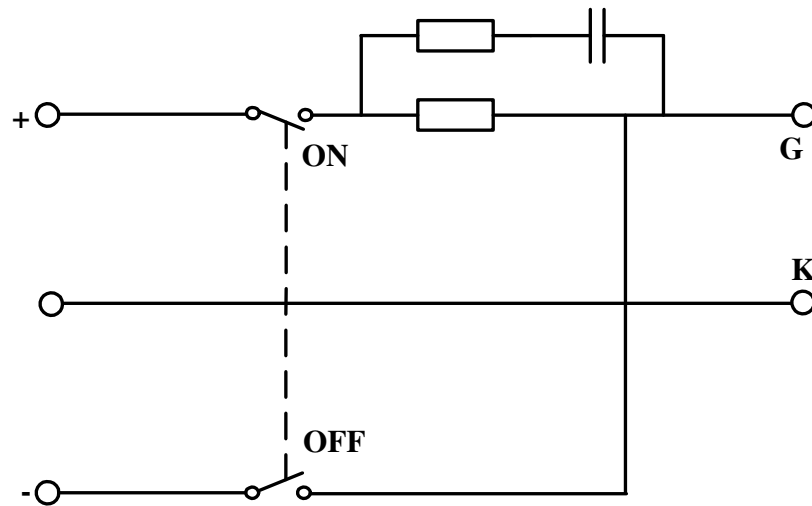


Figure 3.11: Typical Turn Off Waveform of GTO

Figure 2.11 shows the concept for a typical gate drive circuit.

3.2.10 ADDITIONAL PROTECTION

- Minimum ON time.
(To completely discharge snubber capacitor).
- Minimum OFF time.

(To complete switch off transient).

- Power supply

(To ensure that gate drive power supplies are healthy and established after power on).

- Over temperature

(To limit device dissipation).

- Over current

(To ensure guaranteed turn-off).

Chapter 4

MOSFETs and IGBTs Characteristics and Drive Considerations

Power MOSFET and the Insulated Gate Bipolar Transistor (IGBT) are both voltage controlled devices as opposed to current controlled devices such as BJTs, SCRs and GTOs. This desirable feature makes them very attractive as power switches. In principle, they can both be controlled directly from the ICs. However, as will be discussed, some amount of current sourcing/sinking ability is required on the part of the gate drive to improve the switching behavior. In the following, the operation of these two devices is reviewed and basic considerations in designing their gate circuits are discussed.

4.1 The MOSFET [1]

Like the BJT, the MOSFET is a three terminal device. The main terminals are source (S) and the drain (D). The control terminal is the gate (G). The gate is insulated from the rest of the device by an oxide layer and therefore draws no current in steady state. When the gate is placed at a suitable potential with respect to the source, a conducting path known as the channel is established between the source and the drain and current flow becomes possible. MOSFETs used for power switching applications are of the enhancement type, i.e., the channel comes in to existence only when a suitable gate to source voltage is applied. Otherwise the drain and source are isolated from one another, with ideally infinite drain to source resistance. Depending on the nature of the semiconductor material constituting the drain, the source and the channel, MOSFETs are classified as N-channel or P-channel types. N-channel power MOSFETs are more commonly used, although P-channel types are also commercially available.

Figure 4.1 shows the internal structure of an N-channel MOSFET. If the drain D is at a positive potential with respect to the source and the gate G is raised to a positive potential

with respect to the source, an n-type channel is established in the P region and current flow takes place in the device by movement of the electrons from the source to the drain. This will, of course, be regarded as a current flowing through the device from the drain to source.

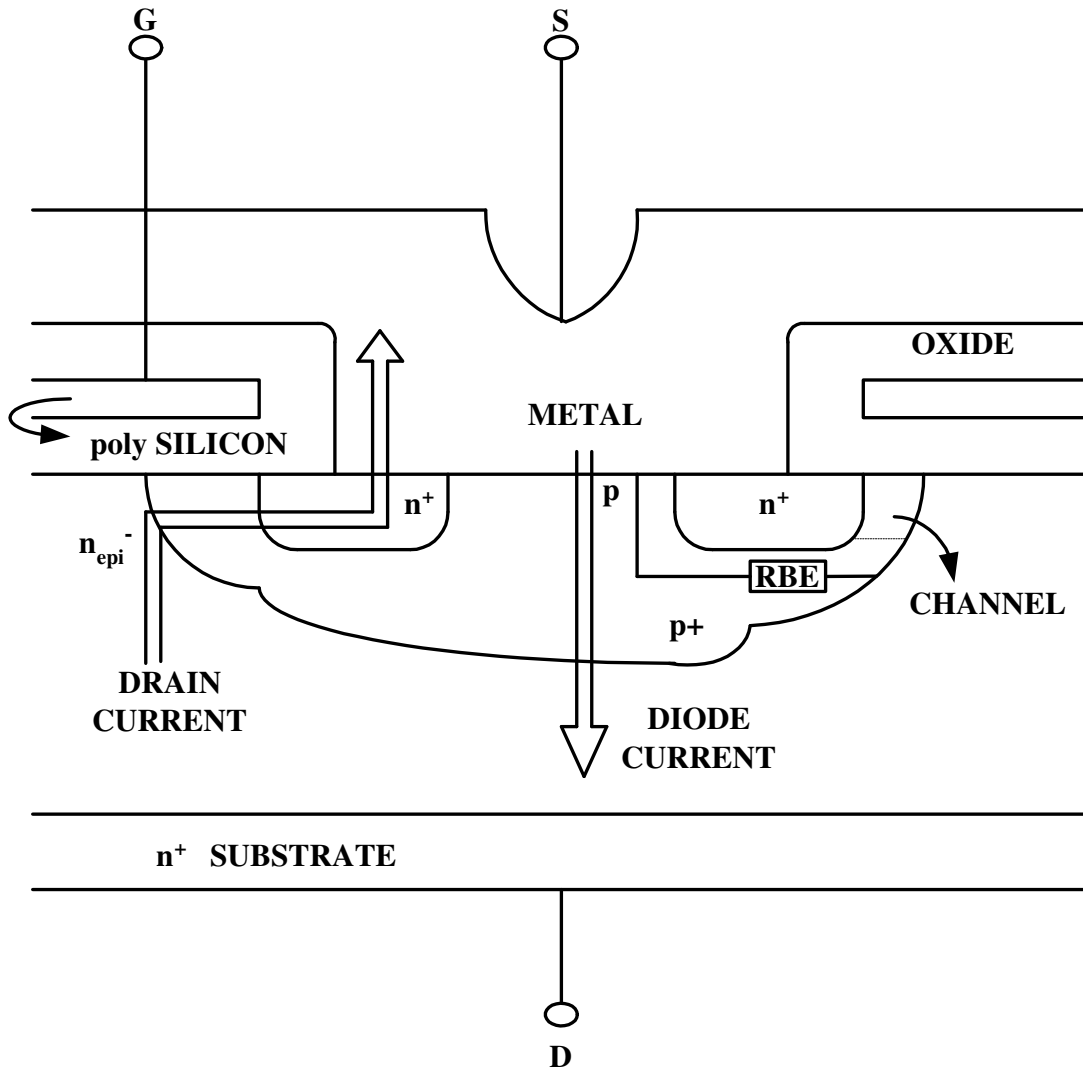


Figure 4.1: Internal structure of an N channel MOSFET

Note that the gate lead draws no current, unlike the base terminal of a BJT which requires a base current of sufficient magnitude relative to the collector current. The MOSFET is thus a voltage controlled device, requiring very little gate drive power.

Note also that flow of drain current is due to the movement of electrons in the N type region, i.e. due to the flow of majority carriers, unlike in a BJT. Because of this, the phenomenon of current hogging and second breakdown are absent in MOSFETs. The MOSFET

has a positive temperature coefficient of resistance and thermal runaway does not occur. Paralleling of MOSFETs is also consequently easier.

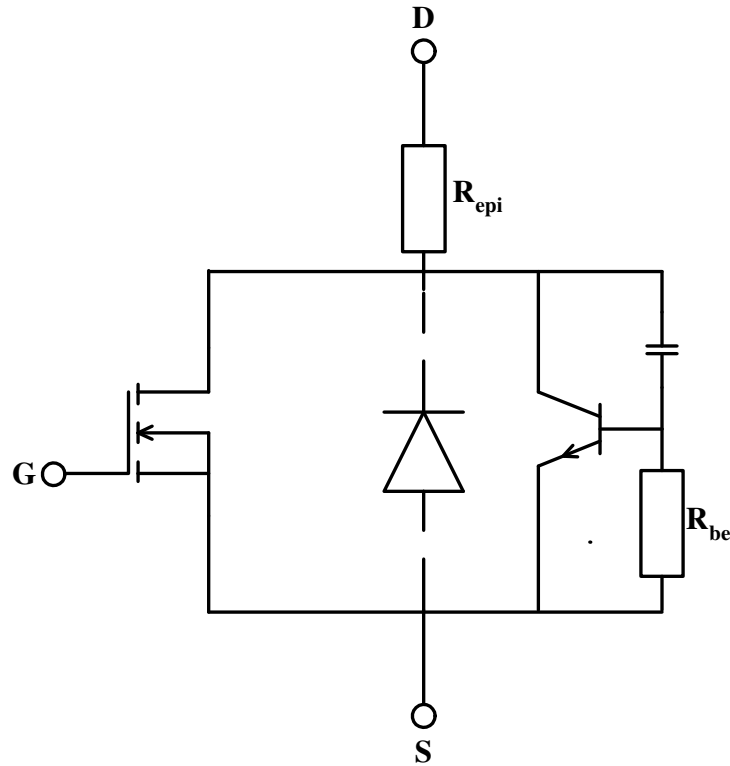


Figure 4.2: Circuit equivalent of an N channel MOSFET

It can be seen from Figure 4.1 that there exists within the MOSFET a parasitic npn transistor. The circuit equivalent of the MOSFET structure is shown in Figure 4.2. Because of the emitter base short at the source metallization, the transistor acts as reverse diode across the MOSFET. This diode can carry as much current as MOSFET itself and can be used as a feedback diode in inverter applications. However it is a slow diode and can limit the switching frequency of the MOSFET. In applications where high frequencies are required, the internal diode has to be blocked out.

Further, when the MOSFET is attempting to revert to the OFF state, especially after conducting reverse current through the diode, excessive $\frac{dv}{dt}$ across drain and source can turn on the npn transistor due to capacitive current injected in to the base. This results in the device ‘latching’ and can result in destruction of the device. The base emitter resistance r_{be} is minimized by the manufacturer to prevent latching. In addition it may be necessary to connect $\frac{dv}{dt}$ snubber across the device.

The resistance R_{epi} is due the n^- epitaxial region. It contributes to the ON state re-

sistance $R_{DS(ON)}$ of the MOSFET, and consequently increases the conduction losses. The n^- region is thicker in high voltage devices with correspondingly higher $R_{DS(ON)}$ values. The voltage rating commonly available MOSFETs are therefore around 500V. Generally the conduction losses of MOSFETs are higher than those of BJTs of the same rating. The current ratings of the MOSFETs are also limited to a maximum of 100A. MOSFETs are therefore to be found in inverters with rating less than 10kVA.

4.1.1 Switching Behavior and Gating Considerations

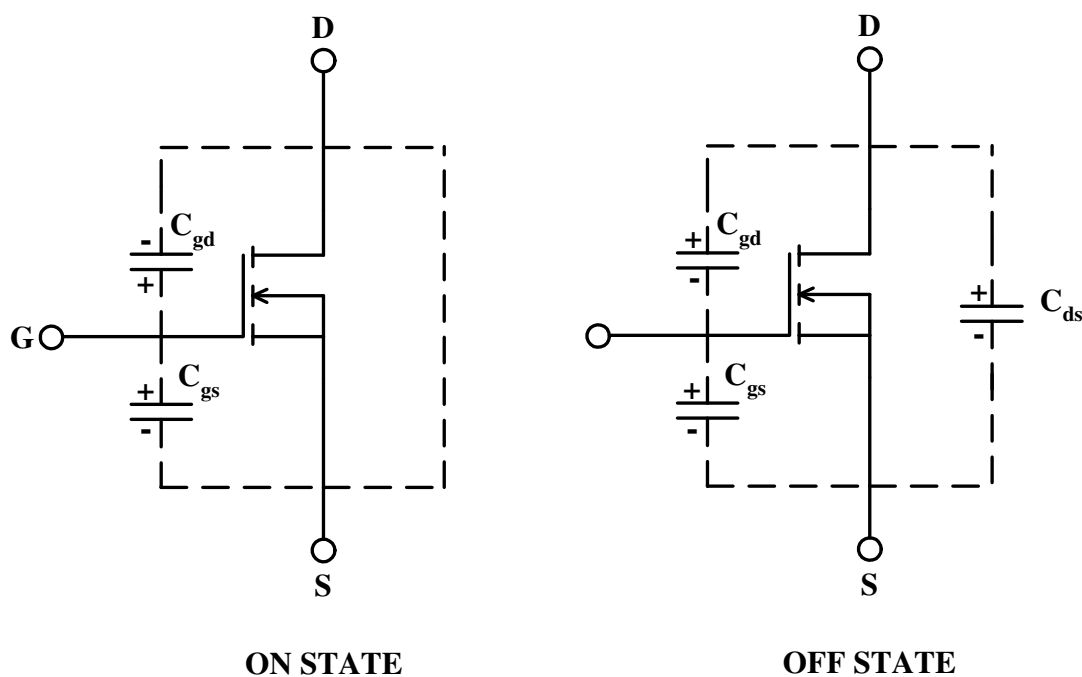


Figure 4.3: Capacitances associated with an N channel MOSFET during ON and OFF conditions

Since current conduction in a MOSFET is due to the movement of majority carriers, the switching speed of the device is not limited by charge storage effects; MOSFETs can easily switch at frequencies of 100kHz. The main limitation on switching frequency is due to the device capacitances. Figure 4.3 shows the three capacitances associated with a MOSFET and the voltage polarities to which they are charged in the ON state and the OFF state.

These capacitances are specified on the device data sheets as:

The input capacitance

$$C_{iss} = C_{gd} + C_{gs}$$

The output capacitance

$$C_{oss} = C_{gd} + C_{ds}$$

The reverse transfer capacitance

$$C_{rss} = C_{gd}$$

The charging and discharging time required by the device capacitances limits the switching frequency. In order to attain high switching frequencies it is essential that the gating circuit be capable of sourcing/sinking sufficient current at the time of switching so as to bring about the changes in the capacitor voltage quickly. This also helps to reduce the switching losses.

The switching times of the MOSFET can be explained with reference to Figure 4.4:

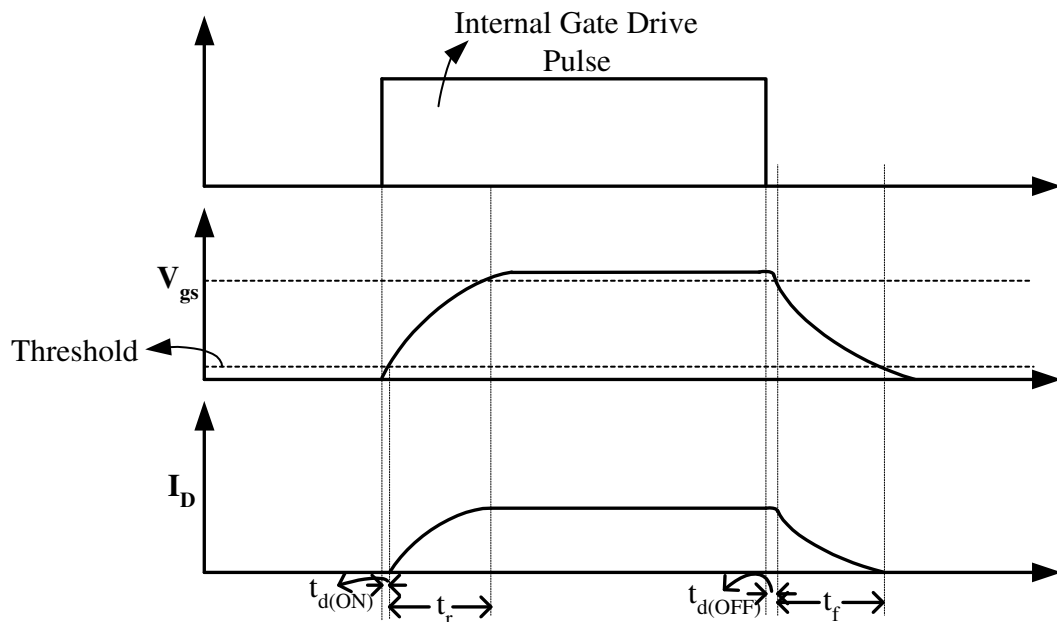


Figure 4.4: Switching times of a MOSFET

The turn-on delay time $t_{d(on)}$ is basically the time for the input capacitance to be charged by the gate drive circuit to the threshold level to bring the device into conduction. The rise

time t_r is the gate charging time required to drive from threshold voltage, through the linear control region to the gate voltage (usually 5 to 8 volts) required for full conduction of drain current. At turn off the procedure is reversed. The turn off delay time is the time required by the gate capacitance to discharge from the gate overdrive saturation voltage (typically 10V) to the active gate control region. Finally the fall time t_f is the time required for the input capacitance to discharge through the active control region to the gate threshold voltage.

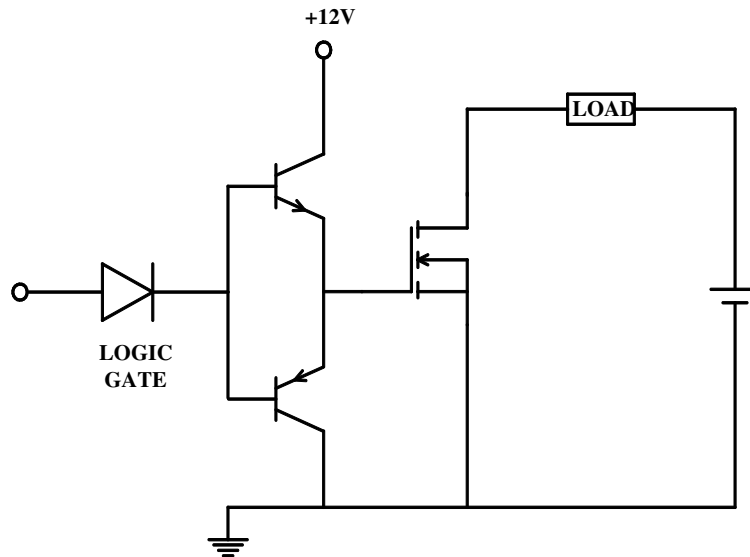


Figure 4.5: Buffering circuit for driving a MOSFET from a logic Gate

The gate drive circuit should therefore act as a voltage source with low output impedance and should source and sink sufficient current to minimize the time spent by the device in the active region during switching. A current capability of about 1A is therefore desirable. Low output impedance is also desirable from another point of view. Because of the Miller capacitance C_{gd} between gate and drain, any voltage transient at the drain is coupled to the gate. If the gate circuit is presents a high impedance to these transients, this may result in a voltage spike at the gate with respect to the source. The ratio in which the drain voltage transients are transferred to the gate is given by $\frac{1}{1+(C_{gs}/C_{dg})}$ which can be about $\frac{1}{6}$. Thus a 300V spike at he chain will cause a 50V spike at the gate. The gate-source voltage of the MOSFETs has an absolute maximum rating of about 20V and so device failure may occur. A protective zener is usually used to clip gate-source voltage spikes. Further the Miller effect results in the device spending time in the active region at every switching resulting in greater power dissipation. These problems are mitigated by designing the gate device circuit to have low output impedance. Thus, although in principle MOSFETs can be directly driven from CMOS or TTL ICs, some amount of buffering and amplification is necessary to

achieve good performance. Also, in case the gate is driven through a pulse transformer, the leakage inductance will present a high impedance to fast transients and therefore buffering is necessary. Figure 4.5 shows a simple circuit that has been suggested for buffering.

Special purpose gate drive ICs are also available from some manufacturers.

4.2 The IGBT

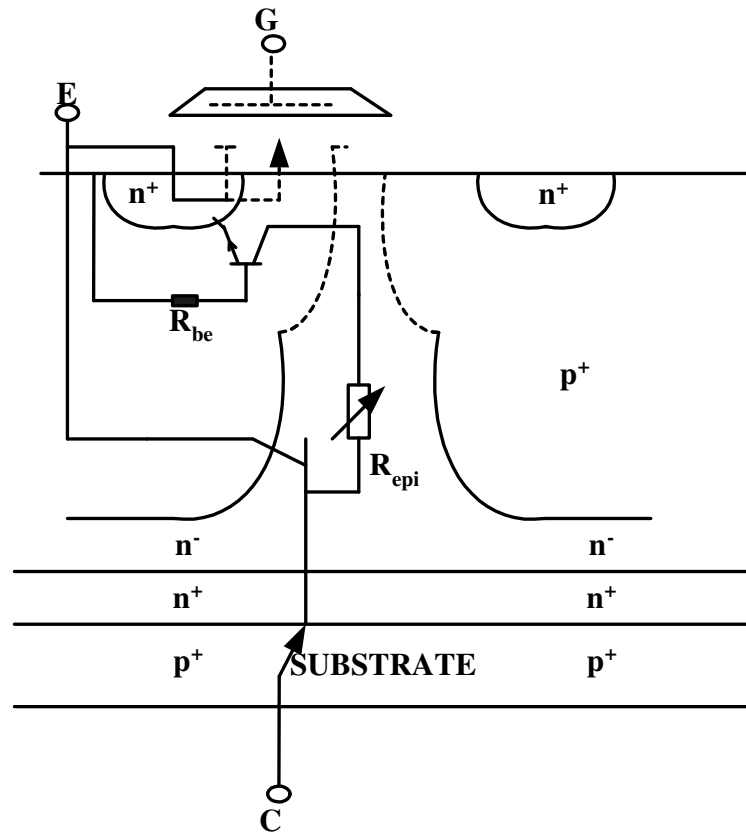


Figure 4.6: Internal structure of an IGBT

The insulated gate bipolar transistor - variously referred to as IGT, IGBT, COMFET, etc. - has recently emerged as an alternative to BJTs and MOSFETs. The BJT furnishes good current carrying ability with low conduction losses, but suffers from drawbacks such as large base drive requirements, limited safe operating area and thermal runaway. The power MOSFET, as discussed above, has low gate power requirements, does not suffer from second breakdown phenomena and can switch much faster. But devices designed for high voltage have high $R_{DS(ON)}$ values, which severely restricts their current handling ability. The IGBT was born out of the attempt to combine the low ON drops of BJTs with the low gate power requirements of MOSFETs.

Figure 4.6 shows the internal structure of an IGBT. As can be observed, it is a four layer p-n-p-n device. By comparing the structure of the MOSFET shown in Figure 4.1, it can be seen that the IGBT has an additional p^+ substrate. The terminals of the IGBT are referred to as the collector (C), the emitter (E) and the gate (G).

The internal equivalent circuit elements are also depicted in Figure 4.6. The equivalent circuit for the IGBT structure and its circuit symbol is shown in Figure 4.7.

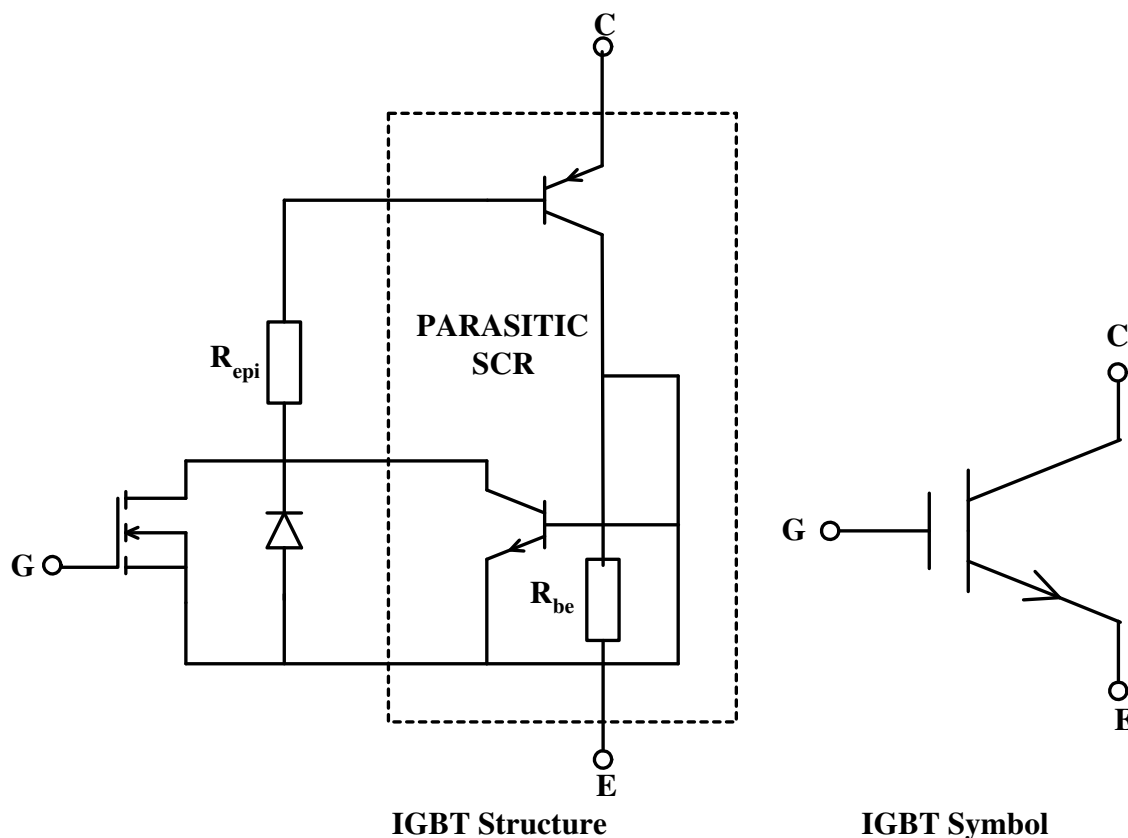


Figure 4.7: Circuit equivalent of IGBT structure and its circuit symbol

When the collector is at a positive potential with respect to the emitter, and the gate is raised to a suitable positive potential with respect to the emitter, a channel is formed in the p^+ region. Electrons pass from the n^+ emitter to the n^- epitaxial region through the channel. This in turn forward biases the pn junction between the p^+ substrate and the n^- regions and holes are injected in to the high resistivity n^- region. The excess electrons and holes modulate or increases the conductivity of the n^- region, thereby reducing the ON resistance of the device.

The reduction in the ON drop is however is achieved at the expense of the switching speed. When the gate pulse is removed, the injected minority carriers in the n^- region have

to be removed and this increases the turn off time of the IGBTs as compared to MOSFETs. Devices with turn-off times as high as $15\mu s$ or as low as $0.5\mu s$ can be produced, by accepting correspondingly lower or greater ON drops. It can also be seen that there is present in the IGBT a parasitic SCR which can cause latching due to high currents and fast turn-off $\frac{dv}{dt}$ effects. As with the MOSFET, this effect is sought to be minimized by minimizing the resistance R_{be} .

In general IGBTs score over BJTs and MOSFETs in applications at 600V and above. IGBTs with 1000V, 300A rating are currently available. However, the switching frequencies are limited to about 20kHz.

4.2.1 Switching Behavior and Gating Requirements of IGBTs

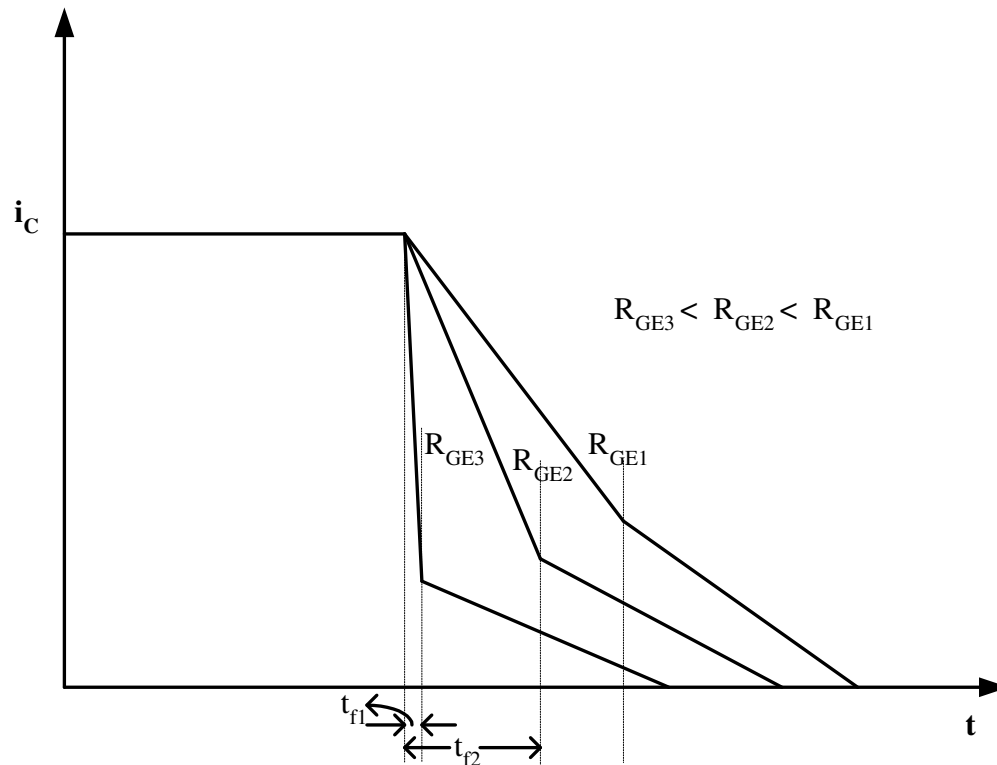


Figure 4.8: Fall times of an IGBT

The IGBT being a voltage controlled device, collector current flows once the gate-emitter voltage exceeds the threshold value. Like the MOSFET, the gate lead draws no current in the steady-state. To turn the IGBT off, the gate pulse should be removed and a resistor R_{GE} should be connected across the gate and emitter in order to discharge the input capacitance

of the device. The resistance R_{GE} has a pronounced effects on the turn off behavior of the IGBT. The fall time of the IGBT has two distinct parts, t_{f1} and t_{f2} as shown in Figure 4.8.

The two intervals are clearly discernible for a slow IGBT, but not so evident for a fast one. t_{f2} is a constant for a given device and constitutes a current tail during turn off leading to switching losses. t_{f1} can be controlled by changing R_{GE} . The lower R_{GE} , the smaller is t_{f1} . However, as R_{GE} is reduced, the maximum controllable current that the device can handle also comes down. This is because of the danger of latching at high currents with fast turn-off.

Although the conduction losses of IGBTs are much smaller than those of MOSFETs and may almost be the same as for BJTs, switching losses are higher than for MOSFETs. Total losses, including both conduction and switching losses, must be evaluated while selecting a device for an application. From the point of view of reducing the switching losses as well as reducing the risk of latching, provision of snubbers is beneficial.

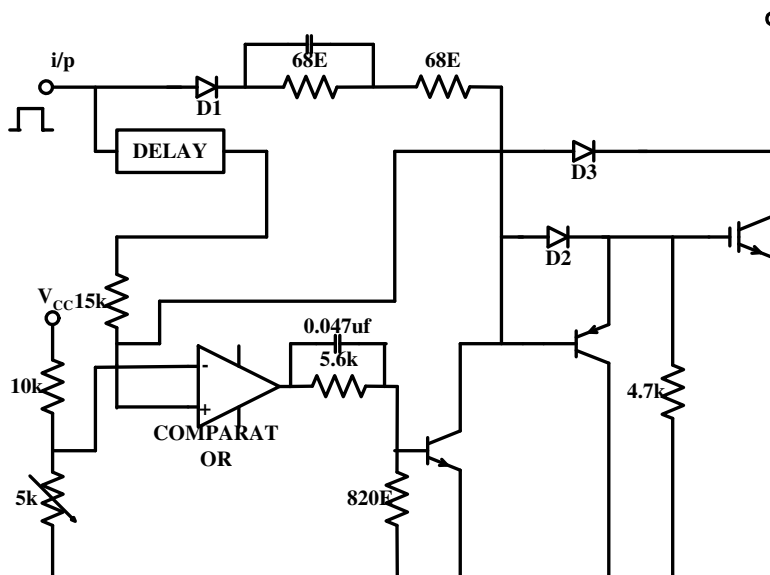


Figure 4.9: Gate drive circuit for IGBT

As with BJTs, over current in IGBTs can be sensed by sensing the collector voltage. This provides a convenient way of protecting the device. In the case of MOSFETs, the $R_{DS(ON)}$ varies markedly with temperature and therefore the drain to source voltage does not provide a reliable means of protecting the device. Even with the protection feature incorporated into the gate drive of the IGBT, it may be advisable to provide a current limiting reactor to limit the $\frac{di}{dt}$ in case of a fault.

Figure 4.9 shows the gate drive circuit for an IGBT. The circuit uses a speed-up capacitor

for reducing turn on time and incorporates over current protection by sensing the collector voltage during the conduction period of the device. The delay circuit has provided to inhibit the protection at turn-on, so that the device is not prevented from turning on.

4.3 REFERENCES

- 1) 'HEXFET Databook', International Rectifiers
- 2) B.J. Baliga and Marvin Smith, 'Modulated Conductivity Devices Reduce Switching Losses', EDN, September 29, 1983, pp.153-162
- 3) AEG, 'Technical Information on IGBT Modules', 1989.
- 4) Dubhashi A.U., Pelly B.R., 'A Comparison Of IGBTs And Power MOSFETs For Variable Frequency Motor Drives', Conference Record of Applied Power Electronics Conference APEC 89, pp 67-74.

Chapter 5

Review of Induction Motors

The squirrel cage induction motor is the work horse of industry. Traditionally it has been a constant speed device. With the advent of static inverters, speed control through frequency variation has become practical. This has opened up a wide range of applications. The basic theory of the squirrel cage induction motor is reviewed here.

5.1 Basic Principle of Operation

The induction motor has a three phase winding on the stator and a rotor cage with end rings which electrically behaves as another three phase winding. When the stator windings are supplied with balanced three phase currents, a revolving magnetomotive force is produced in the air gap. If the stator winding is designed properly, the spatial distribution of the stator *mmf* at any instant of time can be assumed to be sinusoidal. The location of the positive peak (north pole) of this *mmf* is taken as its instantaneous position. The speed of rotation of stator *mmf* wave is given by

$$N_e = \frac{120f_s}{P} \quad \text{revolution per minute} \quad (5.1)$$

where: f_s is the frequency of the stator currents; P is the number of poles.

Because of the stator *mmf* a rotating flux wave is produced in the air gap of the machine. This flux wave also has a sinusoidal spatial distribution at any instant of time and rotates in space in the same direction and with the same speed as the stator *mmf*. Speed of the stator *mmf* (or the flux) is referred to as the synchronous speed.

As the flux sweeps past the rotor conductors, *emfs* are induced in these conductors. Since the rotor bars are shorted by the end rings, currents flow in the rotor conductors. The interaction of rotor currents and the flux produces torque and the rotor begins to turn. The rotor attempts to catchup with the flux. However, since this would result in the disappearance of torque, an equilibrium is reached where the rotor runs at a speed such that the relative motion of the flux is sufficient to produce enough torque to sustain the rotor

speed. If the rotor runs at a speed of N revolutions per minute, the relative speed of the flux with respect to the rotor is given by

$$N_r = N_s - N \quad (5.2)$$

The slip 's' of the machine is defined as the ratio $\frac{N_r}{N_s}$.

i.e.

$$s = \frac{N_r}{N_s} = \frac{N_s - N}{N_s} = 1 - \frac{N}{N_s} \quad (5.3)$$

The frequency of the currents in the rotor is given by

$$f_r = \frac{N_r P}{60 \cdot 2} \quad (5.4)$$

Therefore, the slip can also be defined as

$$s = \frac{f_r}{f_s} \quad (5.5)$$

Let w_r and w_s be the the angular frequencies of the rotor and stator currents respectively. If w is the speed of the rotor in the electrical radians per second, slip is also defined as

$$s = \frac{w_r}{w_s} = \frac{w_s - w}{w_s} = 1 - \frac{w}{w_s} \quad (5.6)$$

When the currents are induced in the rotor, the rotor also produces an *mmf*. The net *mmf* acting on the air gap is the sum of stator and rotor *mmfs* and air gap flux is established due to the resultant *mmf*.

5.2 Mechanism of Torque Production

When the motor is running in the steady state, sinusoidally distributed air gap flux and the *emf* induced in the rotor conductor can be indicated as shown in Figure 5.1.

Air gap flux is moving at a speed w_r electrical radians per second with respect to the rotor conductors. The amplitudes of the induced emfs in the rotor conductors are indicated in Figure 5.1. Due to the induced voltage, current flows in the rotor conductors. However because of the inductance in the rotor circuit, the rotor current is not in phase with the rotor induced *emf*, but lags it in time by an angle θ_r , which is the rotor power factor angle. The inductance is responsible for the presence of θ_r is the leakage inductance of the rotor. Consequently, the rotor conductor current amplitudes with respect to the air gap flux are as shown in Figure 5.2.

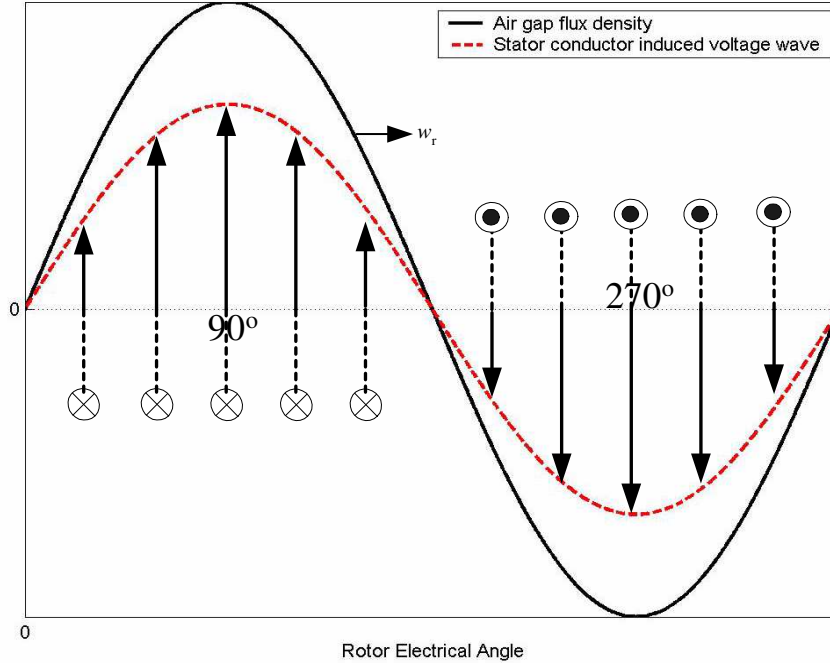


Figure 5.1: Air gap flux and rotor induced voltage wave

The currents in two rotor conductors 180° apart can be regarded as current in a coil, producing an *mmf* along the axis of the coil. Therefore the rotor *mmf* wave will have a spatial position with respect to the air gap flux as shown in Figure 5.3.

The rotor *mmf* also rotates at a speed w_r with respect to the rotor, since the rotor currents alternate at the frequency w_r . Therefore the rotor *mmf* will also rotate at synchronous speed w_s with respect to the stator. The peak of the rotor *mmf* wave is at an angle $90^\circ + \theta_r$ behind the peak of the flux wave.

It can be seen that due to the lag between the rotor voltage and the rotor current the force on some of the rotor conductors oppose the rotation of the rotor. The net torque developed by the machine can be obtained by summing the forces acting on each of the rotor conductors. The expression for developed electromagnetic torque can be shown to be

$$m_d = \pi \frac{P}{2} l r B_p F_p \sin \delta \quad (5.7)$$

where:

P is the number of poles

l is the axial length of the machine

r is the radius of the rotor

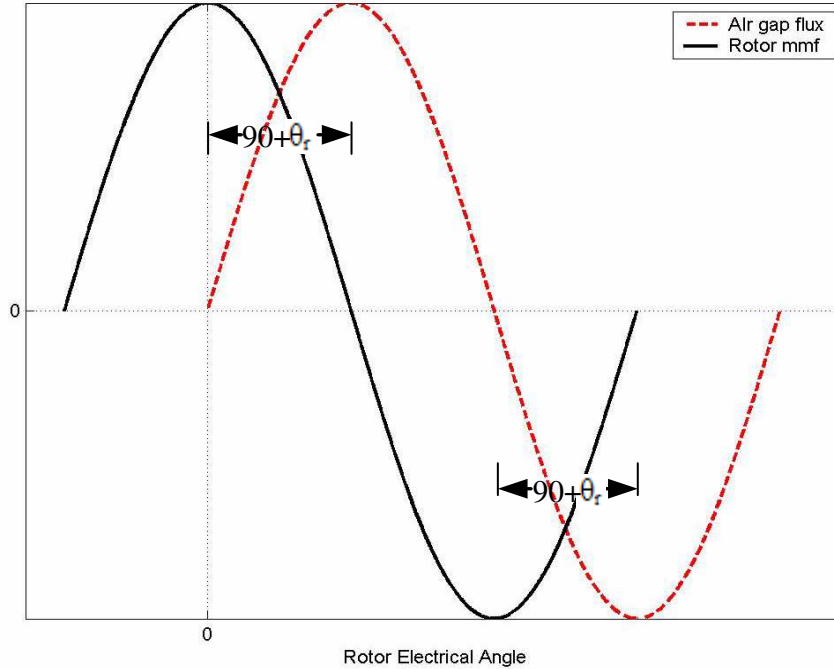


Figure 5.3: Air gap flux and rotor mmf waves

5.3 Steady-State Equivalent Circuit of Induction Motor

The air gap flux rotating at w_s electrical radians per second induces back emf V_m in the stator. The flux also moves at a speed w_r with respect to the rotor. The corresponding emf induced in the rotor can be written as

$$E'_r = n s V_m \quad (5.10)$$

where:

n is rotor to stator turns ration

s is slip

Therefore, the machine can be represented by an equivalent circuit as shown in Figure 5.4.

Here the two sides of the transformer work at different frequencies, namely, w_s and w_r . The rotor current I'_r is given by

$$I'_r = - \frac{n s v_m}{R'_r + j w_r L'_{lr}} \quad (5.11)$$

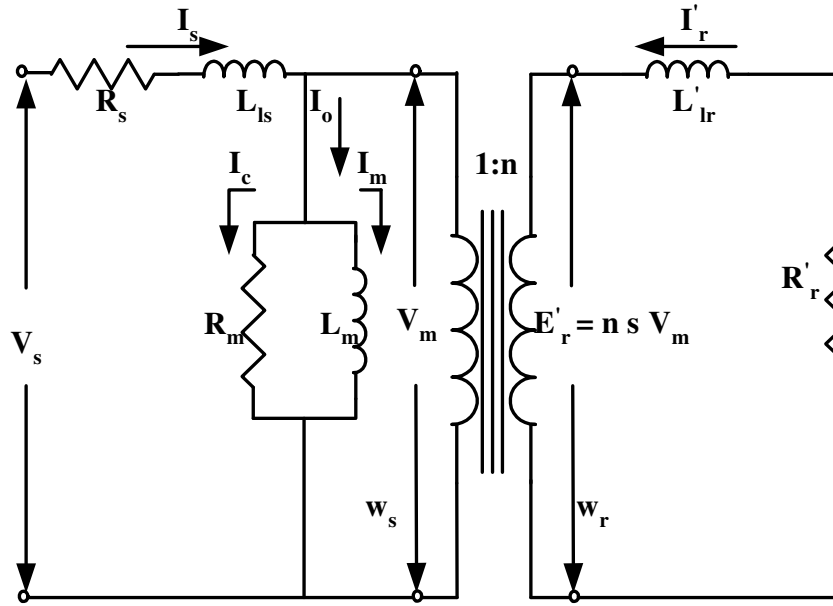


Figure 5.4: First attempt at equivalent circuit

$$\begin{aligned}
 I'_r &= - \frac{n v_m}{\frac{R'_r}{s} + j \frac{\omega_r}{s} L'_{lr}} \\
 &= - \frac{n v_m}{\frac{R'_r}{s} + j \omega_s L'_{lr}} \quad (5.12)
 \end{aligned}$$

using equation 10.12, the above equivalent circuit can be reduced to one in which both sides operate at the same frequency ω_s . In addition, if the usual technique of referring all quantities to the primary (stator) turns is resorted to, the equivalent circuit shown in Figure 5.5 of the induction motor is obtained.

Note that the current I_r is shown and not the component I_2 of stator current. Of course $I_2 = -I_r$. The phasor diagram associated with the above equivalent circuit shown in Figure 5.5 can be drawn as shown in Figure 5.6. For a machine with the sinusoidally distributed windings, the time phase angles between different quantities in the phasor diagram translate in to the spatial angle between them expressed in electrical radians per second. In drawing the phasor diagram, the core loss component I_c of the stator current has been neglected for convenience.

The developed torque can now be written as

$$M_d = K \psi_M I_r \sin \delta \quad (5.13)$$

where

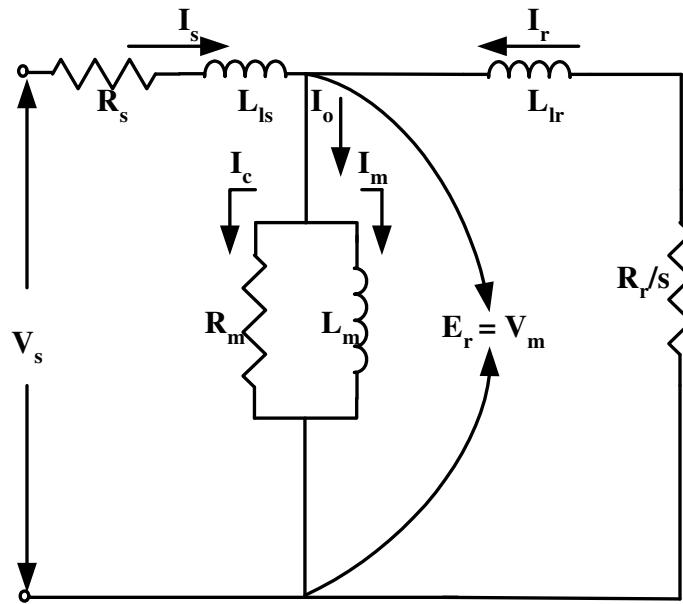


Figure 5.5: Equivalent circuit of induction motor referred to stator

ψ_M and I_r are the *rms* values of the air gap flux and referred rotor current respectively.

Therefore

$$M_d = K' I_M I_r \sin\delta \quad (5.14)$$

Also,

$$I_r \sin\delta = I_s \sin\theta \quad (5.15)$$

Thus,

$$M_d = K' I_M I_s \sin\theta \quad (5.16)$$

$$= K' I_M I_a \quad (5.17)$$

where

I_a is the component of the stator current in phase quadrature with the flux.

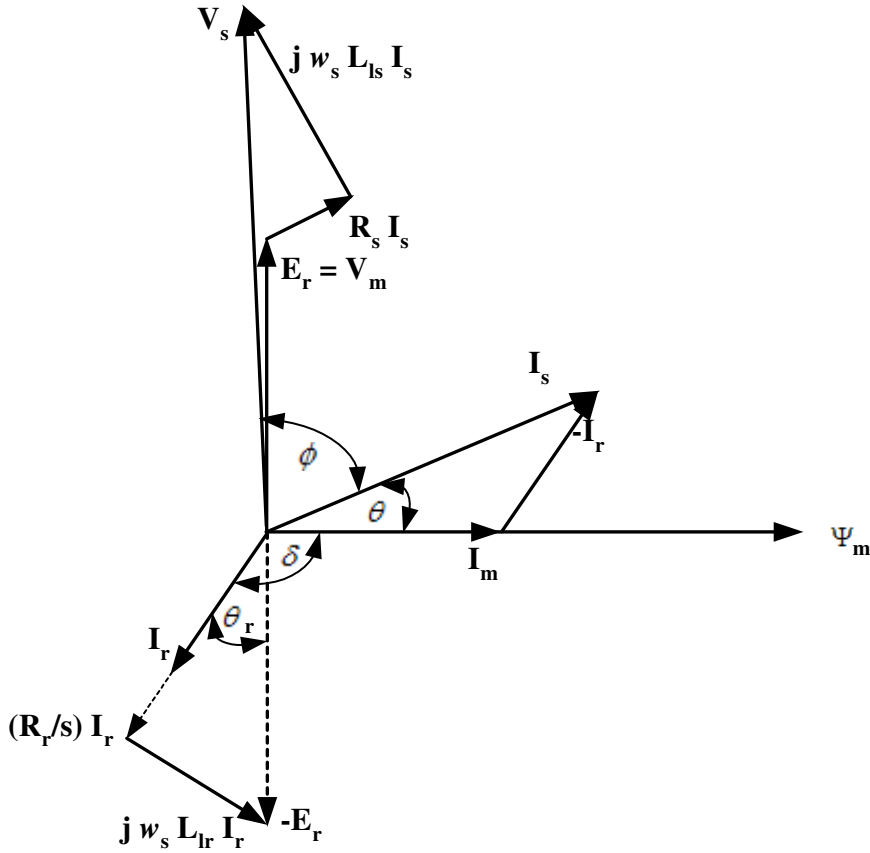


Figure 5.6: Phasor diagram of induction motor

5.4 Steady-state Performance Based On Approximate Equivalent Circuit

The equivalent circuit of Figure 5.5 can be approximated by neglecting the core-loss component and pushing the magnetizing inductance to the stator terminals. The resulting circuit is shown in Figure 5.7.

The circuit shown in Figure 5.7 is a little more convenient than the original one in getting an appreciation of the performance of the machine. Based on this equivalent circuit, rotor current

$$|I_r| = \frac{V_s}{((R_s + \frac{R_r}{s})^2 + \omega_s^2(L_{ls} + L_{lr})^2)^{\frac{1}{2}}} \quad (5.18)$$

The air gap power

$$P_{ag} = 3 |I_r|^2 \frac{R_r}{s} \quad (5.19)$$

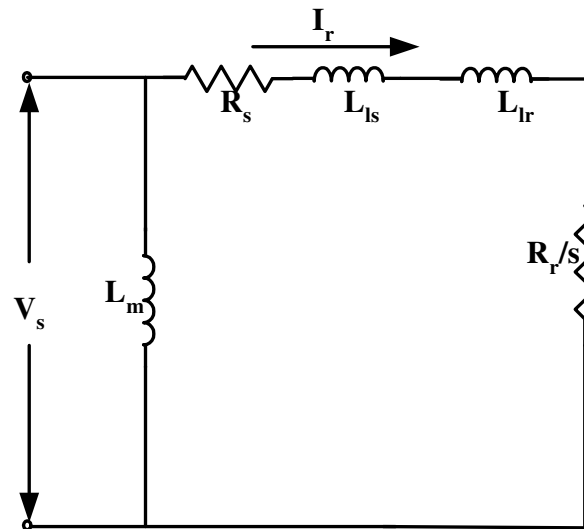


Figure 5.7: Approximate equivalent circuit of induction motor

The electromagnetic torque

$$M_d = \frac{P_{ag}}{\text{synchronous speed}}$$

$$M_d = 3 \frac{P}{2} \frac{R_r}{s w_s} \frac{V_s^2}{(R_s + \frac{R_r}{s})^2 + w_s^2 (L_{ls} + L_{lr})^2} \quad (5.20)$$

The starting torque is obtained by setting $s = 1$ in equation 5.20. The torque speed characteristic based on equation 5.20 is shown in Figure 5.8.

Note that for supersynchronous speeds of rotation (i.e. negative values of slip) the machine acts as a generator. The torque becomes negative, i.e., braking torque. In variable frequency drives, the machine can be made to enter the generating region of the characteristic by reducing the stator frequency w_s to a value below the running speed w of the machine. In the plugging region, the field rotates in the opposite direction to the rotor; slip is greater than unity and there is excessive heating. The machine draws power from the electrical as well as the mechanical system to which it is connected.

The characteristics show that there is a value of slip ' s ' at which the torque is maximum, in the motoring as well as generating mode. The maximum torque is called the pull-out torque and is usually about 1.5 to 2 times the rated torque of the machine.

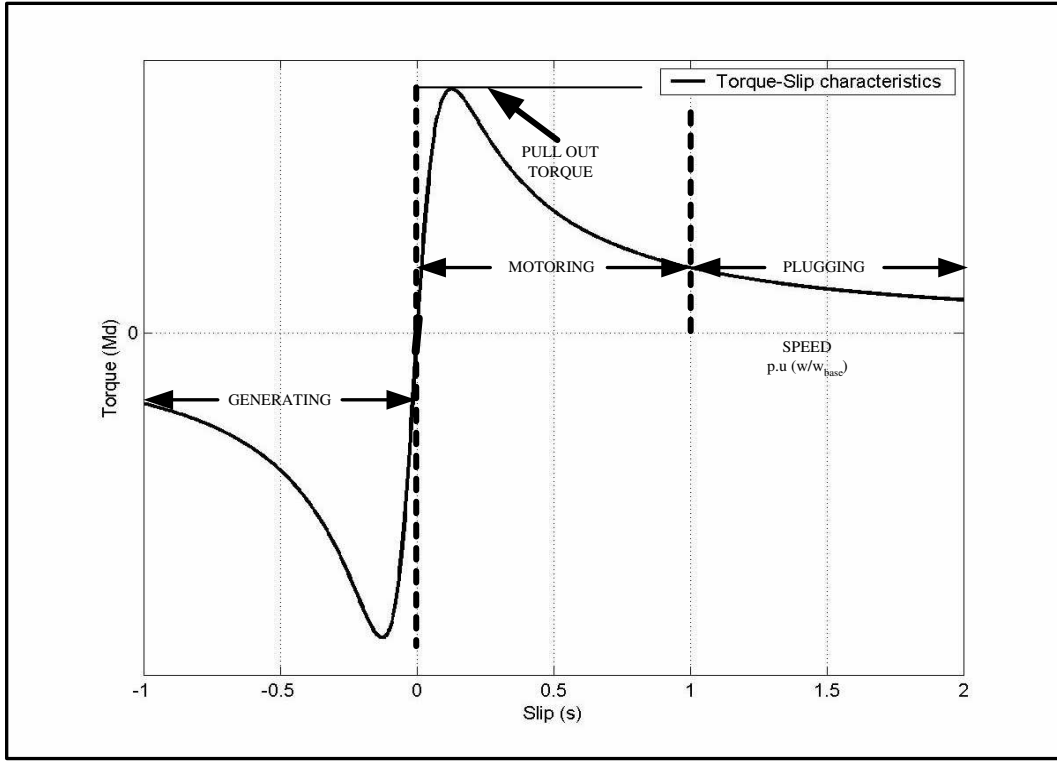


Figure 5.8: Torque-Slip characteristics of induction motor at constant voltage and frequency

Further approximate relationships can be obtained if the stator resistance and the leakage inductances are neglected. Such an approximation is fairly accurate for integral horse power machines at speeds above 10% of rated speed. The approximate expression for the torque is

$$M_d = 3 \frac{P}{2} \left(\frac{V_s}{w_s} \right)^2 \frac{w_r R_r}{R_r^2 + (w_r L_{lr})^2} \quad (5.21)$$

Rotor current

$$I_r = \frac{s V_s}{(R_r^2 + (w_r L_{lr})^2)^{\frac{1}{2}}} \quad (5.22)$$

$$\cos \theta_r = \frac{R_r}{(R_r^2 + (w_r L_{lr})^2)^{\frac{1}{2}}} \quad (5.23)$$

The air gap flux ψ_m is expressed as

$$\psi_m = \frac{V_s}{w_s} \quad (5.24)$$

For very small values of slip, $R_r \gg w_r L_{lr}$ and the torque expression given in the equation 5.20 simplifies to

$$M_d = 3 \frac{P}{2} \psi_m^2 w_r \frac{1}{R_r} \quad (5.25)$$

Therefore, it can be said that at constant flux ψ_m , torque is directly proportional to the slip frequency w_r . At constant w_r , torque is proportional to the square of the flux.

5.5 Operation from Non-Sinusoidal Sources

When an induction motor is operated from an inverter, the applied voltages are not sinusoidal. They contain, besides the fundamental, odd harmonics. For example, in the six step inverter, harmonics of order $6m \pm 1$ are present. Therefore, it becomes necessary to study the response of the machine to these harmonic voltages. The equivalent circuit offers a convenient starting point for this study. The equivalent circuit of induction motor shown in Figure 5.7 is redrawn in Figure 5.9 for a general harmonic of order k . All reactances get multiplied by the harmonic order k . It is assumed that resistance values remain same, i.e. skin effect is neglected.

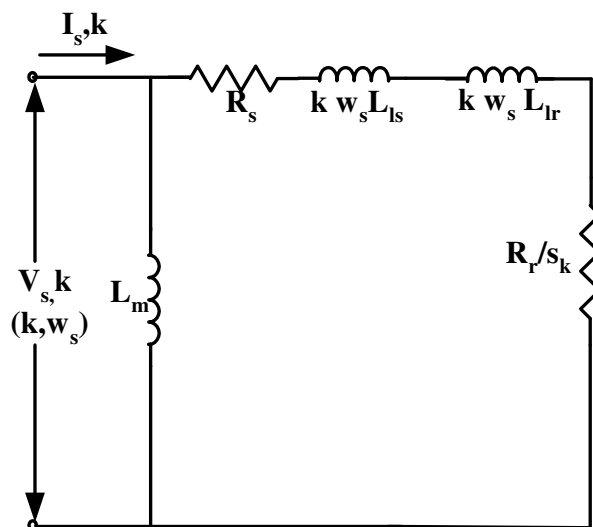


Figure 5.9: Equivalent circuit for any harmonic

The value of the slip s_k has to be interpreted properly. The slip is the ratio of rotor speed to the synchronous speed. The rotor speed is the same, whatever be the harmonic considered. But the synchronous speed, i.e., the speed at which the stator mmf is rotating, depends on the harmonic being considered. In general, the mmf due to the k^{th} harmonic will rotate at k times the speed of the fundamental. However not all the harmonic mmf s rotate in the same direction as the fundamental. It has been pointed out that harmonics of the order $6m - 1$ (5,11,17,etc.) have a negative phase sequence and so the mmf produced by these harmonics will rotate in the opposite direction to the fundamental. Therefore, the

slip for the 5th harmonic is given by

$$s_5 = \frac{-5w_s - w}{5w_s} = 1 + \frac{1}{5} \frac{w}{w_s} = 1 + \frac{1}{5} (1 - s_1) \quad (5.26)$$

Since s_1 is very small, it can be approximately said that

$$s_5 = 1 + \frac{1}{5}$$

Similarly, $s_{11} = 1 + \frac{1}{11}$; $s_{17} = 1 + \frac{1}{17}$; etc.

On the other hand, for a positive sequence harmonic such as 7th,

$$s_7 = \frac{7w_s - w}{7w_s} = 1 - \frac{1}{7} \frac{w}{w_s} = 1 - \frac{1}{7} (1 - s_1) \quad (5.27)$$

$$s_7 = 1 - \frac{1}{7}$$

similarly, $s_{13} = 1 - \frac{1}{13}$; $s_{19} = 1 - \frac{1}{19}$; etc.

In general, therefore, the slip corresponding to the harmonics is very close to unity. Therefore the equivalent circuit of Figure 5.10 can be successively simplified as follows.

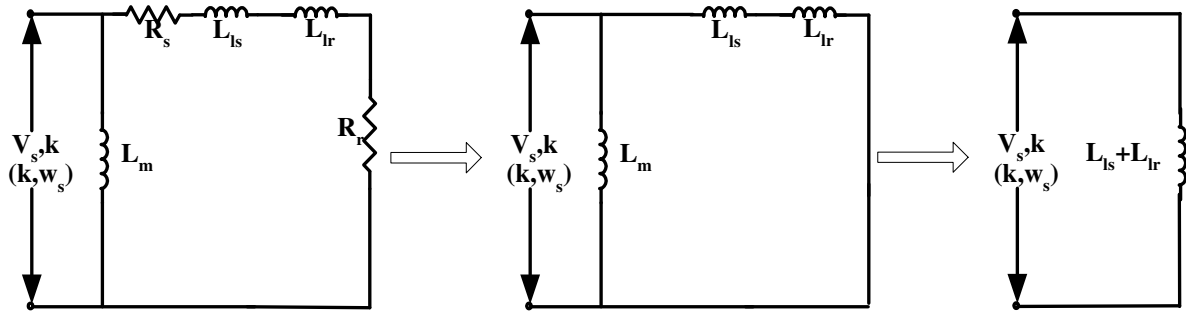


Figure 5.10: Simplification of harmonic equivalent circuit

The resistances can be neglected in comparison with the leakage reactance at the harmonic frequencies and further the magnetizing impedance can be neglected compared to the leakage reactance (in parallel connection). Thus machine offers only the leakage impedance to the harmonics in the applied voltage.

In the case of the six-step inverter, harmonics of the output voltage have amplitude which are inversely proportional to the harmonic order. If X_l is the leakage impedance of

the machine at fundamental frequency, various harmonic currents can be written as

$$I_5 = \frac{V_1}{5 \times 5X_1} = \frac{V_1}{25}$$

$$I_7 = \frac{V_1}{49}; \quad I_{11} = \frac{V_1}{121}, \quad \text{etc.} \quad (5.28)$$

The total *rms* stator current is therefore given by

$$I_{rms}^2 = I_1^2 + \left(\frac{V_1}{X_1}\right)^2 \left[\frac{1}{25^2} + \frac{1}{49^2} + \frac{1}{121^2} + \dots\right]$$

$$= I_1^2 \left[1 + \left(\frac{V_1}{I_1 X_1}\right)^2\right] \left[\frac{1}{25^2} + \frac{1}{49^2} + \frac{1}{121^2} + \dots\right] \quad (5.29)$$

Considering a machine with 10% leakage impedance, $\frac{V_1}{X_1}$ corresponds to 10 times rated current. Therefore the harmonic currents, expressed in p.u. with rated current as base, can be calculated as:

$$I_5 = \frac{10}{25} = 0.4p.u$$

$$I_7 = \frac{10}{49} = 0.2p.u$$

$$I_{11} = \frac{10}{121} = 0.083p.u$$

an so on.

Therefore the harmonic currents considerably increase the *rms* stator current and contribute to the increased copper losses in the motor. Further, the maximum instantaneous current handled by the inverter switches can also go up by a factor of 1.5 to 2 and the inverter devices have to be suitably rated. Thus some amount of derating for the whole inverter drive system becomes inevitable. A further important effect created by the current harmonics is that they produce a torque pulsations in the motor. The mechanism by which torque pulsation are produced is explained below.

5.6 Effects of Harmonics on the Torque

The basic mechanism of torque production in the motor is due to the interaction of the rotor current with the air gap flux. In a machine which is excited by purely sinusoidal voltages, only fundamental flux and rotor current are produced and these rotate in synchronism, i.e., a constant spatial angle is maintained between the flux and the current. Since torque is proportional to the magnitudes of the flux and the current and also the *sine* of the spatial angle between two, a steady torque is produced.

In inverter fed machines, however, fluxes and currents at various harmonic frequencies are also produced. If the interaction between flux at one frequency and the current at same frequency is considered, steady torque is produced. In the case of positive sequence harmonics, this adds to the torque produced by the fundamental and in the case of negative sequence harmonics, it opposes the torque due to the fundamental. However, the contributions of the harmonics to the steady output torque of the motor are negligible in magnitude and it can be said that the useful output torque is only due to the fundamental.

When the interaction between flux at one frequency and rotor current at another frequency is considered, the two are in relative motion as they rotate at different speeds and possibly in the opposite directions. The torque produced by such interactions therefore pulsates with respect to time at the frequency of relative motion between the flux and current considered. Such interactions can be understood by looking at the phasor diagram of Figure 5.11.

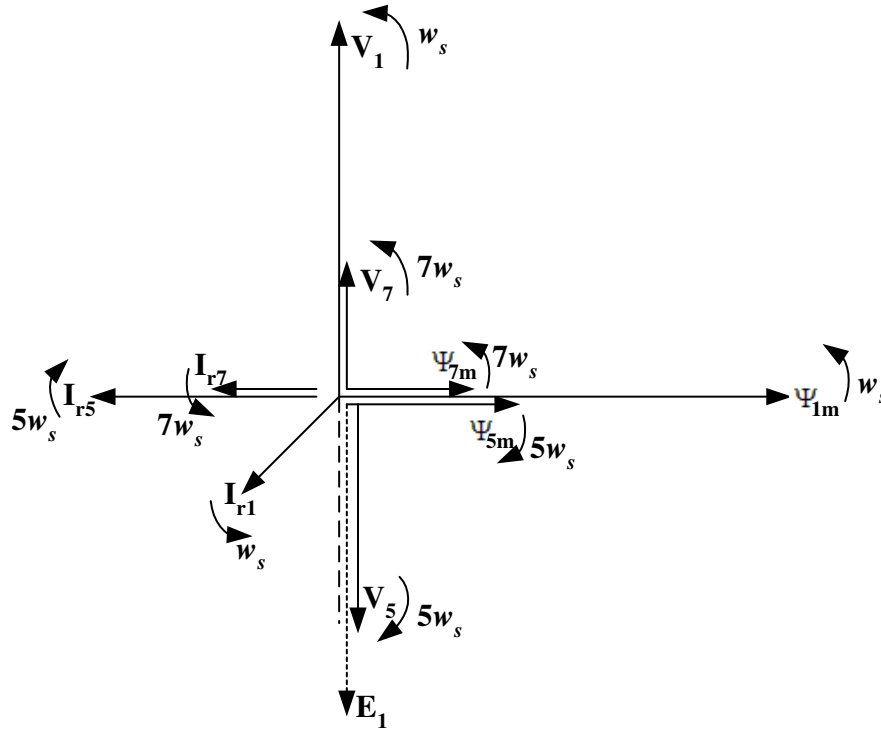


Figure 5.11: Phasor diagram showing harmonic fluxes and currents

The phasor diagram has been drawn taking the time origin as the instant at which the fundamental flux ψ_{1m} has the peak value. Correspondingly, the fundamental applied voltage will be at its negative zero crossing and is therefore pointing upwards. Now, it has been mentioned that due to the symmetry of the inverter output voltage waveform,

it can be expressed as a Fourier series containing only sine terms, i.e., the zero crossings of fundamental coincide with the zero crossings of the harmonics. Therefore the harmonic voltages V_5 and V_7 should also be at there negative zero crossings. However, V_5 is a negative sequence component and rotates in the clockwise direction. Therefore the phasor of the V_5 points downwards. Once the voltage phasors are drawn, corresponding flux phasors can be located at a lag angle of 90° with respect to the voltage, taking the direction of rotation into account.

For each harmonic flux, the rotor induced *emf* lags by 90° . Also at the harmonic frequencies, rotor leakage reactance dominates over the resistance and therefore the rotor can be taken to lag the induced voltage by 90° . The currents I_{r5} and I_{r7} are drawn in Figure 5.11 taking into account the above considerations. The diagram of Figure 5.11 can be given a clockwise rotation at a speed w_s , thereby making the fundamental quantities stationary. The resulting diagram is shown in Figure 5.12.

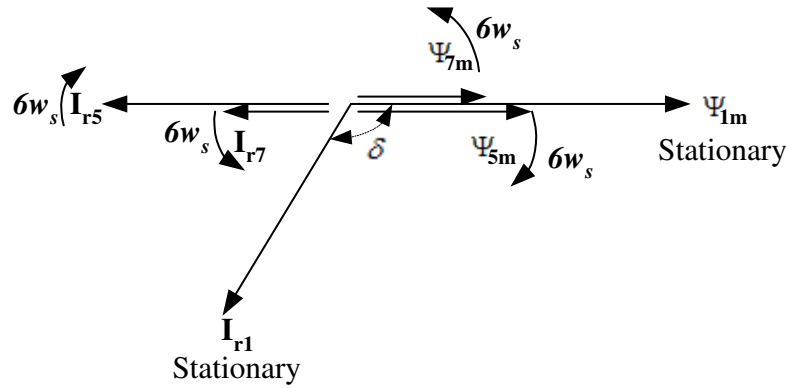


Figure 5.12: Phasor diagram with stationary fundamental quantities

From the Figure 5.12, it is clear that I_{r5} and I_{r7} are rotating with respect to ψ_{1m} at 6 times the fundamental speed, but in the opposite direction. They will both produce torque components pulsating at 6 times the fundamental frequency w_s . These torque components can be expressed as

$$M_{d6,1} = k [\psi_{1m} I_{r5} \sin(\pi + 6w_s t) + \psi_{1m} I_{r7} \sin(\pi - 6w_s t)] \quad (5.30)$$

Similarly the flux components ψ_{5m} and ψ_{7m} will interact with I_{r1} and produce 6^{th} harmonic torque pulsation. These components can be expressed as

$$M_{d6,2} = k [\psi_{5m} I_{r1} \sin(\delta - 6w_s t) + \psi_{7m} I_{r1} \sin(\delta + 6w_s t)] \quad (5.31)$$

If δ is approximately taken as 90° , the total 6^{th} harmonic torque pulsation due to all the four flux currents pairs is

$$M_{d6} = k [\psi_{1m}(I_{r5} - I_{r7})\sin(6w_s t) + (\psi_{7m} + \psi_{5m})I_{r1}\cos(6w_s t)] \quad (5.32)$$

The harmonic fluxes ψ_{7m} and ψ_{5m} are generally very small and in any case the second term adds to the first in quadrature. Therefore the 6^{th} harmonic torque pulsation can be expressed as

$$M_{d6} = k [\psi_{1m}(I_{r7} - I_{r5})\sin(6w_s t)] \quad (5.33)$$

Thus the fundamental flux interacting the 7^{th} and 5^{th} harmonic currents produces 6^{th} harmonic torque pulsation. Note that there is a cancelling effect between the contribution of the two currents. Similarly torque pulsation at the 12^{th} , 18^{th} , etc. harmonics are also produced, although the 6^{th} harmonic pulsation is the predominant one. The time variation of the instantaneous developed torque in the induction machine fed by a six step inverter therefore is as shown in Figure 5.13.

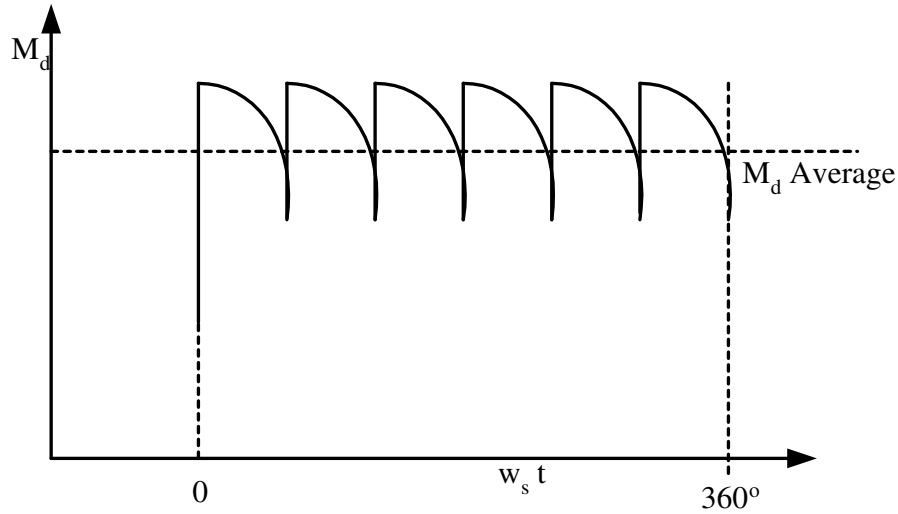


Figure 5.13: Phasor diagram with stationary fundamental quantities

It is even possible that the instantaneous torque is negative, for low values of average torque.

Such a pulsating torque may result in jerky motion of the motor, especially at low speeds (frequencies). Even at higher frequencies, where the torque pulsations are too fast for mechanical system to respond, increased stress on the shaft and bearings results.

5.7 REFERENCES

- 1) B.K. Bose, 'Power Electronics and AC Drives', Prentice-Hall.
- 2) J.M.D. Murphy, 'Thyristor Controlled AC Motors'.
- 3) Fitzgerald, Kingsley and Ullman, 'Electric Machinery', McGraw-Hill, New York, 1983.
- 4) S.B.T. Robertson and K.M. Hebbar 'Torque Pulsation in Induction Motors with Inverter Drives', IEEE Trans. Industry Applications, vol. IA7, pp. 318-323, March-April 1971.

Chapter 6

Basic Principles of Voltage Source Inverters

6.1 Single Phase Inverters

The circuit diagram of a single phase voltage source inverter, along with the gating signals for the power switches, is shown in Figure 6.1 and 6.2 respectively. The switches may be any one of the devices considered so far, namely BJTs, MOSFETs, IGBTs, or GTOs.

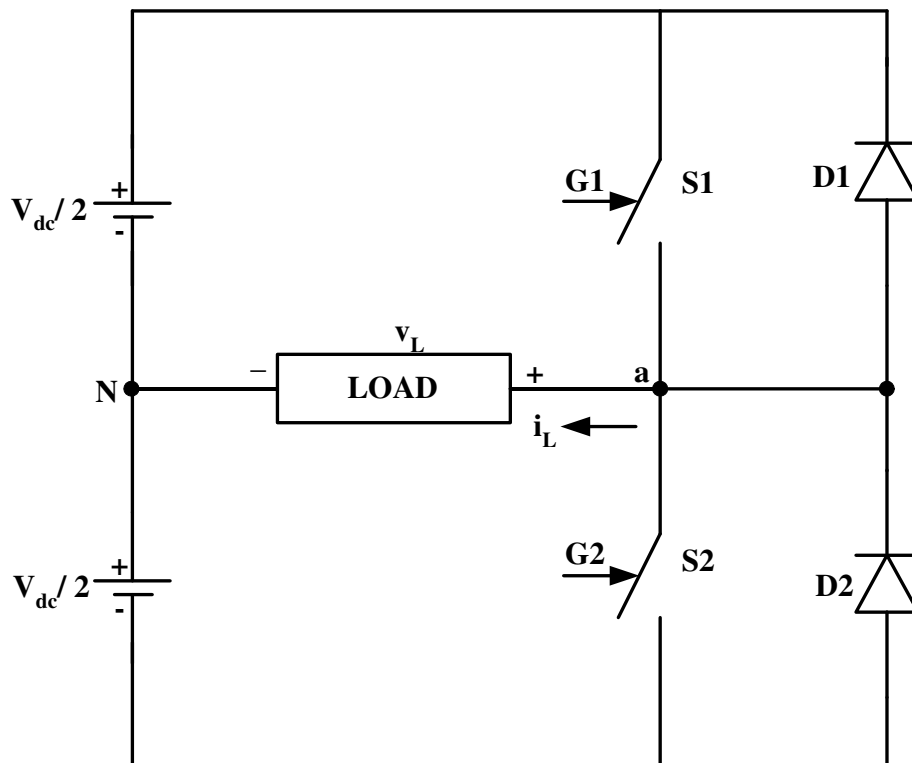


Figure 6.1: Circuit diagram of single phase voltage source inverter

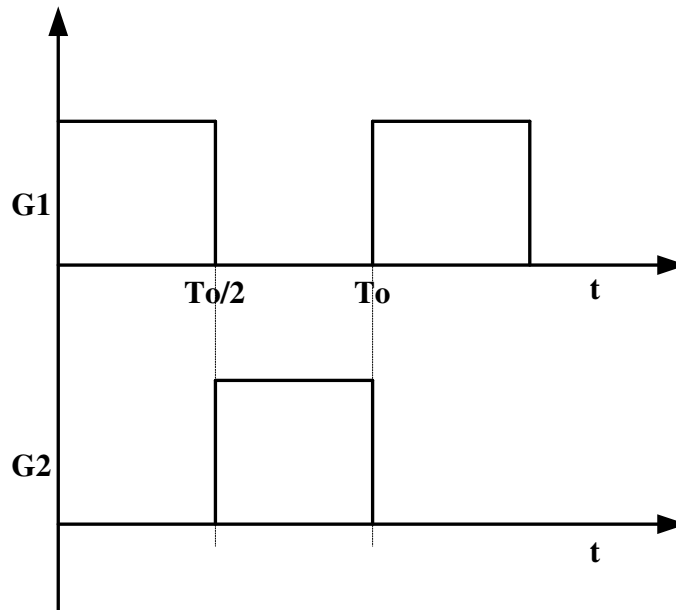


Figure 6.2: Gating signals for single phase voltage source inverter

The gating signals shown are such that each switch receives a gate pulse for half the period of the output frequency. The gating signals are complementary, i.e. at no instant of time do both the switches receive gating pulses. Also, there is no instant of time at which neither of the devices receives a gating pulse. These two features are characteristic of voltage source inverters. If the load current is continuous, as it usually is especially in motor drives, the output voltage $V_L = V_{ON}$ of the inverter is entirely decided by the gating pulses, irrespective of the polarity of the load current i_L , i.e. irrespective of the load power factor. This can be explained as follows.

If S_1 is receiving a gating pulse at a particular instant of time, then S_2 will not receive a gating pulse and will be off. The diode D_2 becomes reverse biased as S_1 is gated ON. Therefore, only S_1 or D_1 can conduct current. If the load current is positive it will flow through S_1 , otherwise through D_1 . Thus irrespective of the load current polarity, the voltage $V_{ON} = +\frac{V_{dc}}{2}$.

Thus, provided the load current is continuous, the output voltage of a voltage source inverter can be decided purely by looking at the gating signals of the switches. In the above inverter, voltage V_{ON} will be a symmetrical square wave of the amplitude $\frac{V_{dc}}{2}$. The output voltage V_{ON} and superimposed, sinusoidal load current for the lagging and the leading conditions are shown in Figure 6.3 and 6.4 respectively. The sequence in which the four devices conduct is also indicated in each case.

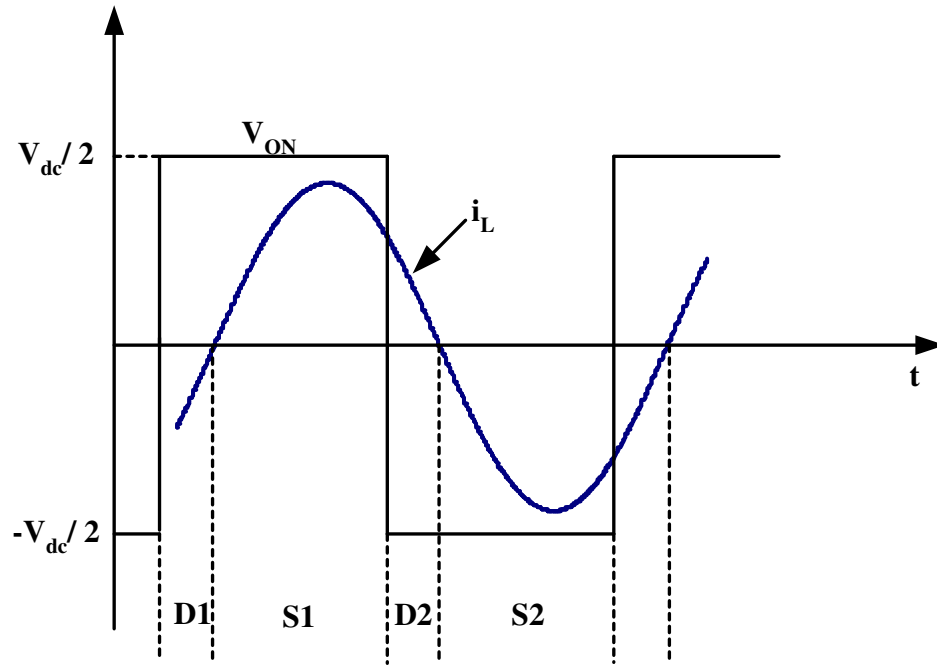


Figure 6.3: Inverter output voltage and current for lagging load

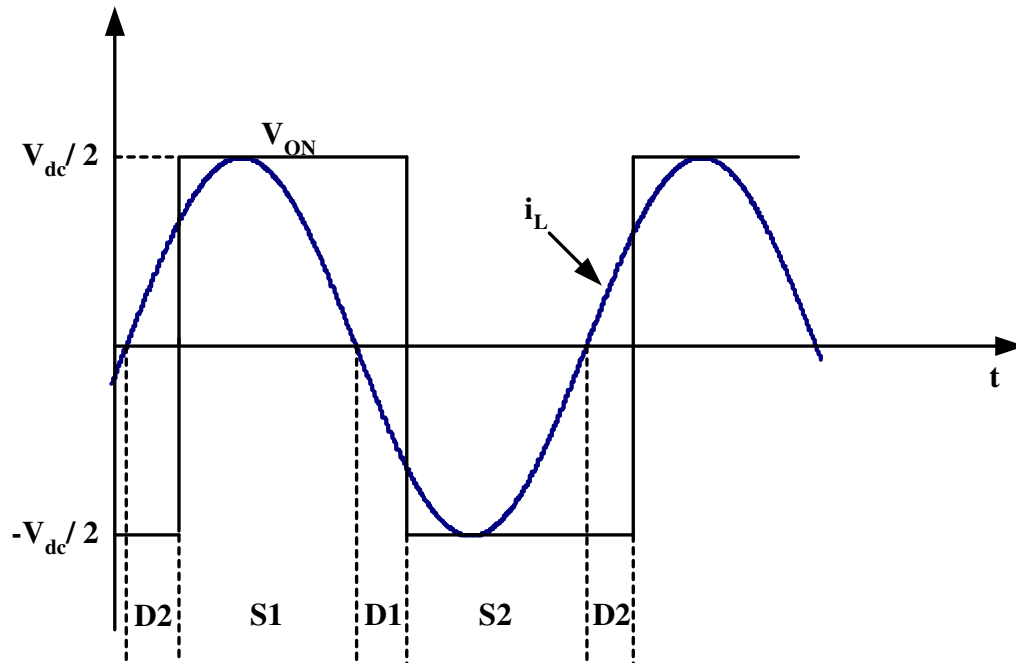


Figure 6.4: Inverter output voltage and current for leading load

For inductive loads, i.e. lagging loads, the sequence of conduction of devices is such that each of the switches S_1 and S_2 takes over current from its own antiparallel diode, whereas each diode takes over current from the complementary switch. Thus even though the switches receive the gating pulses at the transition of the voltage, current transfers into them only later and in a smooth fashion as decided by the load inductance. By the same token, the decay of current in the diodes also takes place in a smooth fashion, the $\frac{di}{dt}$ is being limited by the load inductance. Therefore there is no need for inductances to limit the $\frac{di}{dt}$ and consequently there is no associated energy loss. At turn-off of the switches, current transfers from switch to the complementary diode. Turn-off snubbers, in the form of capacitors across each switch are therefore required in order to limit the $\frac{dv}{dt}$. However, it can be verified that the charging and discharging of these capacitors is accomplished by the load current itself, i.e. the energy stored in these capacitors is not lost.

On the other hand, for leading loads, it can be seen that each switch takes over current from the opposite feedback diode. In the absence of $\frac{di}{dt}$ limiting, large reverse recovery currents occur in the diodes and these current peaks will have to be handled by the switches on top of the load current. The energy stored in the $\frac{di}{dt}$ snubber is transferred to the turn-off $\frac{dv}{dt}$ snubber at the time of turn-off and causes overvoltages across the switch turning off, in addition to energy loss at each switching.

With the above method of gating, it is seen that the output voltage of the inverter is a symmetrical square wave. Therefore, this is referred to as the square wave mode of operation. The output voltage can be resolved into various frequency components by Fourier analysis and expressed as

$$V_{ON}(t) = \sum_{n=1(n \text{ odd})}^{\infty} \frac{4}{\pi} \frac{V_{dc}}{2} \frac{1}{n} \sin(nwt) \quad (6.1)$$

where w is the angular frequency given by

$$w = \frac{2\pi}{T} \quad (6.2)$$

The amplitude of the fundamental

$$= \frac{4}{\pi} \frac{V_{dc}}{2} \quad (6.3)$$

The various harmonics have amplitudes which are inversely proportional to their order. Because of the fact that the square wave possesses quarter wave and half wave symmetries, the Fourier series contains only odd *sine* terms. Note that the frequency of the output voltage can be changed by changing the frequency of the gating signals. However, the amplitudes of the output voltage is proportional to the V_{dc} and can be changed only by changing V_{dc} . The *dc* voltage is usually taken from the *ac* mains through a simple diode rectifier. If the V_{dc} is to be variable, the rectifier has to be a controlled converter or alternatively has to be followed by a chopper to vary the *dc* voltage input to the inverter.

6.2 Three Phase Voltage Source Inverter

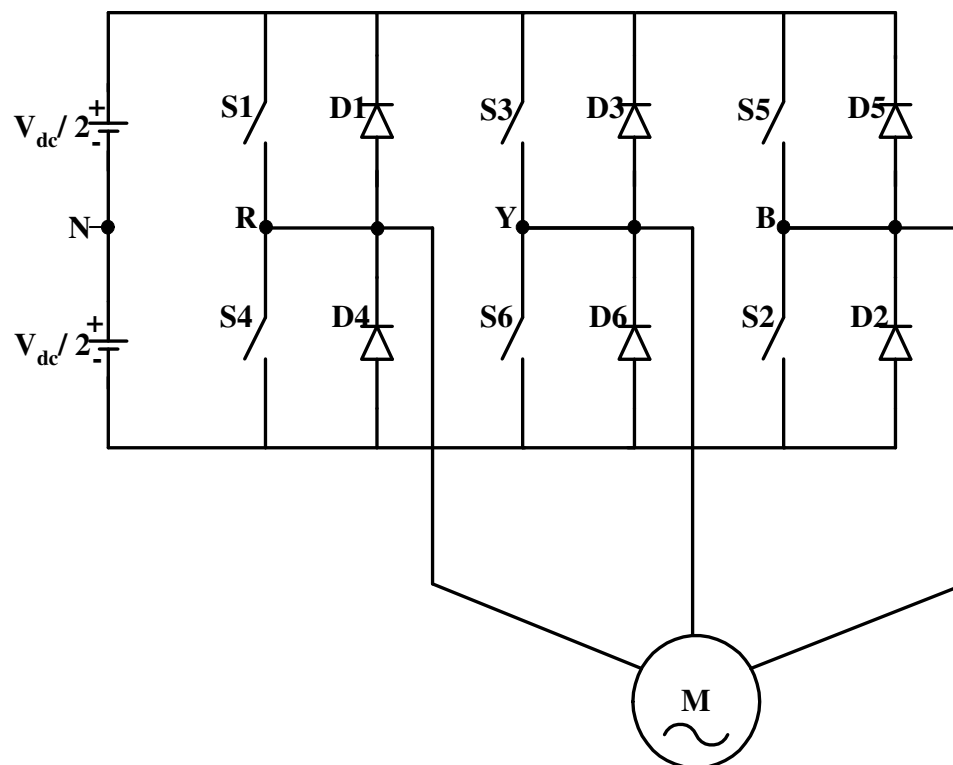


Figure 6.5: Three phase half bridge inverter

A three phase inverter can be realized by using three single phase inverters and arranging the there gating signals to be phase shifted by 120° with respect to one another. The center-tap of the dc supply does not have to be physically accessible, although it is convenient to speak of output voltages with respect to a fictitious center tap. Figure 6.5 shows the circuit diagram of a three phase half-bridge inverter. Note the numbering of the devices. The numbering is in the same order as the gating signals. The gating signals are shown in Figure 6.6. The three output voltages V_{RN} , V_{YN} and V_{BN} of the three phases are as shown in Figure 6.7. Note that these are the voltages of the phases with respect to the imaginary center-tap of the dc supply. From these voltages, the line voltages V_{RY} , V_{YB} and V_{BR} of the motor can also obtained as follows.

$$\begin{aligned}
 V_{RY} &= V_{RN} - V_{YN} ; V_{YB} = V_{YN} - V_{BN} ; \\
 V_{BR} &= V_{BN} - V_{RN}
 \end{aligned}
 \tag{6.4}$$

These voltages are also indicated in Figure 6.7.

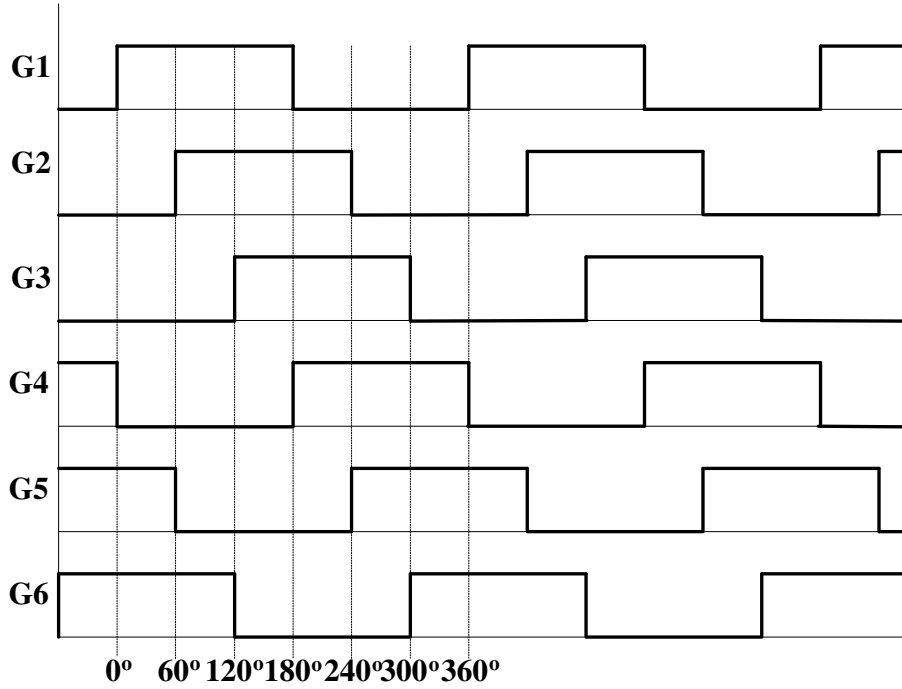


Figure 6.6: Gating signals of the three phase inverter

Since the phase to phase voltages are obtained as the difference between two square waves displaced by 120° , all the triplen harmonics are absent in these waveforms. Thus, besides the fundamental, phase to phase voltages contain only harmonics of order $6m \pm 1$, $m = 1, 2, 3, \dots$; of these, harmonics of order 7, 13,(*i.e.* $6m + 1$) have the same phase sequence as the fundamental and are spoken of as positive sequence harmonics. Harmonics of order 5, 11, ...(*i.e.* $6m - 1$) have the opposite phase sequence and are spoken of as negative sequence harmonics. But every harmonic component in the three phase to phase voltages forms a balanced three phase set. Taking advantage of this, phase to neutral voltages of a star-connected motor can be determined as follows.

$$V_{Rn} = \frac{1}{3} (V_{RY} - V_{BR}) \tag{6.5a}$$

$$V_{Yn} = \frac{1}{3} (V_{YB} - V_{RY}) \tag{6.5b}$$

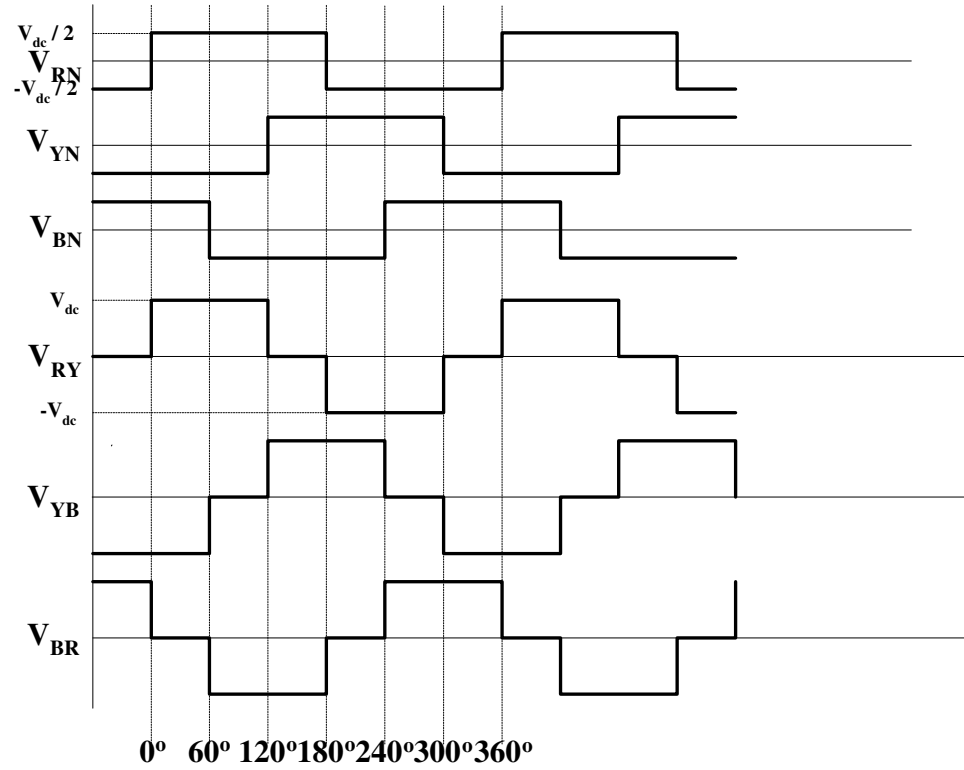


Figure 6.7: Phase to center and phase to phase voltage waveforms

$$V_{Bn} = \frac{1}{3} (V_{BR} - V_{YB}) \quad (6.5c)$$

There the letter 'n' represents the motor neutral. The waveforms of the motor phase to neutral voltages are shown in Figure 6.8.

Since these voltages have six steps in one cycle, this mode of inverter operation is referred to as six-step operation. The inverter itself is sometimes referred to as a six step inverter, although the same inverter circuit can be operated in other modes also.

The *rms* line to line voltage of the motor

$$\begin{aligned} &= \sqrt{3} \frac{1}{\sqrt{2}} \frac{4}{\pi} \frac{V_{dc}}{2} \\ &= \frac{\sqrt{6}}{\pi} V_{dc} = 0.78 V_{dc} \end{aligned} \quad (6.6)$$

The *rms* phase to neutral voltage of the motor

$$= \frac{\sqrt{2}}{\pi} V_{dc} = 0.45 V_{dc} \quad (6.7)$$

The peak phase to neutral voltage of the motor

$$= \frac{2}{\pi} V_{dc} = 0.637 V_{dc} \quad (6.8)$$

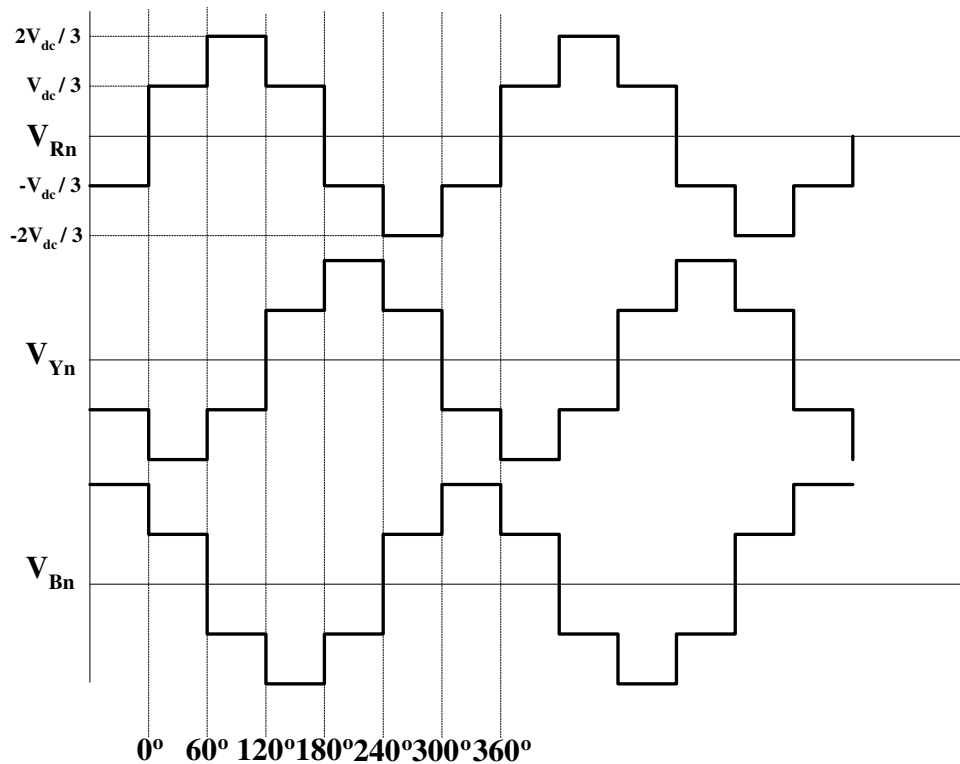


Figure 6.8: Motor phase to neutral voltages

Since the motor voltages are derived from the phase to center square wave outputs of the individual inverter phases, they contain odd harmonics of the form $6m \pm 1$ $m = 1, 2, 3, \dots$ and the amplitude of each harmonic is inversely proportional to its order.

6.3 Pulse Width Modulation

The single phase inverter phase to center output voltage can only attain two possible values viz. $\frac{V_{dc}}{2}$ and $-\frac{V_{dc}}{2}$. In the square wave mode of operation each output voltage prevails for a half period continuously. In this mode of operation, each switch is turned on and off only once per cycle. It is possible to operate the inverter with more than one switching per cycle and thereby modify the output voltage waveform. In any such attempt, the basic quarter wave and half wave symmetries of the square wave are usually preserved, so that the output voltage still contains only odd harmonics. Consider the output voltage waveform shown in Figure 6.9. The square wave has been modified by introducing one ‘notch’ per quarter cycle. The corresponding gate drive signals are also indicated in Figure 6.9.

It can be shown that the inverter output voltage can be expressed in terms of a Fourier

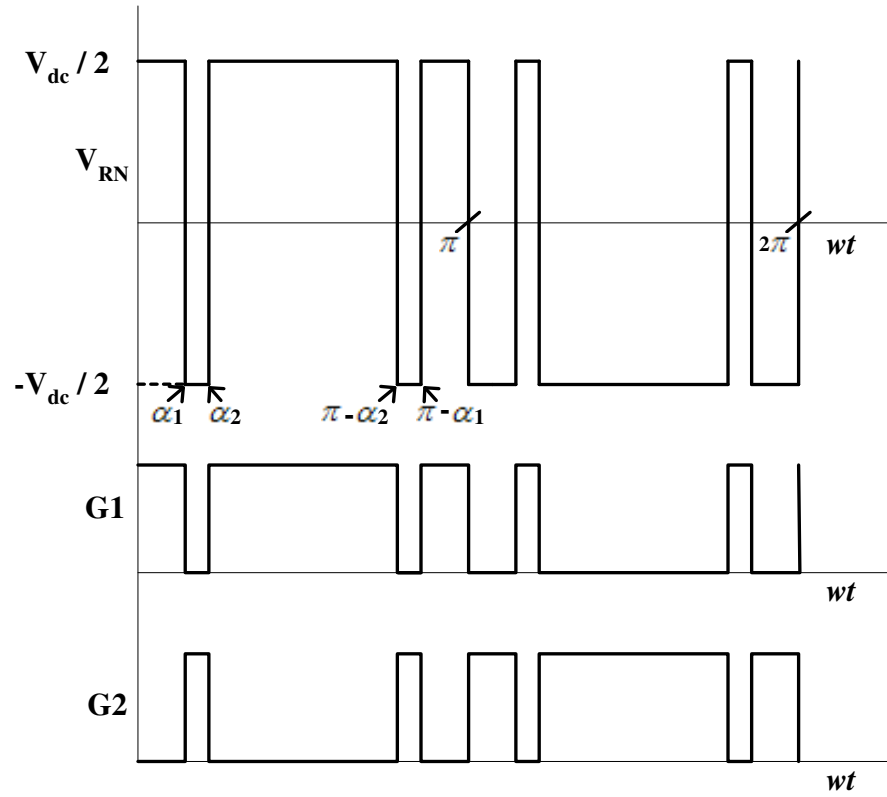


Figure 6.9: Output voltage and gating signals for pulse width operation

series as follows:

$$V_{RN}(t) = \sum_{n=1, n \text{ odd}}^{\infty} \frac{4}{n\pi} [1 - 2\cos(n\alpha_1) + 2\cos(n\alpha_2)] \frac{V_{dc}}{2} \sin(n\omega t) \quad (6.9)$$

Therefore the amplitudes of the n^{th} harmonic can be expressed as

$$V_{RN,n} = \frac{4}{n\pi} [1 - 2\cos(n\alpha_1) + 2\cos(n\alpha_2)] \frac{V_{dc}}{2} \quad (6.10)$$

The two switching angles α_1 and α_2 can be selected so as to control the amplitudes of any two harmonics. For example, they can be calculated to yield a required amplitude of fundamental and to eliminate one harmonic, which is usually the one with the lower order. But in this process, eight additional switchings have been introduced per cycle. Further, it is obvious that this method will only yield fundamental voltages of the lower amplitudes than the square wave. Therefore, for a given dc bus voltage, the maximum amplitude of the fundamental is obtained in the square wave (six step for a three phase inverter) mode. Further, with the above technique of controlling or eliminating certain frequency components, some other frequency components will increase in magnitude. The inverter is said to operate in the pulse width modulation (PWM) mode.

6.4 Reference

- 1) B.K. Bose, 'Power Electronics and AC Drives', Prentice-Hall.
- 2) K. Thorborg, 'Power Electronics'.

6.5 Questions for Tutorial

- 1) Assume that a 3-phase six step inverter is supplying a balanced 3-phase currents to a lagging load. Sketch the waveform of the dc input current to the inverter.
- 2) The line to line voltages of two 3-phase six step inverters operating at the same frequency with a phase difference of 30° are added (through a transformer with delta connected primaries and secondaries in series). Sketch the resulting output waveform. What techniques can be employed to cancel out the 5^{th} and 9^{th} harmonics in the resultant output?

Chapter 7

Pulse-Width Modulation Techniques

An induction motor driven by a six step inverter draws currents at the harmonic frequencies in addition to the fundamental current. Useful output power is produced by the fundamental only. The harmonics contribute to the additional copper losses in the machine and create torque pulsations. They also stress the inverter switches by way of large instantaneous current peaks. As has been pointed out, harmonics in the six-step voltage source wave are of order of $6m \pm 1$, the most dominant being the 5th (20%) and the 7th (14%). In addition the six step inverter requires an additional power converter to vary the *dc* bus voltage and the machine voltage.

In high power units, some amount of reduction in harmonics can be achieved even with the six step inverters by suitably phase shifting and adding the output voltages of two or more six step inverters. Because of the phase shift involved, the fundamentals add vectorially rather than arithmetically and some reduction in the output voltage has to be accepted. Further, control of the fundamental amplitude still requires a variable *dc* voltage.

With present day power switching devices, switching frequencies of between $500Hz$ to $1000Hz$ can be comfortably achieved even at high power ratings. Therefore, the trend is towards pulse width modulated (PWM) inverters for driving induction motors; achieving a favorable harmonic profile as well as control of fundamental amplitude are both accomplished within the inverter itself by suitably designed switching patterns. Various techniques are available for determining switching patterns. The basic principles underlying a few of these are discussed in the following.

7.1 Basic Motivation for PWM

The basic attempt in all PWM methods is to produce the required amplitude and frequency of the fundamental, while moving the energy in the harmonics to a higher range in the frequency spectrum. The expectation is that at such higher frequencies, even the machine leakage inductance will exhibit appreciable reactance, thereby limiting the harmonic currents

drawn from the inverter. Also, since the torque pulsations created by these high-frequency harmonics are also at high frequencies, the motor should be able to run smoothly. The constraint on the PWM process is the fact that the additional switchings per cycle are required in order to accomplish the modulation. This increases the losses in the inverter. Moreover, as the switching pattern becomes more complicated, an individual inverter phase may be required to produce pulses or notches of very small width. The switching times of the devices used in the inverter impose a limitation here.

There are basically two types of PWM implementations. In one, the switching instants are decided in real time (by either analog or digital means) by comparing a high frequency ‘carrier’ wave with a low frequency ‘reference’ or ‘modulating’ wave. The second class of PWM methods makes use of precalculated switching patterns corresponding to each possible frequency and voltage command for the fundamental. The switching pattern is calculated so as to eliminate a certain number of low order harmonics or to optimize some performance index such as the *rms* current or the *peak* current drawn from the inverter. Amongst carrier based PWM techniques the so called *sine triangle* or *the subharmonic* modulation technique is the oldest and best known. Amongst stored waveform techniques, the method of selective harmonic elimination is widely used.

7.2 Selective Harmonic Elimination

In this method the basic square wave produced by each inverter phase (phase to *dc* center tap voltage) is modified by the introduction of the additional switching angles $\alpha_1, \alpha_2, \dots, \alpha_p$ in each quarter cycle. At each of these switching angles, there is a reversal of the phase to center voltage and so these angles are also referred to as angles of reversal.

The angles are introduced in such a manner that the resulting waveform possesses quarter-wave symmetry, i.e. contains no even harmonics and is antisymmetric about the 180° point. It can be expanded in a Fourier series containing only sine terms by suitably choosing the time origin. Note that in addition to the switchings at the angles of reversal, there are two switchings at the 0° point and at the 180° point as in the square wave. In Figure 7.1 shows some examples of the resulting phase to center voltage waveforms.

Depending on whether the number of angles of reversals are even or odd, the transition at 0° is either positive going or negative going respectively. The harmonic component of any such waveform can be determined by Fourier analysis. Recognizing that due to the symmetry of the waveform, it is necessary to perform integration over the interval 0 to $\frac{\pi}{2}$, the *rms* value of the n^{th} harmonic component in a waveform containing reversals at $\alpha_1, \alpha_2, \dots, \alpha_p$ can be

written as

$$v_n = \frac{1}{\sqrt{2}} \frac{4}{\pi} \frac{V_{dc}}{2} \left| \left[\int_0^{\alpha_1} \sin(n\theta) d\theta - \int_{\alpha_1}^{\alpha_2} \sin(n\theta) d\theta \dots - \int_{\alpha_p}^{\frac{\pi}{2}} \sin(n\theta) d\theta \right] \right|, \quad n \text{ odd} \quad (7.1)$$

In writing the above, advantage has also been taken of the fact that the series will only contain sine terms. Whether a particular interval α_k to α_{k+1} contributes a positive or negative integral is decided by whether the voltage is $\frac{+V_{dc}}{2}$ or $\frac{-V_{dc}}{2}$ during the interval. The above equation 7.1 can be evaluated as

$$v_n = \frac{0.45}{n} V_{dc} \left[[1 - 2\cos(n\alpha_1) + 2\cos(n\alpha_2) - 2\cos(n\alpha_3)\dots] \right] \quad (7.2)$$

From equation 7.2, it can be observed that each angle of the reversal constitutes a degree of freedom in controlling the amplitudes of the various frequency components. In general, in 3 phase inverters, any triplen harmonic components present in phase to center waveforms get eliminated in the phase to phase waveforms. Therefore control or elimination of triplen harmonic through switching is not attempted. Harmonics of order $6k \pm 1$, $k = 1, 2, \dots$ as well as the fundamental are only controlled.

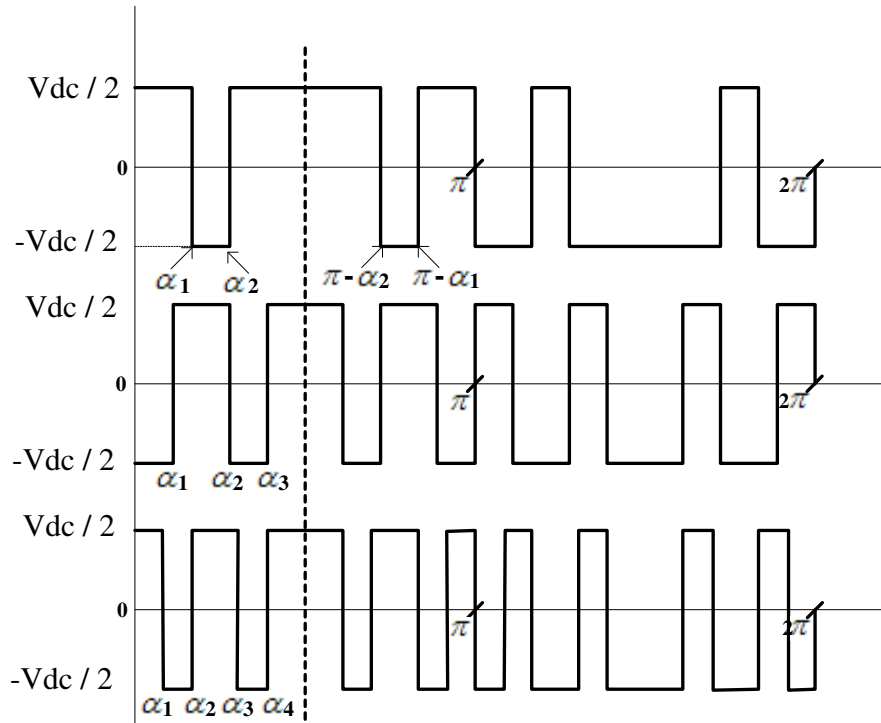


Figure 7.1: Inverter phase-center waveforms for selective harmonic elimination

As an example, consider a waveform with three angles of reversal α_1 , α_2 , and α_3 . If the criterion for determining the angles is that the fundamental should have a required amplitude

and that the 5th and 7th harmonic should be eliminated, the equations for calculating the angles are:

$$\begin{aligned} 2\cos(\alpha_1) - 2\cos(\alpha_2) + 2\cos(\alpha_3) - 1 &= \frac{u_{1rms}}{0.45V_{dc}} = a \\ 2\cos(5\alpha_1) - 2\cos(5\alpha_2) + 2\cos(5\alpha_3) - 1 &= 0 \\ 2\cos(7\alpha_1) - 2\cos(7\alpha_2) + 2\cos(7\alpha_3) - 1 &= 0 \end{aligned} \quad (7.3)$$

These are nonlinear equations and have to be solved by numerically methods. Note that the angles have to be recalculated for every value of ‘a’, i.e. every value of fundamental required. Once the solution is obtained, the ratio of any of the other harmonics such as 11th, 13th, 17th, 19th, etc. to the fundamental can be expressed as

$$\frac{V_{nrms}}{V_{1rms}} = \frac{\frac{V_{nrms}}{0.45V_{dc}}}{\frac{V_{1rms}}{0.45V_{dc}}} = \left| \frac{1}{a} \frac{1}{n} [2\cos(n\alpha_1) - 2\cos(n\alpha_2) + 2\cos(n\alpha_3) - 1] \right| \quad (7.4)$$

Figure 7.2 shows the variation of α_1 , α_2 and α_3 as a function of the voltage control ratio ‘a’. Figure 7.3 shows the magnitudes of the 11th and 13th harmonics of the voltage with this technique, expressed as a percentage of the fundamental, as the voltage control ratio is varied. It can be observed that while the 5th and 7th harmonics are eliminated, the amplitudes of the 11th and 13th harmonics increases over their values for the six step voltage. Thus, although the lower order harmonics may be eliminated, the amplitudes of some of the higher order harmonics increase. This is characteristic of all PWM methods.

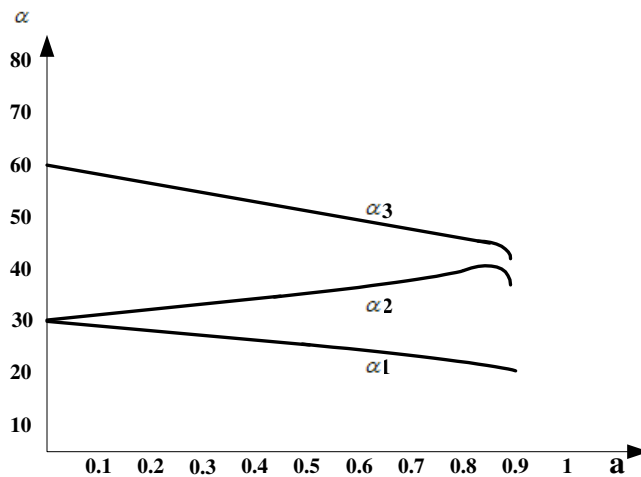


Figure 7.2: Variation of α_1 , α_2 and α_3 as a function of the voltage control ratio ‘a’

A PWM circuit can be developed for a variable frequency AC motor drive by employing the above technique. The total voltage range has to be quantized into a discrete number of

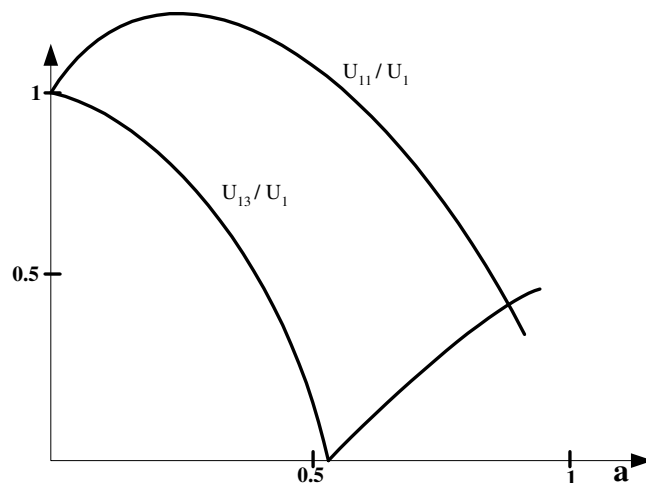


Figure 7.3: Magnitudes of the 11th and 13th harmonics of the voltage

voltage levels, the number of levels deciding the resolution. Corresponding to each voltage level, the reversal angles $\alpha_1, \alpha_2, \dots$ have to be calculated and the resulting waveform stored in memory. Thus each voltage level for the fundamental requires one segment of memory. The length of the each segment is decided by the accuracy with which it is desired to reproduce the switching angles. The usual technique is to store the gating signals for the six inverter switches and step through the cycle using a high frequency clock. The frequency of this clock is a multiple of the fundamental frequency required. The higher the clock frequency, the more the size of the each memory segment and the better the resolution in reproducing the angles of reversal. Savings in memory size can also be effected by making use of the fact that the waveforms possess symmetry. It is sufficient to store only 90° of the waveform; the gating signals appropriate to the rest of the cycle can be obtained by suitable logic.

When deciding the voltage waveform for a particular value of fundamental, cognizance has to be taken of the fact that at higher voltages, the fundamental frequency will also be greater, in order to maintain the $\frac{v}{f}$ ratio in the motor. Therefore, the number of reversals has to be gradually reduced, as the fundamental approaches the value for the six step wave. Otherwise, number of switchings per second i.e. the switching frequency may become too high for the switches. The strategy generally followed is that at low speeds corresponding to low fundamental frequency and amplitudes, a large number of reversals are incorporated in the waveform, so that a large number of low order harmonics get eliminated. Number of reversals is reduced in steps as the fundamental frequency (and hence amplitude) is increased. Ultimately, the waveform approaches the square wave mode.

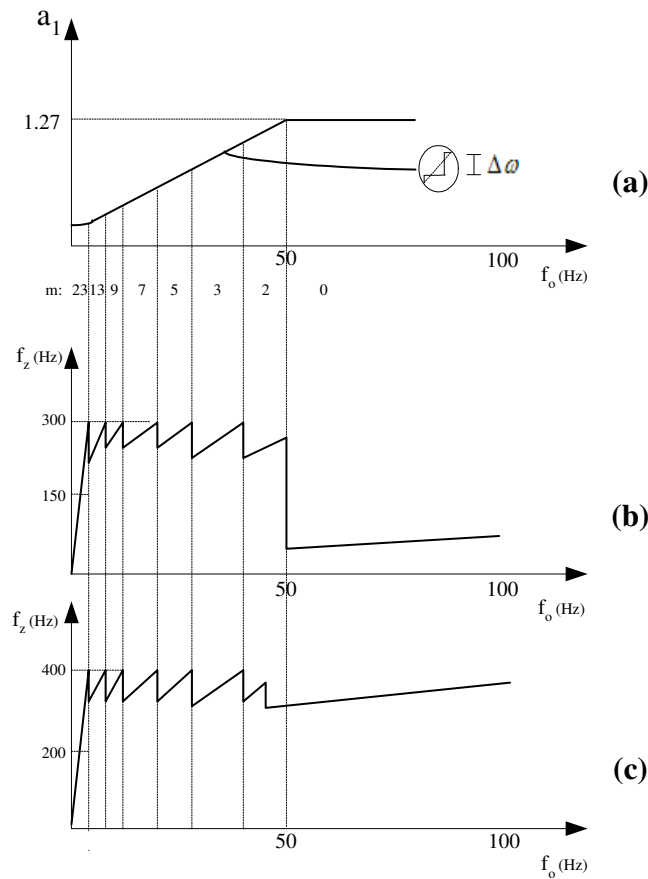


Figure 7.4: **a.** $\frac{v}{f}$ characteristics for constant flux operation **b.** Inverter switching frequency **c.** Frequency of lower order nonzero harmonic f_z

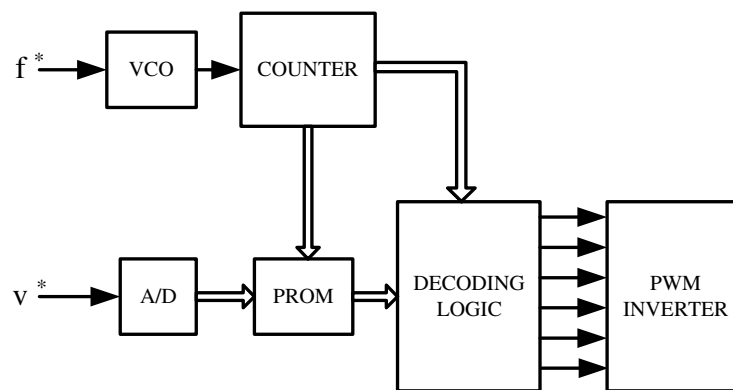


Figure 7.5: Block diagram of modulator for analog frequency and voltage command

Moreover, as the voltage control ratio ‘a’(equation 7.3) exceeds about 0.82, no solution exists for the equation 7.3. In this region, therefore, criterion of elimination of harmonics has to be replaced by some other criterion, perhaps the minimization of harmonic distortion.

The variation of the fundamental voltage, the inverter switching frequency and the frequency of the lowest order harmonic with non-zero amplitude for a modulator based on the above principles are described by Pollmann [2] and are shown in Figure 7.4.

The simplified block diagram of of the modulator incorporating the stored waveform technique is shown in Figure 7.5.

The harmonic elimination technique is only one method of stored waveform PWM. Other criteria can also be employed in optimizing the gating pattern. For example, the motor current can be calculated taking into account a large number of harmonics; the voltage waveform can then be optimized to give minimum *rms* current, minimum *peak* current, minimum losses in the system, etc. Such techniques, however, require extensive computational effort and resulting voltage waveform is machine dependent.

7.3 Sub-Harmonic Sine-Triangle PWM

This method was first discussed extensively by Schonung and Stemmler and is the oldest of the ‘carrier’ based PWM techniques. The basis of the method can be explained as follows.

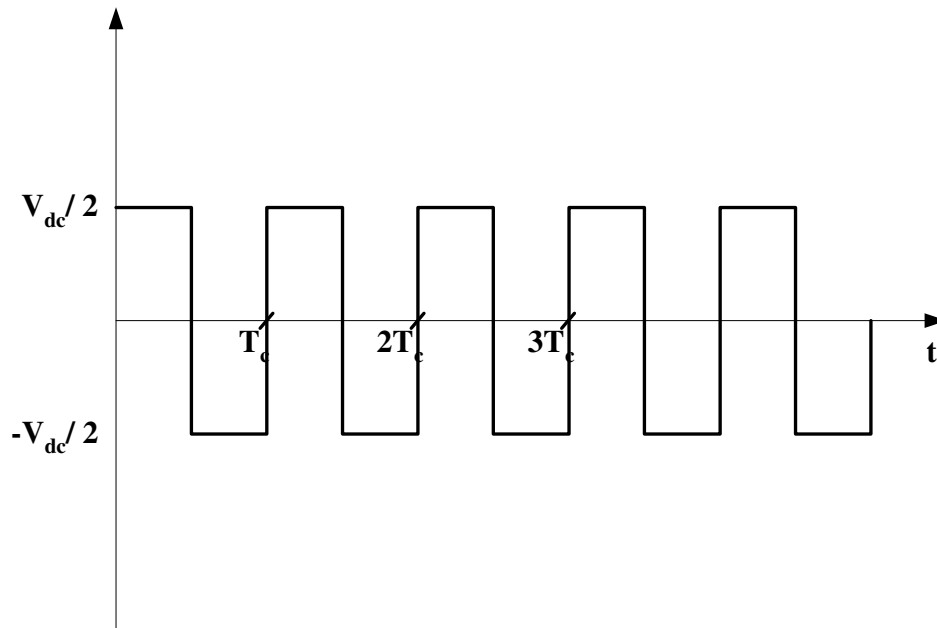


Figure 7.6: Symmetrical square wave

Consider the symmetrical square wave of voltage, with a period T_c , as shown in Figure 7.6. Such a voltage can be produced by one phase of a voltage source inverter switching at a frequency of $f_c = \frac{1}{T_c}$. The positive and negative volt-seconds balance in each cycle and the average value is zero. If the duty cycle of the each cycle is increased above 50%, i.e., the positive volt-seconds are more than the negative volt-seconds, the average value will be positive. Similarly, if the duty cycle reduced below 50%, average voltage will be negative. If the duty cycle is varied with time in a sinusoidal manner about the 50% level, average value of the voltage in each cycle will also vary in a sinusoidal manner with respect to time. The frequency at which the duty cycle is varied or ‘modulated’ is referred to as the modulating frequency f_m . The modulated waveform contain besides the component at the modulating frequency, other components in the neighborhood of the pulse frequency f_c . If the f_m is small compared to f_c , unwanted components will be far removed from the wanted frequency f_m . Such a waveform can therefore can be used to feed an induction motor. The modulating frequency f_m is the fundamental and the other components are the unwanted harmonics. Since these harmonics are at frequencies well away from the fundamental, the currents at these harmonics should be small.

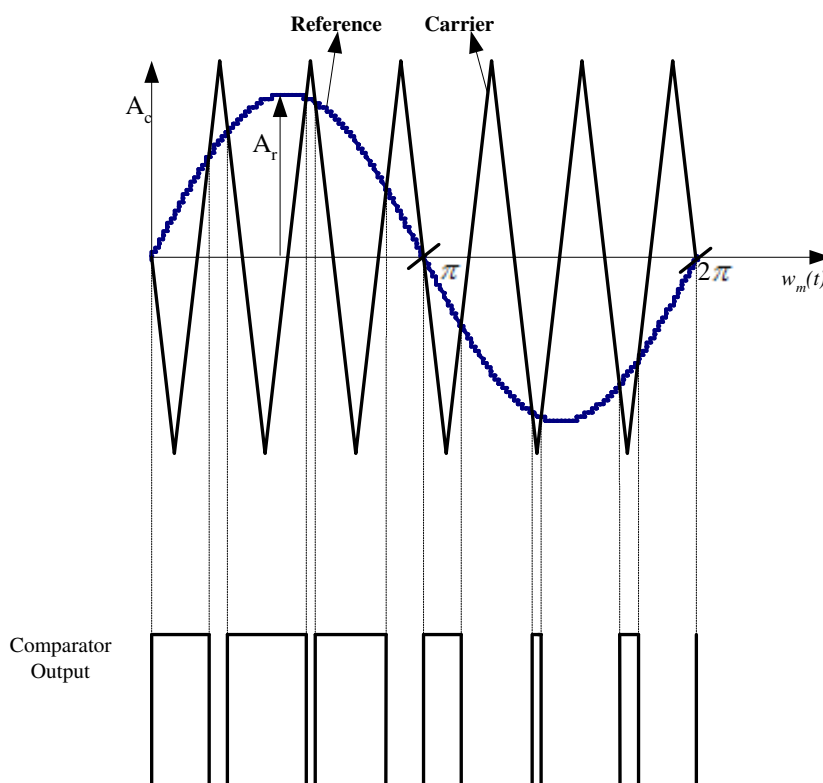


Figure 7.7: Carrier, reference and comparator outputs

The gating pulses for the inverter switches are generated by the following technique. A constant amplitude triangular waveform at frequency f_c is generated. This is referred to as the carrier waveform. This carrier waveform is then compared with a sinusoidal waveform at the modulating frequency f_m . The amplitude of the sinusoidal waveform is less than that of the triangle. The sine-wave is known as the reference waveform. The carrier, the reference and the output of the comparator are shown in Figure 7.7.

The comparator gives a 1 output whenever the reference wave is greater than the carrier wave and 0 output whenever the carrier is greater than the reference. The 1's are used as gating pulses for the top switch and 0's for the bottom switch. In this manner the phase to center-tap output voltage of the inverter will be the desired modulated square-wave.

The carrier has an amplitude A_c and the reference wave an amplitude A_r . The ratio of the reference to carrier amplitudes is defined to be the modulation index m .

$$\text{i.e. } m = \frac{A_r}{A_c} \quad (7.5)$$

By varying A_r while keeping A_C constant, i.e. by varying the modulation index, the amplitude of the fundamental component in the output voltage can be varied. Similarly by varying the frequency of the sine waves, the fundamental frequency in the output can be varied.

There are several significant features to be noted in Figure 7.7. First of all, one period of the reference waveform is shown to contain an integral number of cycles of the triangles (9 in Figure 7.7). By this means, synchronization between carrier and reference is achieved, i.e. every cycle of the inverter output waveform will be the same. This feature is essential if the number of triangles per cycle of the reference, i.e., the frequency ratio $\frac{f_c}{f_r}$, is less than about 21. Otherwise, adjacent cycles of the inverter output voltage waveform will differ from one another and their differences will repeat periodically at a frequency lower than that of the reference, i.e. sub-harmonic or beat frequency components will begin to appear in the inverter output.

Moreover, in three-phase inverters, gating patterns have to be generated for three inverter phases. This is accomplished by employing a common carrier waveform and three sinusoidal waveforms having identical amplitude and frequency, with mutual phase displacement of 120° . In this case, in order to ensure that the output voltage waveforms produced by each inverter phase is the same, it has to be ensured that there are integral number of triangles in 120° of the reference waveforms. Therefore the carrier waveform f_c has to be made a multiple of three times the reference frequency f_r . It has been shown that the unwanted harmonic frequency components in the inverter output voltage waveform occur at frequencies $Nf_c \pm Mf_r$, where M and N are integers and $N + M$ is odd. Therefore, there occur bands

of harmonics around each multiple of the carrier frequency f_c as follows:

$$\begin{aligned} f_c, f_c \pm 2f_r, f_c \pm 4f_r \dots & \text{first band} \\ 2f_c, 2f_c \pm f_r, 2f_c \pm 3f_r \dots & \text{second band} \\ 3f_c, 3f_c \pm 2f_r, 3f_c \pm 4f_r \dots & \text{third band} \end{aligned}$$

The amplitudes are largest for the first band and decrease progressively as further bands

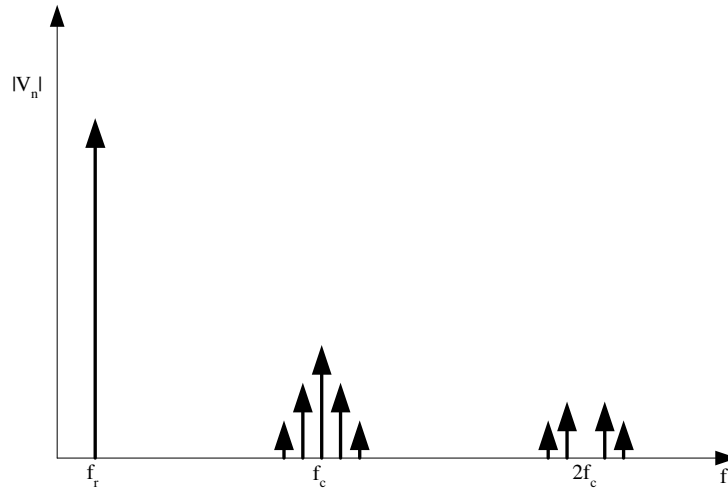


Figure 7.8: Output voltage spectrum with sine triangle modulation

are considered. A typical spectrum of the inverter output voltage is shown in Figure 7.8.

The component at f_c is a triplen harmonic and gets cancelled in the inverter line voltages. Moreover, by selecting f_c to be an odd multiple of f_r , it can be ensured that no even harmonics appear in the output. The necessity for keeping the carrier and the reference synchronized implies that as the reference frequency is changed, in a variable frequency drive, f_c also has to change correspondingly to keep the ratio $\frac{f_c}{f_r}$ constant. Also, as the amplitude of the *sine* wave reference is increased, some of the pulses and notches in the inverter gating pulses becomes very narrow and may be difficult to reproduce accurately in the inverter. The situation where the *sine* and the *triangle* amplitudes are equal i.e. modulation index $m = 1$, represents the maximum value of the fundamental voltage in the output. It is easy to see that the amplitude of the fundamental component of the inverter output voltage in this case is given by

$$V_{1peak} = \frac{V_{dc}}{2} \tag{7.6}$$

Therefore,

$$V_{1rms,m=1} = \frac{1}{\sqrt{2}} \frac{V_{dc}}{2} = 0.35V_{dc} \quad (7.7)$$

This can be compared to the maximum value of $0.45V_{dc}$ for square wave operation

Therefore,

$$\frac{V_{1rms,m=1}}{0.45V_{dc}} = 0.78 \quad (7.8)$$

Therefore the maximum *rms* value of the fundamental component that can be obtained with *sine triangle* modulation is only 78% of the value corresponding to the *square wave* operation. If the amplitude of the *sine* is increased further, the *sine* will not intersect the triangle during some of the carrier cycles, i.e. some of the pulses starts disappearing. This type of operation is referred to as *overmodulation*. In overmodulation, low frequency components such as the 5th, the 7th, etc. begin to appear in the inverter output voltage.

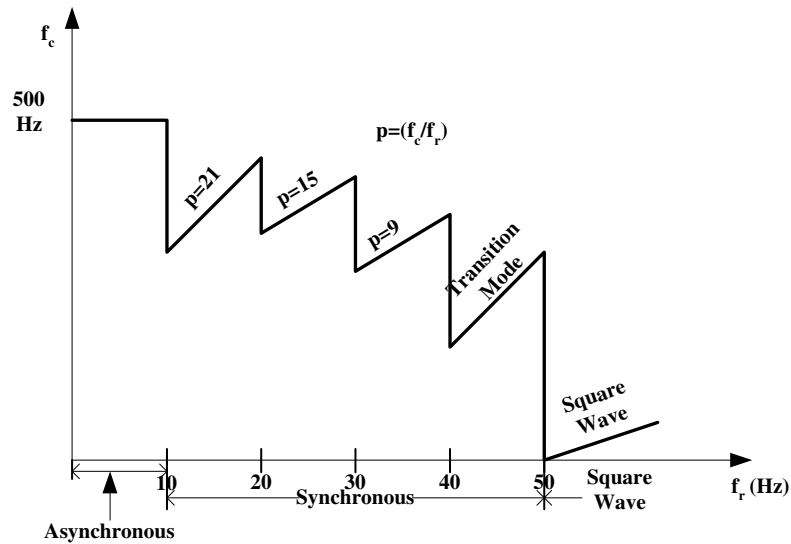


Figure 7.9: Profile of switching frequency with respect to reference frequency

While designing a modulator for a variable frequency AC drive based on the *sine triangle* modulation, the characteristic features mentioned above have to be kept in mind. Generally, maintaining a constant frequency ratio $\frac{f_c}{f_r}$ is not feasible, especially in high power drives where the switching times of the devices are large. As the fundamental frequency f_r is increased, the switching frequency may become unmanageably large. The ratio $\frac{f_c}{f_r}$ has to be made variable and should be progressively reduced as the fundamental frequency is increased. At the same time, the ratio should be kept a multiple of three and synchronization between

reference and carrier waveforms should be maintained. Figure 7.9 shows a typical profile of carrier frequency as a function of reference frequency.

At low reference frequencies below 10Hz, asynchronous PWM is used i.e. the carrier frequency is kept constant and the carrier and the reference waveforms are not synchronized. As the carrier to reference frequency ratio is high (more than 50) over this range, adverse effects due to beat frequencies are negligible. Beyond 10Hz, synchronous PWM is used, i.e. the carrier frequency is made a multiple of the reference frequency and *sine* and *triangles* are synchronized. To begin with the frequency ratio of $P = 21$ is used until $f_r = 20Hz$. The maximum switching frequency over this range is therefore 420Hz. Similarly frequency ratios of 15 and 9 are used over the ranges 20-30Hz and 30-40Hz. As the frequency f_r increases, the modulation index also has to be increased correspondingly to keep the $\frac{v}{f}$ ratio constant. It has already been pointed out that the maximum *rms* value of the line to line voltage that can be attained is only $0.78V_{dc}$ for operation in the sine-triangle mode. Therefore at a frequency of about 40Hz the amplitude of the sine wave reference and the triangular carrier becomes equal.

As the reference amplitude approaches the carrier amplitude, some of the transitions in the inverter voltage waveform occur very close to each other; resulting pulse or notch widths demanded by the control circuit may be too small to be reproduced by the power circuit. Therefore some kind of logic to limit the minimum width of the pulses and the notches becomes necessary. Two approaches are possible. Pulses below the minimum width can be extended to the minimum width or can be dropped altogether.

As the reference frequency is increased from 40 to 50Hz therefore, the pulse pattern should gradually get transformed from the sine-triangle to square wave mode. The inverter works in a transition mode of PWM over this frequency range. This mode can be obtained in several ways: (a) by using a modified carrier waveform [4], (b) by using so called level interactions method [5], (c) by resorting to stored waveform over this frequency range. The optimization of the pulse pattern over this frequency range may be done by either taking the *rms* current or the peak current as the performance criterion and requires some computation.

7.4 Current Regulated PWM

In AC drives applications it is necessary to control the stator current of the motor rather than the stator voltage. If the inverter uses any of the PWM methods described above, it acts as the voltage source only and current control has to be achieved by closing a current loop around the inverter. An alternative technique is the so-called *current regulated* PWM technique. This method, is suitable for inductive loads such as motors. In this method, instantaneous stator current is compared with the reference current waveform, usually sinusoidal. Suppose

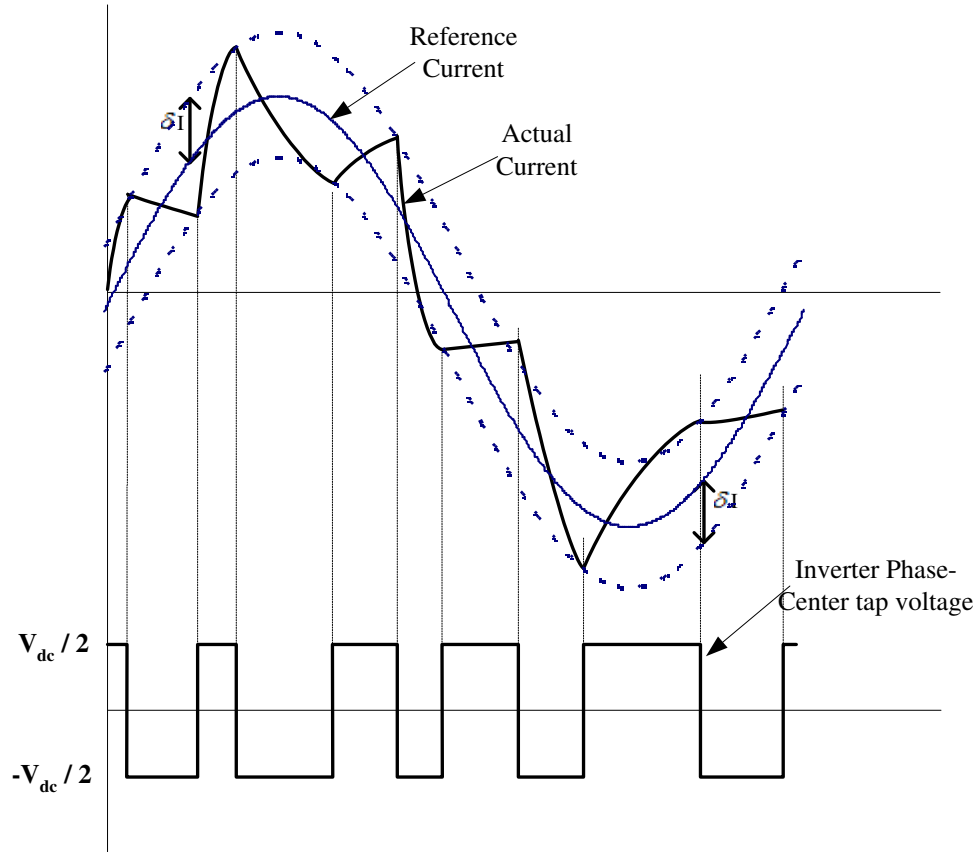


Figure 7.10: Current and voltage waveforms for current regulated PWM

that the top switch of the inverter phase is gated on, the phase to center tap voltage of that phase will then be $+\frac{V_{dc}}{2}$; this voltage will force the machine current to rise. When the current exceeds the reference by a margin δI , gating pulse of the top switch is turned off and the bottom switch is gated on. The current now begins to fall. When the current falls below the reference by δI , the bottom switch is turned off and the top switch is again turned on. Typical load current and inverter phase to center tap voltage are shown in Figure 7.10.

The switching instants of the inverter are therefore decided by the current margin δI and the load impedance. The switching frequency of the inverter is therefore not constant in this technique and this may not be acceptable in some of the applications. Also a current sensor with the good bandwidth is required to accurately reproduce the load current waveform.

In drive applications, the load on the inverter consists of a *back emf* corresponding to the airgap voltage of the rotor, in series with the stator resistance and inductance. As the

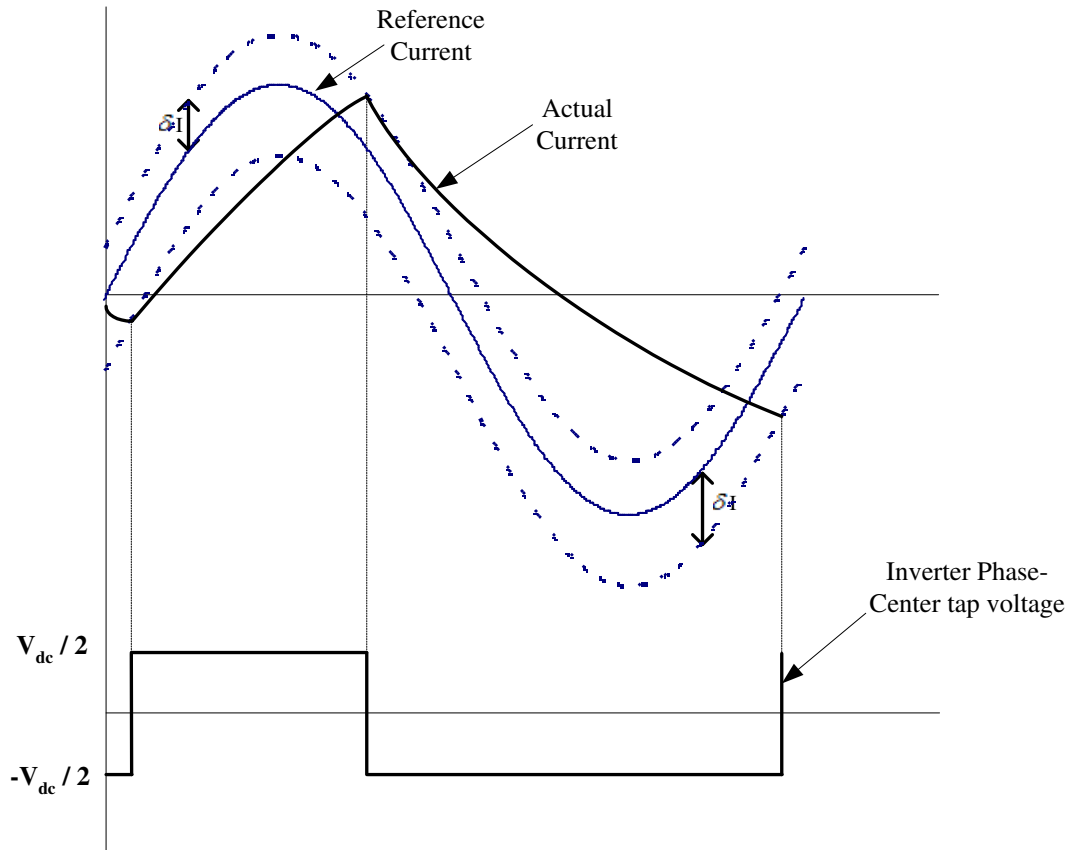


Figure 7.11: Current and voltage waveforms for current regulated PWM at high motor speeds

speed of the motor increases, the *back emf* also increases, once the flux is almost constant. Therefore at high speeds, *back emf* may approach the bus voltage and the inverter may not be able to force the current into the stator. As a result, the stator current will not follow the reference accurately. Figure 7.11 shows the possible current and voltage waveforms corresponding to this situation. The inverter is now operating in the square wave mode and the actual current no longer reproduces the reference.

7.5 Discussion

Several variations on the PWM techniques discussed above are possible. As has been already pointed out, stored waveform PWM modulators can use some inertia other than harmonic elimination for optimizing the pulse patterns. Amongst the carrier based PWM modulators also, several variations are possible. For example, instead of a sinusoidal reference waveform,

a trapezoidal reference can be used. Although this introduces some amount of the low frequency harmonics such as the 5th and the 7th in the output voltage, the technique is amenable to implementation through software and is suitable for μp based modulators. Yet another variation is the so called ‘regular sampled’ or ‘True’ sinusoidal PWM. In this method, the fundamental period of the output voltage is divided into equal intervals (the number of intervals = the number of pulses per cycle). The pulsewidth in each interval is made proportional to the amplitude of the reference sine wave at the midpoint of the interval. This method is also suitable for fully digital implementation. Whatever be the PWM technique used the basic considerations are the minimization of the torque pulsations, the reduction of *rms* current drawn from inverter, and the minimization of the peak current drawn from the inverter without appreciably increasing the losses either in the inverter or in the machine.

7.6 References

1. Thorborg, K, ‘Power Electronics’, Prentice-Hall, 1988.
2. Pollmann, A, ‘A Digital Pulsewidth Modulator Employing Advanced Modulation Techniques,’ IEEE Trans. Industry Applications, Vol. IA-19, May-June 1983, pp 409-413.
3. Schonung, A and Stemmler, H, ‘Static Frequency Changer with Subharmonic Control in Conjunction with Reversible Variable Speed AC drives, ’ The Brown Boveri Review, August-September 1964, pp. 555-577.
4. Green, R.M and Boys, J. T, ‘PWM Sequence Selection and Optimization: A Novel Approach’ IEEE Trans. Industry Applications, Vol. IA-18, No. 2, March-April 1982, pp 146-151.
5. Kliman, G.B and Plunkett, A.B, ‘Development of a modulation Strategy for a PWM Inverter Drive, ’ IEEE Trans. Industry Applications, Vol. IA-15, No. 1 Jan-Feb 1979 pp 72-79.
6. Bose, B.K, ‘Power Electronics and AC Drives,’ Prentice-Hall, 1986.

Chapter 8

Simple Drive Schemes for Inverter Fed Induction Motors

It has been shown that the torque developed in an induction motor is proportional to the square of the flux and is also proportional to the rotor (or slip) frequency w_r . Therefore, in order to obtain the full torque capability of the motor at any speed, the flux must be maintained at the rated value. If speed control is attempted by varying the stator voltage, keeping the frequency constant, flux and consequently torque capability of machine get drastically reduced. The torque speed characteristics under this method of control are shown in Figure 8.1.

Since the stator frequency is constant, the synchronous speed remains the same in all cases. As the voltage is reduced, the peak torque ability of the motor gets reduced. Although speed is controlled, the motor operates at high values of slip and high currents. This type of control is thus not very efficient and is only used sometimes with the fan type load, whose torque demand comes down with speed. In order to preserve the torque capability of the motor at all speeds over the control range, the preferred method is variable frequency control.

8.1 Variable Frequency Control

Consider the equivalent circuit of the induction motor, reproduced in Figure 8.2. The rotor current I_r is given by

$$I_r = -\frac{V_m}{\frac{R_r}{s} + jw_s L_{lr}} \quad (8.1)$$

The airgap power

$$P_{ag} = 3|I_r|^2 \frac{R_r}{s} \quad (8.2)$$

$$\begin{aligned} &= 3 \frac{V_m^2}{\left(\frac{R_r}{s}\right)^2 + (w_s L_{lr})^2} \frac{R_r}{s} \\ &= 3 \frac{V_m^2 s}{R_r^2 + (w_r L_{lr})^2} R_r \end{aligned} \quad (8.3)$$

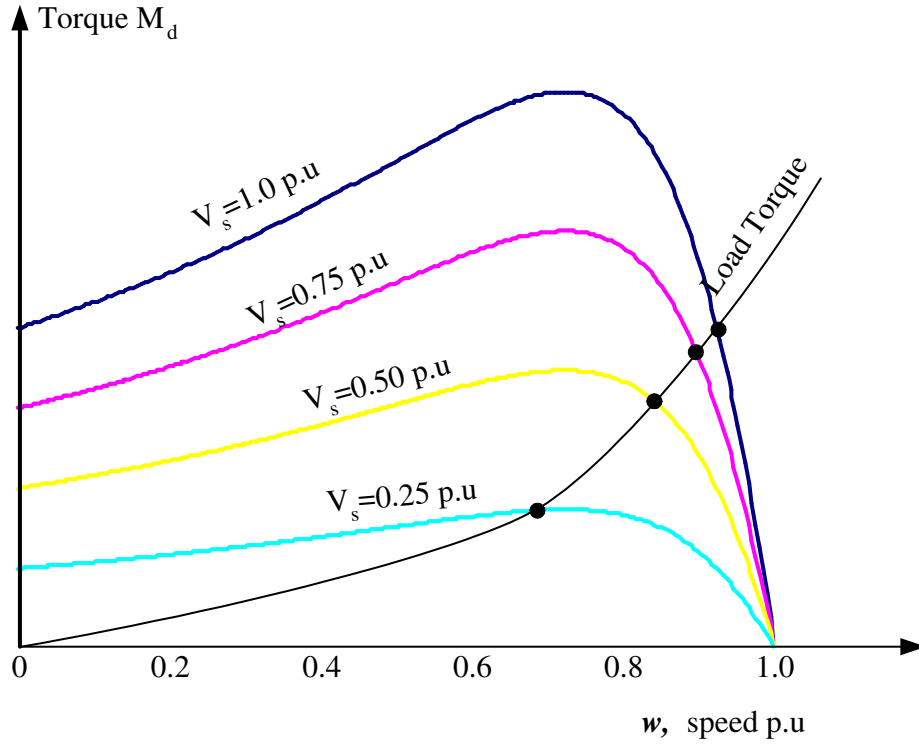


Figure 8.1: Torque-speed characteristics with stator voltage control.

The output torque

$$\begin{aligned}
 M_d &= \frac{P_{ag}}{\text{synchronous speed in Mech rad/sec}} \\
 &= 3 \frac{P}{2} \frac{1}{w_s} \frac{V_m^2 s}{R_r^2 + (w_r L_{lr})^2} R_r \\
 &= 3 \frac{P}{2} \left(\frac{V_m}{w_s} \right)^2 \frac{w_r}{R_r^2 + (w_r L_{lr})^2} R_r \quad (8.4)
 \end{aligned}$$

The above equation implies that the developed torque of the machine will depend only on w_r , irrespective of the stator frequency w_s , provided the ratio $\frac{V_m}{w_s}$ is kept constant. This ratio is nothing but the amplitude of the airgap flux. Thus by keeping the airgap flux constant, and varying the stator frequency w_s , a family of torque speed curves can be obtained for the motor as shown in Figure 8.3. This method of speed control is referred to as constant flux control. Note that constant flux control is only possible up to rated voltage and frequency. For further increase in the frequency beyond rated frequency, if the voltage be increased proportionally this would exceed the rating of the machine. Therefore, beyond the rated

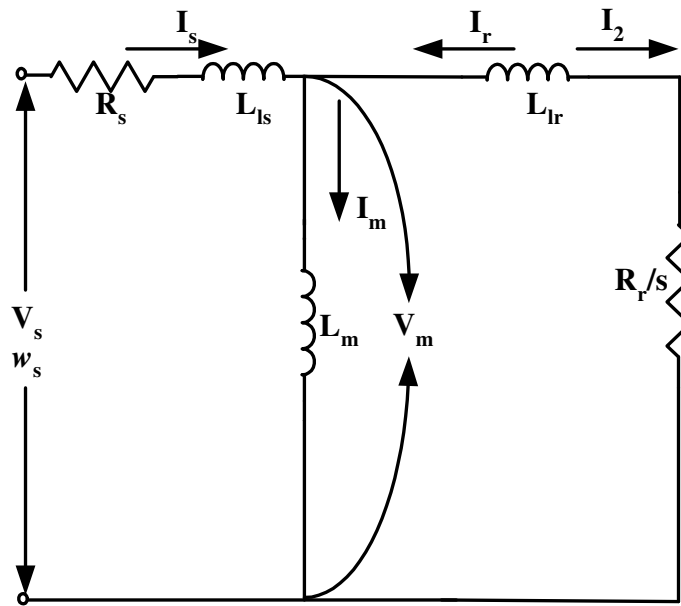


Figure 8.2: Equivalent circuit of induction motor.

frequency, the peak torque ability of the motor decreases as the ratio $\frac{V_m}{w_s}$ is less than the rated value. This region of operation is referred to as the field weakening region.

It can be seen that any load torque demand within the capability of the machine can be met at all speeds up to the rated speed. Further, it is possible to obtain high torques for starting the motor by operating at reduced frequency.

However, the above method is difficult to implement as the airgap voltage V_m cannot be measured directly. It can be calculated by measuring the motor terminal voltages and currents, but this results in considerable complexity of the control circuits. Alternately the airgap flux can be measured directly by incorporating flux sensing coils or hall sensors in the motor and integrating their output voltages. This requires modification of the motor. However, it is difficult to carry out integration at low frequencies. Therefore, in practice, the above technique is implemented in an approximate manner, by keeping the ratio of the terminal voltage V_s to w_s constant.

The terminal voltage and the airgap voltage are reasonably close in magnitude at speeds above 10% of rated speed. At very low speeds (and hence stator frequencies) the drop in the stator resistance and leakage reactance becomes appreciable in magnitude compared to the airgap voltage. Therefore, at low speeds, keeping $\frac{V_s}{w_s}$ constant is not equivalent to keeping the flux constant. The torque capability of the machine therefore comes down. The family of torque speed curves for constant $\frac{V_s}{w_s}$ control (or constant $\frac{V}{f}$ control as it is referred to)

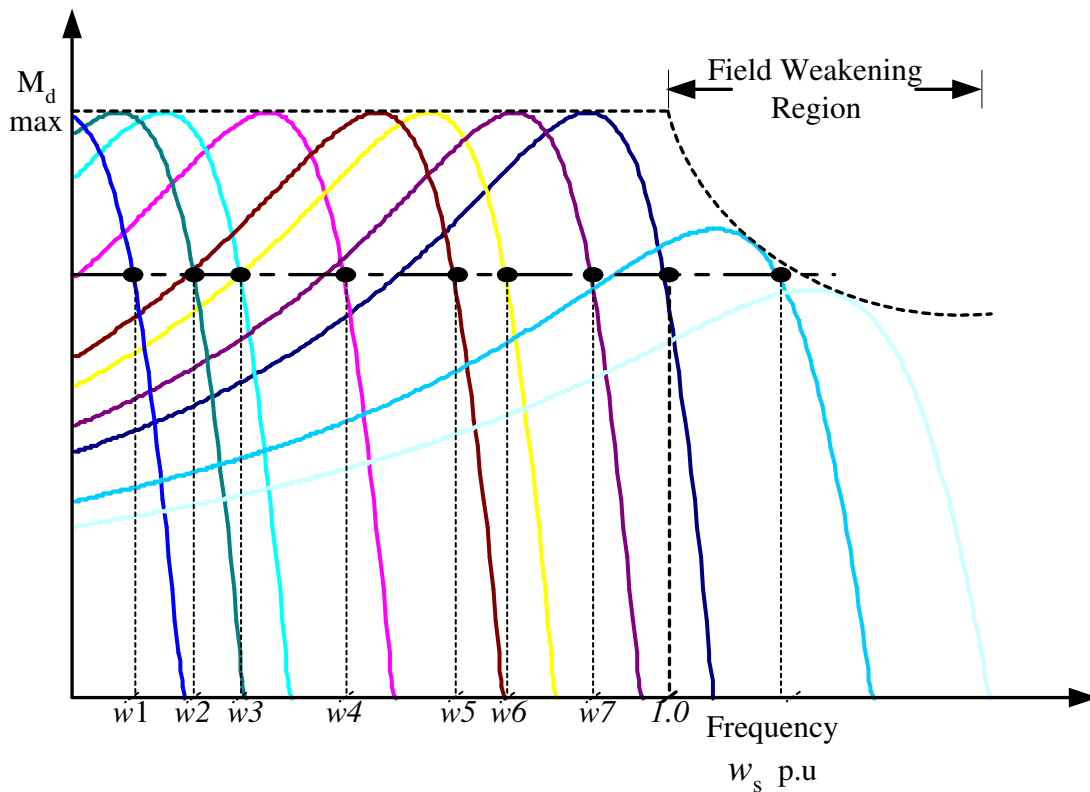


Figure 8.3: Torque-speed characteristics with constant flux control.

is shown in Figure 8.4. To some extent the drop in torque ability at low speeds can be counterbalanced by giving a boost to the stator voltage V_s at low frequencies above the constant $\frac{V}{f}$ value. Figure 8.5 shows two possible $\frac{V}{f}$ relationships that can be employed.

In a variety of industrial drive applications, speed range is limited to 1:2 or 1:3. The drive is not required to operate in the steady state at very low speeds. In such applications, the motor only traverses through the low frequency range while starting. Therefore inaccuracies in the $\frac{V}{f}$ ratio are tolerable, (provided the machine is able to develop enough torque to accelerate). The constant $\frac{V}{f}$ method is then suitable for adjustable speed drives. The method can be used in conjunction with either six-step or PWM inverters. In the former, at low frequencies, the 5th and 7th harmonics also have low frequencies and the torque pulsations may become objectionable. In addition, a second power converter is needed in cascade to vary the DC link voltage. With present day power switches, PWM inverters can be economically realized. In the following, therefore, drives using PWM inverters only are considered. Both voltage and frequency can be controlled within the inverter itself.

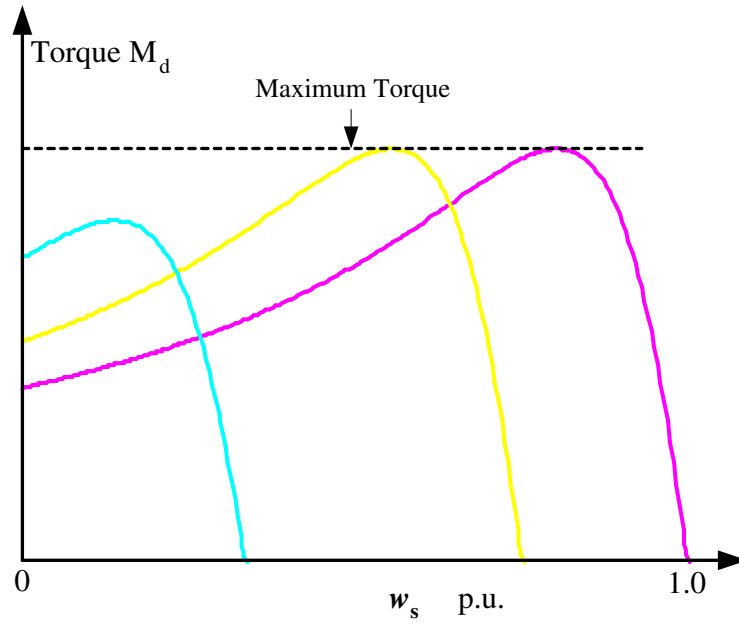


Figure 8.4: Torque-speed characteristics for constant $\frac{v}{f}$ control.

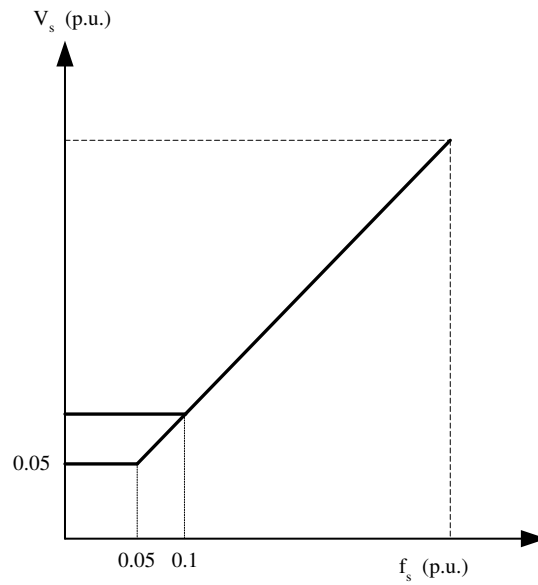


Figure 8.5: $\frac{v}{f}$ relationship including low frequency boost of voltage.

8.2 Block diagram of inverter fed drive

The block diagram of an adjustable speed drive incorporating a PWM inverter and an induction motor is shown in Figure 8.6. Power is normally available as AC. Therefore a

front-end rectifier and filter are needed to create the DC voltage for the inverter. The simplest type of rectifier is the uncontrolled diode rectifier, as shown in Figure 8.6. Any fluctuations in the mains voltage will therefore cause fluctuations in the DC bus voltage also. A controlled rectifier can be used to regulate the DC bus voltage. Note that in either case, power flow cannot be reversed, i.e., regeneration is not possible. In the majority of industrial drives, regeneration is not required and so this is not a limitation.

The drive control system accepts as inputs the speed command and any feedback signals available from the motor. It generates the stator frequency command f^* and voltage command v^* . The PWM circuit then generates the gating signals required to impress the commanded voltage and frequency on the motor.

8.3 Open loop drives with $\frac{V}{f}$ control

In a speed control system, evidently the actual speed of the motor should be measured through a tacho generator in order to accurately control the speed. In many industrial drives, it is desirable to avoid the installation of a tacho, from the point of view of cost, installation problems, reliability, etc. Such drives are referred to as open loop drives. No feedback information is available from the motor and the drive control has only the speed command to act upon. As has been pointed out earlier, the voltage and the frequency have to be related to each other through the $\frac{V}{f}$ program. This program generates the voltage command using the frequency command as the input. Therefore, the task of the drive control reduces to that of generating the frequency command using the speed command as input.

Since the rated or full load slip of an induction motor is usually small, the simplest approach to generating the frequency command is to directly use the speed command as the frequency command. The resulting drive control block diagram is shown in Figure 8.7. With such an arrangement the motor will always run at a speed which is less than the commanded speed by the slip speed corresponding to the prevailing load torque. If this speed error is accepted, then the system will run satisfactorily in the steady state.

However, the above simple arrangement may result in the motor pulling out when the speed command is suddenly changed. This may be explained as follows. Referring to Figure 8.8, let the machine operate initially at frequency f_{s1} , at the point A on the torque speed characteristic. If the speed command is suddenly changed resulting in a sudden change of frequency to f_{s2} , the new torque speed curve prevails. Because of the inertia of the mechanical system, machine speed cannot change suddenly. Therefore, the operating point jumps to B on the new curve. The slip at B is large and will result in large stator current. The developed torque is, however, larger than the load torque and the motor will accelerate. The

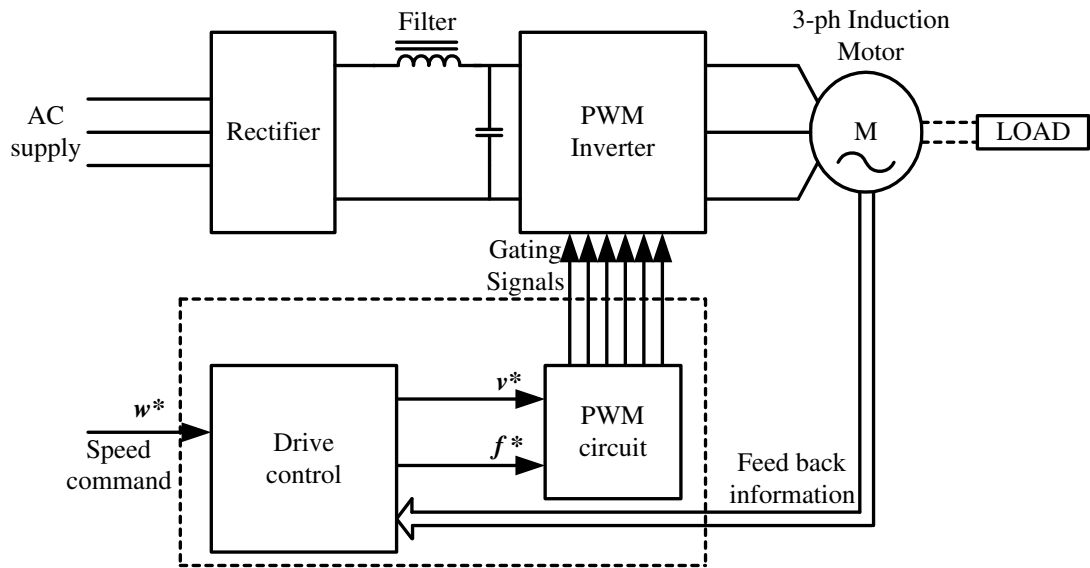
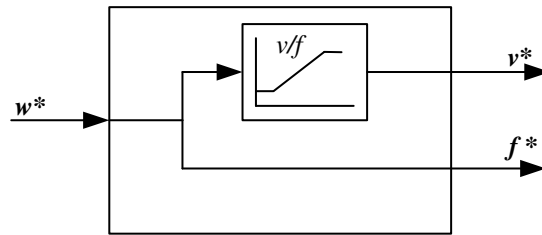
Figure 8.6: Block diagram of *PWM* inverter fed induction motor drive.

Figure 8.7: Drive control block diagram.

operating point will move along the characteristic and settle at C .

The above transient may be acceptable provided the resulting transient overcurrents can be handled by the inverter. Consider, however, the situation depicted in Figure 8.9. In this case, when the operating point jumps from B to A the resulting developed torque is less than the load torque. The motor decelerates, resulting in further reduction of developed torque and further deceleration. The motor will eventually pull out and come to a stop. In the process, large currents may be drawn from the inverter. Similar arguments can be advanced for sudden reduction of frequency also.

Therefore, the simple drive control scheme of Figure 8.7 has to be modified to prevent the sudden changes in the frequency command f^* . This can be achieved by making the frequency command f^* track the speed command w^* at a finite speed, through what is referred to as a 'slow start' circuit. In the simplest case, this consists of a RC circuit. The rate of change

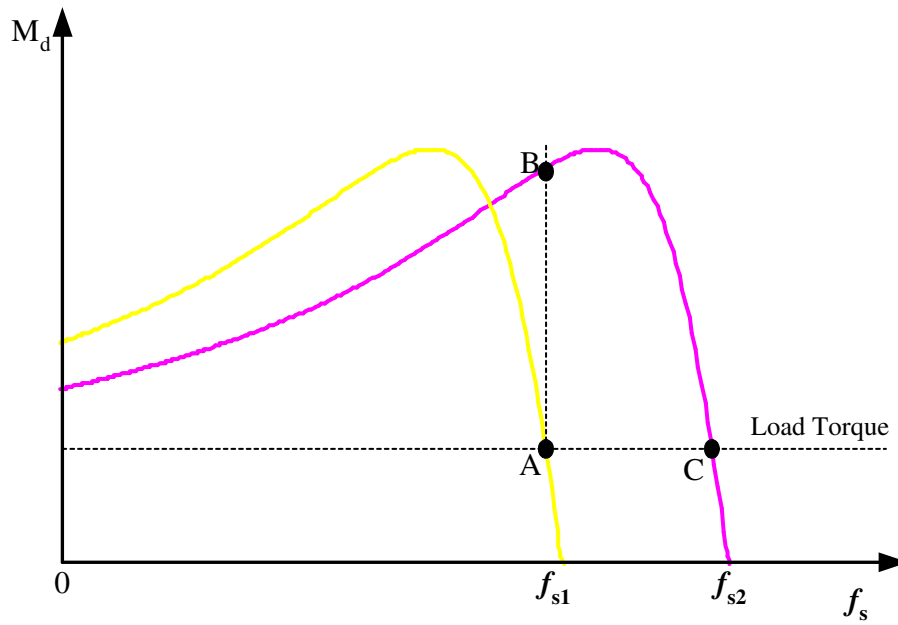


Figure 8.8: Effect of change in speed command.

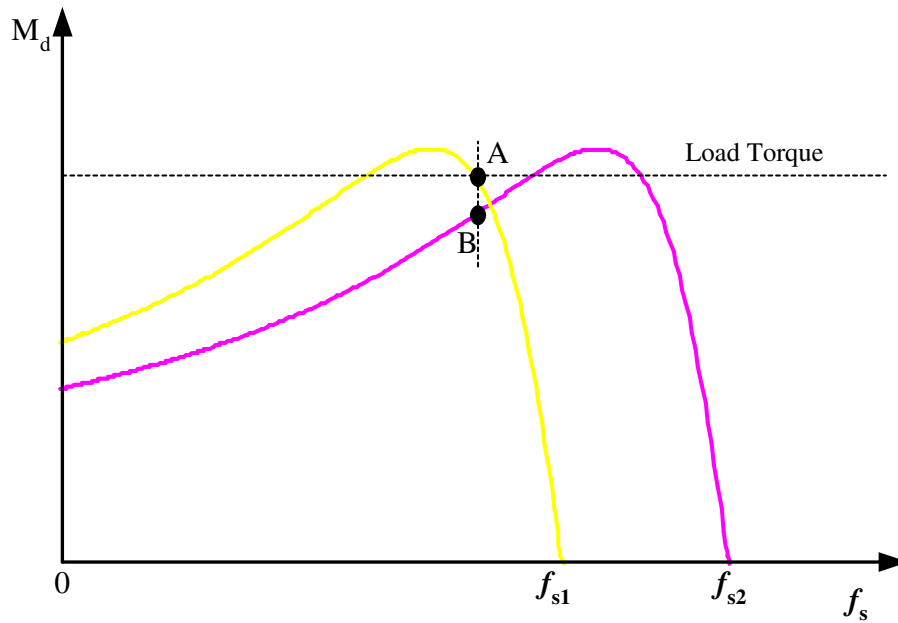


Figure 8.9: Effect of change in speed command.

of f^* must be limited to such an extent that the motor speed variation is able to track of

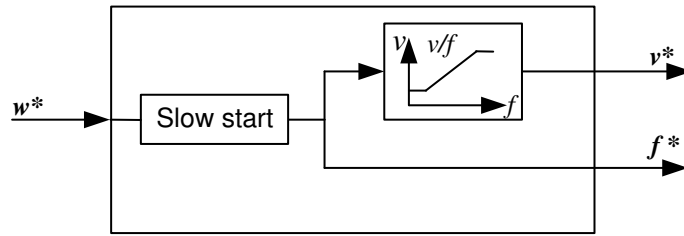


Figure 8.10: Drive control incorporating slow start.

changes in f^* . The resulting block diagram in Figure 8.10.

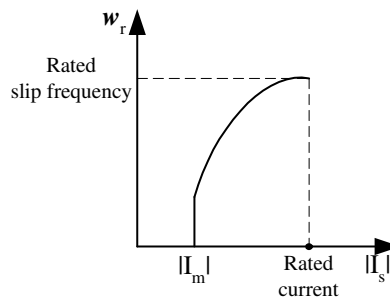


Figure 8.11: Slip frequency vs stator current relationship.

Note that in the steady state f^* will be equal to w^* . However, the speed of the response of the drive to changes in the speed command is now very much limited. This is not a drawback in many drives, as speed changes are commanded only once in a while.

8.4 Slip Compensation to Improve Speed Regulation

It was pointed out in the above method of control that the motor speed will always be less than the commanded speed due to the slip speed. For a given speed command, therefore, the speed will drop as load is increased. The speed regulation of drive can be improved, without, however, incorporating a tacho, by a technique known as slip compensation. This makes use of the fact that the amplitude of the stator current I_s and the slip frequency w_r of the machine are related to one another. The method therefore requires knowledge of the stator current in order to inject a correction to the frequency command. Measurement of current can be accomplished in a relatively easy manner and therefore slip compensation can be employed if speed regulation better than that obtained in the previous method is required. The principle of slip compensation can be explained as follows.

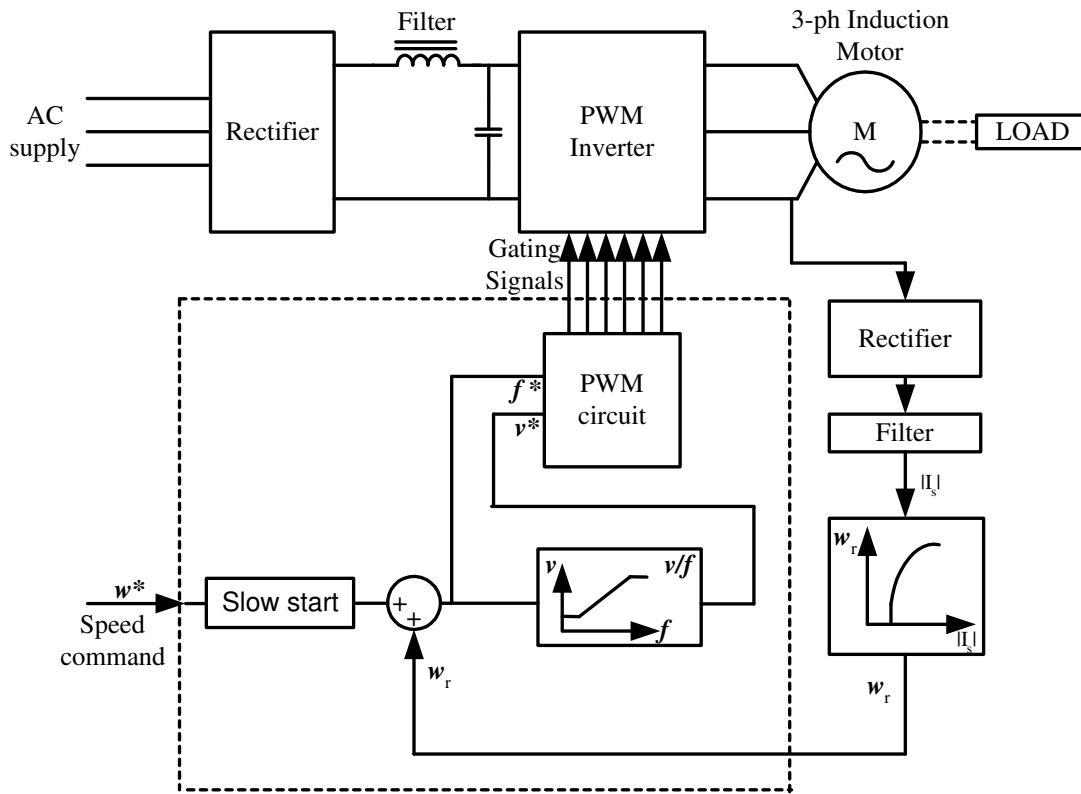


Figure 8.12: Drive control incorporating slip compensation.

From the equivalent circuit of Figure 8.2 magnetizing current and the stator current can be related by

$$I_m = I_s \frac{\frac{R_r}{s} + j\omega_s L_{lr}}{\frac{R_r}{s} + j\omega_s (L_{lr} + L_m)} \quad (8.5)$$

or

$$I_s = I_m \frac{R_r + j\omega_r L_r}{R_r + j\omega_r L_{lr}}, \quad L_r = L_{lr} + L_m \quad (8.6)$$

Thus

$$|I_s|^2 = |I_m|^2 \frac{1 + (\omega_r T_r)^2}{1 + (\omega_r T_{lr})^2} \quad (8.7)$$

where

$$T_r = \frac{L_r}{R_r}; \quad T_{lr} = \frac{L_{lr}}{R_r} \quad (8.8)$$

Using equation 8.7, with I_m assumed to be the rated value of the magnetizing current, the magnitude of the stator current I_s can be calculated for different values of rotor frequency ω_r . The resulting relationship between slip frequency and stator current is shown in Figure 8.11.

If the magnitude of the stator current in the machine can be measured, the corresponding slip frequency signal w_r can be generated using a function generator incorporating the graph of Figure 8.11. This signal can then be added to the speed command signal and the sum used as the frequency command. The resulting overall drive control scheme is shown in Figure 8.12.

The line current of the motor is sensed using a current sensor. Note that the frequency of the current is variable. Current signal is then rectified and filtered to get a DC signal proportional to the amplitude of the stator current. This signal is then used to generate slip compensation signal which is then added to the output of the slow start circuit to obtain the frequency command. Since the slip frequency at rated load is small, good speed regulation of the motor of the order of 1% can be achieved even in the presence of errors in the motor parameter values and magnetizing current assumed to generate the slip compensation signal.

Note that slip compensation constitutes a positive feedback. Excessive compensation may result in the motor pulling out following an increase in the speed command.

8.5 Drive with Speed Feedback

If a tacho generator can be provided to measure speed, then the motor speed can be directly controlled. The block diagram of the drive can then be as shown in Figure 8.13.

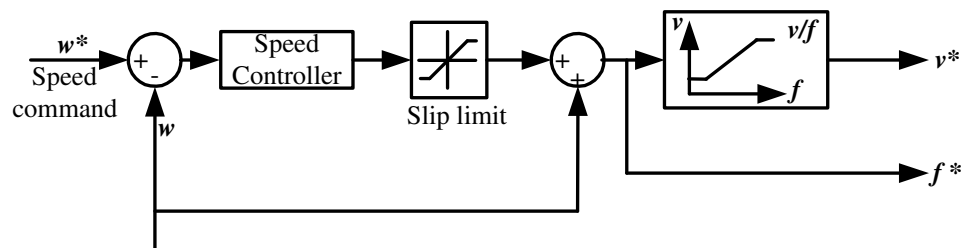


Figure 8.13: Control scheme with speed feedback.

The output of the speed controller is directly used as the slip frequency by adding it to the speed feedback signal to generate the stator frequency command. Therefore, by limiting the controller output as shown, the maximum slip frequency can be limited and pullout of the machine can be avoided.

8.6 Conclusion

Simple drive schemes for inverter fed induction motors have been outlined. The control schemes are based on steady state relationships in the machine and are not suitable for applications requiring fast dynamic response. For such applications, more sophisticated algorithms based on the dynamic model of the induction motor become necessary and will be discussed subsequently.

Chapter 9

Field Oriented Control of AC Motor Drives

9.1 Introduction

Until a few years ago, dc motor drives remained the only choice for fast response high performance drives such as steel and paper mill drives, servo drives for machine tool applications, etc., although it was realized that a squirrel cage induction motor enjoys many advantage over a dc motor, such as better power/weight ratio, lower inertia, higher speeds and less maintenance. Partly this state of affairs could be attributed to the fact that inverters for AC motor drives were not as rugged and reliable as the line commutated converters needed for dc motor drives. More importantly, however, dc motors represent simple control systems. This is because the dc motor has two separate physical windings, the armature and the field, whose *mmfs* are always at right angles with respect to one another in space due to the action of the commutator. The armature current can be controlled independently of the field current yielding fast response torque and speed control. This decoupling between control of torque and control of flux is not available readily in AC motors. It was only towards the late 1970s that it was realized that the dynamic behaviour of AC motors could be viewed in a manner analogous to that of the dc motor, provided the machine is modelled in an appropriate manner. The conceptual framework for such a model was then established and control methods could then be proposed for AC motor drives, yielding decoupled control of flux and torque with performance equivalent to that of the dc motor drive . This technique for decoupled control of torque and flux in an AC motor has come to be known as field oriented control or vector control of AC motors [1,2]. At the beginning , this technique could not be readily applied because it required complex signal processing. With present day advances in microelectronics, this is no longer a serious constraint and field oriented AC drives are emerging as a viable alternative to dc motor drives in high performance applications.

In the following, the principle of field oriented control is developed in the context of a squirrel cage induction motor drive. The block diagram of the drive is presented and

explained. The implementation of the control scheme in a microprocessor is discussed.

9.2 Space Phasors (3)

The conceptual foundation for field oriented control lies in the so called space phasor modelling of AC machines. It is therefore necessary to first develop an appreciation of the concept of space phasors. Consider a three phase winding in an AC machine, for example, the stator winding of an induction motor. Figure 9.1 shows the schematic diagram of the three phase coils, each of which has N_s turns. The diagram shows the spatial orientation of the three coils, the angles being in electrical radians.

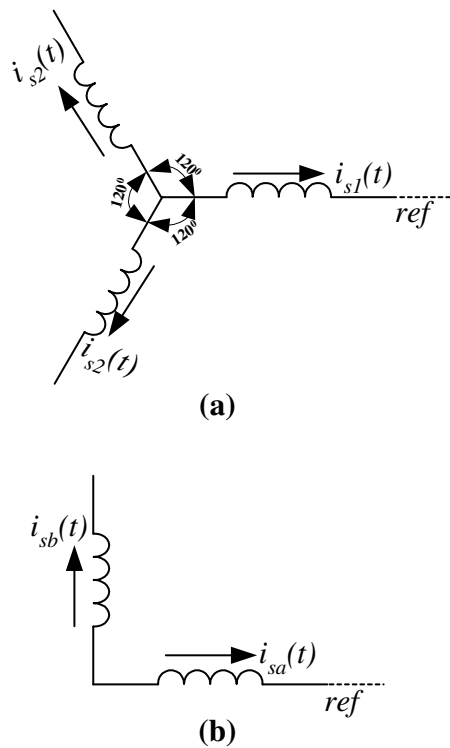


Figure 9.1:

It is assumed that the spatial distribution of mmf produced by each coil is sinusoidal in nature and also that the neutral is isolated, so that the condition

$$i_{s1}(t) + i_{s2}(t) + i_{s3}(t) = 0 \quad (9.1)$$

holds at all instants of time. The currents can have any general variation with respect to time. The axis of coil 1 is taken as the reference for spatial orientation. At any given instant of time, the net mmf produced by the three coils is given by adding the $mmfs$ due to the

individual coils, but with appropriate spatial orientation, i.e. vectorially. The net mmf can therefore in general have components along and perpendicular to the reference direction. If these components are denoted by subscripts a and b respectively, their values are given by

$$mmf_a = N_s[i_{s1}(t) + i_{s2}(t)\cos\gamma + i_{s3}(t)\cos2\gamma] \quad (9.2)$$

$$mmf_b = N_s[i_{s2}(t)\sin\gamma + i_{s3}(t)\sin2\gamma] \quad (9.3)$$

Where $\gamma = 2\pi/3$ electrical radians. Thus it can be seen that the system of three coils can be replaced by a system of two coils a and b shown in Figure 9.1, having the same number of turns N_s as the original coils and carrying currents $i_{sa}(t)$ and $i_{sb}(t)$ given by

$$i_{sa}(t) = \frac{3}{2}i_{s1}(t) - \frac{1}{2}i_{s2}(t) - \frac{1}{2}i_{s3}(t) \quad (9.4)$$

$$i_{sb}(t) = [i_{s2}(t) - i_{s3}(t)]\frac{\sqrt{3}}{2} \quad (9.5)$$

Using the condition (9.1), these can be rewritten as

$$i_{sa}(t) = \frac{3}{2}i_{s1}(t) \quad (9.6)$$

$$i_{sb}(t) = \frac{\sqrt{3}}{2}[i_{s2}(t) - i_{s3}(t)] \quad (9.7)$$

The net mmf produced by the two systems of coils is identical. The net effect of all the currents is thus obtained by adding $i_{sa}(t)$ and $i_{sb}(t)$ with proper spatial orientation. Using complex notation, this can be expressed by defining a so called current phasor $\underline{i}_s(t)$ by

$$\underline{i}_s(t) = i_{sa}(t) + ji_{sb}(t) \quad (9.8)$$

The current space phasor is thus a complex function of time, whose real and imaginary parts give the components of current along two mutually perpendicular directions in space. Pictorially the space phasor $\underline{i}_s(t)$ can be represented by a vector in a two dimensional plane, the real and imaginary components being $i_{sa}(t)$ and $i_{sb}(t)$. This is shown in Figure 9.2.

The space phasor can also be expressed in polar instead of cartesian form as follows:

$$\underline{i}_s(t) = i_s(t)e^{j\zeta(t)} \quad (9.9)$$

Where

$i_s(t)$ - instantaneous amplitude of space phasor

$\zeta(t)$ - instantaneous angle that the space phasor makes with the reference direction.

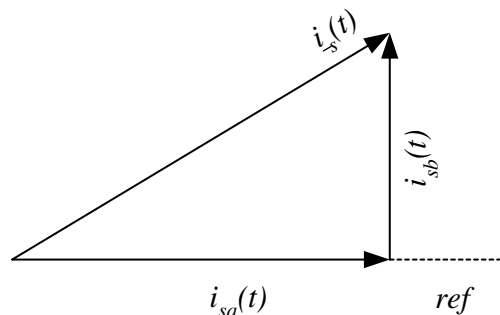


Figure 9.2:

Since the orientations refer to spatial direction in Figure 9.2, it should not be confused with the usual time phasor diagram of sinusoidal steady state analysis. The space phasor $\underline{i}_s(t)$ can also be expressed in terms of the original three phase currents as follows:

$$\underline{i}_s(t) = i_{s1}(t) + i_{s2}(t)e^{j\gamma} + i_{s3}(t)e^{j2\gamma} \quad (9.10)$$

Similarly, space phasors can be defined for other quantities such as voltages and flux linkages associated with a three phase system of windings.

From the study of polyphase windings, it will be seen that if the three individual quantities are balanced three phase sinusoids, then the space phasor will have a constant amplitude and will rotate in space with constant angular velocity. But the definition of space phasors is not limited to sinusoidal quantities alone. Any general time variation is possible for the three individual variables. Thus the concept of a space phasor is a useful tool in the analysis of AC motor drives, because the inverters that drive the motor produce non-sinusoidal voltages. The currents produced by a current source inverter for example have the waveforms shown in Figure 9.3. The corresponding space phasor will therefore occupy a fixed position in space for one sixth of a cycle and jump in position by 60° at every commutation in the inverter.

It will be seen that what was described in the preceding is nothing but a statement of the equivalence between three phase and two phase windings, with the important extension that the two real quantities are composed into one complex quantity known as the space phasor. The advantage as we have seen is that we are now able to visualize the motion of the space phasor.

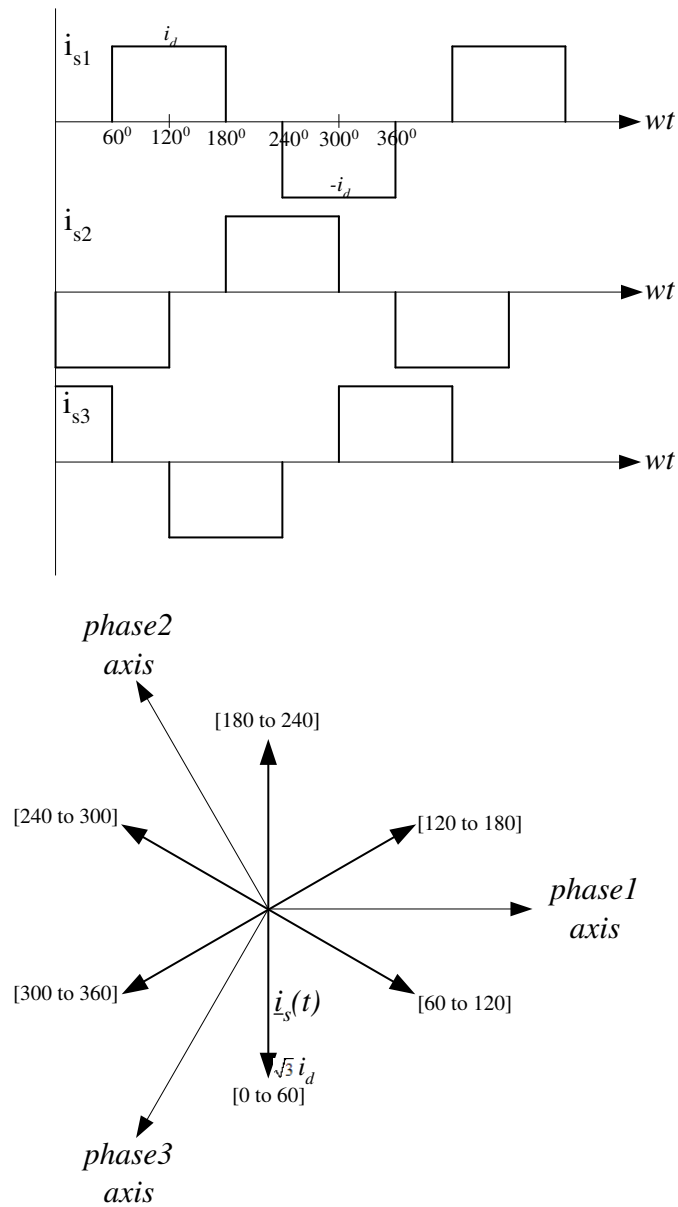


Figure 9.3:

9.3 Induction Machine Equations in Space Phasor Form

The symmetrical three phase squirrel cage induction motor has a three phase system of coils on the stator and a cage on the rotor which can be considered to be equivalent to a three phase winding. The two sets of windings can be represented by two equivalent two phase coils as shown in Figure 9.4. The rotor axis makes an angle $\varepsilon(t)$ with respect to the stator axis. Two current space phasors $\underline{i}_s(t)$ and $\underline{i}_r(t)$ can be defined for the stator and rotor current

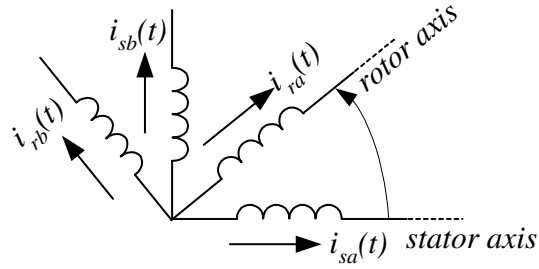


Figure 9.4:

respectively as follows:

$$\underline{i}_s(t) = i_{sa}(t) + j i_{sb}(t) \quad (9.11)$$

$$\underline{i}_r(t) = i_{ra}(t) + j i_{rb}(t) \quad (9.12)$$

Note that the two are defined with respect to different coordinate axes; $\underline{i}_s(t)$ with respect to stator coordinates and $\underline{i}_r(t)$ with respect to rotor coordinates. It is also possible to write down the flux linkages of the various coils as a first step towards writing down the machine voltage equations

$$\psi_{sa}(t) = L_s i_{sa}(t) + M i_{ra}(t) \cos \varepsilon(t) - M i_{rb}(t) \sin \varepsilon(t) \quad (9.13)$$

$$\psi_{sb}(t) = L_s i_{sb}(t) + M i_{ra}(t) \sin \varepsilon(t) + M i_{rb}(t) \cos \varepsilon(t) \quad (9.14)$$

where

L_s - self inductance of stator coils

M - maximum value of mutual inductance between stator and rotor coils. Combining 10.14 and 10.15 to form the stator flux space phasor.

$$\underline{\psi}_s(t) = \psi_{sa}(t) + j \psi_{sb}(t) = L_s \underline{i}_s(t) + M \underline{i}_r(t) e^{j\varepsilon(t)} \quad (9.15)$$

Similarly the rotor flux linkage space phasor can be derived as

$$\underline{\psi}_r(t) = \psi_{ra}(t) + j \psi_{rb}(t) = L_r \underline{i}_r(t) + M \underline{i}_s(t) e^{-j\varepsilon(t)} \quad (9.16)$$

where

L_r - self inductance of rotor coil referred to stator number of turns. The form of equations

9.15 and 9.16 resembles that for a coil with self and mutual inductance except for the expression for current in the second term. It must be remembered that 9.15 is with respect to stator coordinate and 9.16 is with respect to rotor coordinates. Therefore, space phasors defined with respect to another coordinate system have to be transformed to the coordinate system of the equation. Multiplication by $e^{j\varepsilon(t)}$ results in a clockwise rotation of the coordinate system by an angle $\varepsilon(t)$, while multiplication by $e^{-j\varepsilon(t)}$ results in anticlockwise rotation of the coordinate system by the same angle.

The voltage-current equations for the stator and rotor windings can also be written in the space phasor form. First the individual coil equations are written as follows:

$$v_{sa}(t) = R_s i_{sa}(t) + \frac{d\psi_{sa}(t)}{dt} \quad (9.17)$$

$$v_{sb}(t) = R_s i_{sb}(t) + \frac{d\psi_{sb}(t)}{dt} \quad (9.18)$$

$$v_{ra}(t) = R_r i_{ra}(t) + \frac{d\psi_{ra}(t)}{dt} \quad (9.19)$$

$$v_{rb}(t) = R_r i_{rb}(t) + \frac{d\psi_{rb}(t)}{dt} \quad (9.20)$$

where

R_s - stator resistance, R_r - rotor resistance.

Combining equation 9.17 with 9.18 and 9.19 with 9.20 we then obtain two complex equations:

$$\underline{v}_s(t) = R_s \underline{i}_s(t) + \frac{d\underline{\psi}_s(t)}{dt} \quad (9.21)$$

$$\underline{v}_r(t) = R_r \underline{i}_r(t) + \frac{d\underline{\psi}_r(t)}{dt} \quad (9.22)$$

using 9.15 and 9.16 these can be rewritten as

$$\underline{v}_s(t) = R_s \underline{i}_s(t) + L_s \frac{d\underline{i}_s(t)}{dt} + M \frac{d}{dt} [\underline{i}_r(t) e^{j\varepsilon(t)}] \quad (9.23)$$

$$\underline{v}_r(t) = R_r \underline{i}_r(t) + L_r \frac{d\underline{i}_r(t)}{dt} + M \frac{d}{dt} [\underline{i}_s(t) e^{-j\varepsilon(t)}] \quad (9.24)$$

It must be remembered that equation 9.23 refers to the stator and is in stator coordinates whereas equation 9.24 refers to the rotor and is in rotor coordinates. For a squirrel cage induction motor, of course, $\underline{v}_r(t)$ is zero. Each of the above equations is actually two equations combined into one. With these two equations, the electrical behavior of the machine is defined.

It can also be shown that the torque developed by the machine is given by

$$M_d = \frac{2}{3} \frac{P}{2} M \operatorname{Im} [\underline{i}_s(t) [\underline{i}_r(t) e^{j\varepsilon(t)}]^*] \quad (9.25)$$

Where Im stands for imaginary part and $*$ denotes complex conjugate, P is the number of poles. Therefore the complete equations that describe the behavior of the machine are as follows:

$$R_s \underline{i}_s(t) + L_s \frac{d\underline{i}_s(t)}{dt} + M \frac{d}{dt} [\underline{i}_r(t) e^{j\varepsilon(t)}] = \underline{v}_s(t)$$

$$R_r \underline{i}_r(t) + L_r \frac{d\underline{i}_r(t)}{dt} + M \frac{d}{dt} [\underline{i}_s(t) e^{-j\varepsilon(t)}] = 0$$

$$J \frac{d\omega_m}{dt} = \frac{2}{3} M \operatorname{Im} [\underline{i}_s(t) [\underline{i}_r(t) e^{j\varepsilon(t)}]^*] - M_{load}$$

$$\frac{P}{2} \omega_m = \omega = \frac{d\varepsilon(t)}{dt}$$

(9.26)

where

ω_m - rotor speed in mechanical rad/sec

ω - rotor speed in electrical rad/sec

J - moment of inertia

M_{load} - torque load

The above equations describe the dynamic behaviour of the machine. The steady-state behaviour, pertaining to sinusoidal steady state operation, can also be deduced from the above.

9.4 Sinusoidal Steady State Operation (3)

Under sinusoidal steady-state conditions, the applied stator voltage can be expressed as follows:

$$V_{s1}(t) = \sqrt{2} V_s \cos(\omega_1 t + \tau_1)$$

$$V_{s2}(t) = \sqrt{2} V_s \cos(\omega_1 t - \gamma + \tau_1)$$

$$V_{s2}(t) = \sqrt{2} V_s \cos(\omega_1 t - 2\gamma + \tau_1)$$

(9.27)

Where ω_1 is the stator angular frequency.

When composed into a space phasor according to equation 9.10, the stator voltage space phasor is expressed as

$$\underline{v}_s(t) = \frac{3\sqrt{2}}{2} v_s e^{j(\omega_1 t + \tau_1)} \quad (9.28)$$

$$i.e. \quad \underline{v}_s(t) = \frac{3\sqrt{2}}{2} \underline{V}_s e^{j\omega_1 t} \quad (9.29)$$

where \underline{V}_s is a complex constant, with amplitude equal to the *rms* line to neutral voltage and spatial orientation giving the instantaneous position of the peak of the voltage space wave at the instant $t = 0$. With the voltage input, the solution to the stator and rotor equations in 9.26 can be shown to be

$$\underline{i}_s(t) = \frac{3\sqrt{2}}{2} \underline{I}_s e^{j\omega_1 t} \quad (9.30)$$

$$\underline{i}_r(t) = \frac{3\sqrt{2}}{2} \underline{I}_r e^{j\omega_2 t} \quad (9.31)$$

where

$$\omega_2 = \omega_1 - \omega = \omega_1 - \frac{d\varepsilon}{dt} \quad (9.32)$$

The rotor current referred to stator coordinates is given by

$$\underline{i}_r(t) e^{j\varepsilon(t)} = \frac{3\sqrt{2}}{2} \underline{I}_r e^{j\omega_1 t} \quad (9.33)$$

With the definitions $M = L_0$, $L_s = L_0(1 + \sigma_s)$, $L_r = L_0(1 + \sigma_r)$, the stator and rotor equations in 9.26 can then be rewritten as

$$(R_s + j\omega_1 \sigma_s L_0) \underline{I}_s + j\omega_1 L_0 (\underline{I}_s + \underline{I}_r) = \underline{v}_s(t) \quad (9.34)$$

$$(R_r + j\omega_2 \sigma_r L_0) \underline{I}_r + j\omega_2 L_0 (\underline{I}_s + \underline{I}_r) = 0 \quad (9.35)$$

If the ratio between the rotor frequency ω_2 and the stator frequency ω_1 is defined as the slip ' s ' i.e. $s = \frac{\omega_2}{\omega_1}$, equation 9.35 can be rewritten as

$$\left(\frac{R_r}{s} + j\omega_1 \sigma_r L_0\right) \underline{I}_r + j\omega_1 L_0 (\underline{I}_s + \underline{I}_r) = 0 \quad (9.36)$$

Equation 9.34 and 9.36 together yield a steady state equivalent circuit of the induction machine as follows:

It should be remembered that the complex constants \underline{V}_s , \underline{I}_s and \underline{I}_r are proportional to the instantaneous values of the corresponding space phasors \underline{v}_s , \underline{i}_s and \underline{i}_r at the instant $t = 0$.

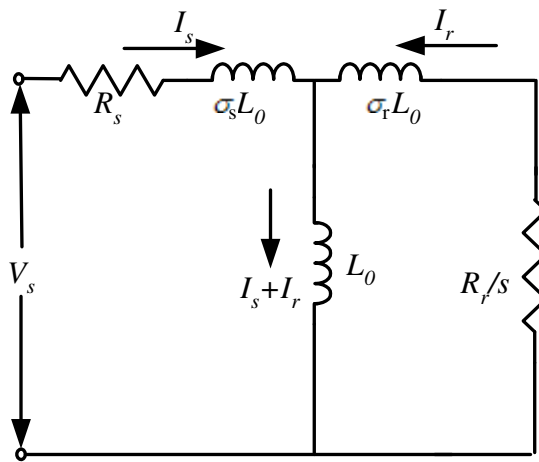


Figure 9.5:

However, because of the assumption that the winding *mmfs* are sinusoidally distributed in space, there is one to one correspondence between the above circuit and the usual one based on time phasors. This means that the parameters of the above circuit can be determined by the usual no-load and locked rotor tests.

All the steady-state characteristics of the machine such as torque-speed characteristics, circle diagram etc. can therefore be deduced from the equivalent circuit of Figure 9.5. However, what is of interest in the development of the concept of field oriented control is to appreciate the position and magnitude of different fluxes in the machine. The space phasor diagram of figure 9.6 below is drawn to show the spatial orientation of different fluxes in the machine. These can be defined as follows:

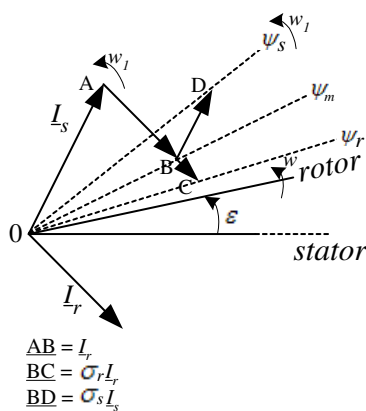


Figure 9.6:

$$\begin{aligned} \text{Mutual or air gap flux } \underline{\psi}_m &= L_0[\underline{I}_s + \underline{I}_r] \\ &\cong L_0\underline{I}_m \end{aligned} \quad (9.37)$$

$$\begin{aligned} \text{Stator flux } \underline{\psi}_s &= \sigma_s L_0 \underline{I}_s + L_0[\underline{I}_s + \underline{I}_r] \\ &= L_0[(1 + \sigma_s)\underline{I}_s + \underline{I}_r] \\ &\cong L_0\underline{I}_{ms} \end{aligned} \quad (9.38)$$

$$\begin{aligned} \text{Rotor flux } \underline{\psi}_r &= \sigma_r L_0 \underline{I}_r + L_0[\underline{I}_s + \underline{I}_r] \\ &= L_0[\underline{I}_s + (1 + \sigma_r)\underline{I}_r] \\ &\cong L_0\underline{I}_{mr} \end{aligned} \quad (9.39)$$

In addition to the magnetizing current \underline{I}_m responsible for mutual flux, two additional magnetizing currents \underline{I}_{ms} and \underline{I}_{mr} have been defined in equation 9.38 and 9.39 to account for stator and rotor fluxes also. Even though this has been done in the context of sinusoidal steady-state operation, identical definitions can be given in the general case of transient non-sinusoidal operation also.

All the fluxes rotate at the synchronous speed ω_1 with respect to the stationary stator axis. The torque developed by the machine can be expressed as the vector product of the stator current and any one of these fluxes.

If it is desired to establish an analogy between the induction motor and the dc machine, with similar decoupling between flux and torque, then the stator current \underline{I}_s should be decomposed into two spatially orthogonal components, along and perpendicular to the flux - but which flux? To decide this question, the machine equations (9.26) have to be recast using stator current components oriented along the different fluxes. It has been established that to obtain decoupling between flux and torque, the equation should be viewed from a frame of reference fixed to the rotor flux $\underline{\psi}_r(t)$. This exercise is carried out in the next section.

9.5 Dynamics of the Induction Motor in the Rotor Flux Frame of Reference (3)

It is assumed here that the machine is operated from a current source which impresses on the machine windings a given stator current space phasor $\underline{i}_s(t)$. This can be realized in practice with a pulse width modulated inverter operating at a switching frequency of a few kilohertz in the current regulated PWM mode. The first of the machine equations 9.26

therefore serves only to determine the stator voltage $\underline{v}_s(t)$ and need not be considered in determining the dynamic response of the machine. It is the second equation, corresponding to the rotor, that determines the machine behaviour. This equation is repeated here, with $M = L_0$ and $L_r = (1 + \sigma_r)L_0$.

$$R_r \dot{i}_r(t) + (1 + \sigma_r)L_0 \frac{d\dot{i}_r(t)}{dt} + L_0 \frac{d}{dt} [\dot{i}_s(t) e^{-j\varepsilon(t)}] = 0$$

The rotor flux space phasor is given by

$$\underline{\psi}_r(t) = L_0(1 + \sigma_r)\dot{i}_r(t) + L_0\dot{i}_s(t)e^{-j\varepsilon(t)} \quad (9.40)$$

in rotor coordinates. The representation in terms of stator coordinates can be obtained by multiplying equation 9.40 by $e^{j\varepsilon(t)}$, giving

$$\underline{\psi}_r(t)e^{j\varepsilon(t)} = L_0[\dot{i}_s(t) + (1 + \sigma_r)\dot{i}_r(t)e^{j\varepsilon(t)}] \quad (9.41)$$

$$= L_0\dot{i}_{mr}(t) \quad (9.42)$$

Therefore

$$\dot{i}_{mr}(t) = [\dot{i}_s(t) + (1 + \sigma_r)\dot{i}_r(t)e^{j\varepsilon(t)}] \quad (9.43)$$

The rotor equation then becomes:

$$\frac{R_r}{1 + \sigma_r} [\dot{i}_{mr}(t) - \dot{i}_s(t)]e^{-j\varepsilon(t)} + L_0 \frac{d}{dt} [(\dot{i}_{mr}(t) - \dot{i}_s(t))e^{-j\varepsilon(t)}] + L_0 \frac{d}{dt} [\dot{i}_s(t)e^{-j\varepsilon(t)}] = 0 \quad (9.44)$$

It must be observed that equation 9.44 is still in terms of the rotor coordinate system. After simplification

$$\frac{R_r}{1 + \sigma_r} [\dot{i}_{mr}(t) - \dot{i}_s(t)]e^{-j\varepsilon(t)} + L_0 \frac{d}{dt} [\dot{i}_{mr}(t) - j \frac{d\varepsilon(t)}{dt} \dot{i}_{mr}(t)L_0]e^{-j\varepsilon(t)} = 0 \quad (9.45)$$

If equation 9.45 is multiplied by $e^{j\varepsilon(t)}$, the resulting equation will be in terms of stator coordinates. Observing that $\frac{d\varepsilon(t)}{dt} = \omega$, the speed of the machine,

$$L_0 \frac{d}{dt} \dot{i}_{mr}(t) + \frac{R_r}{1 + \sigma_r} \dot{i}_{mr}(t) - j\omega L_0 \dot{i}_{mr}(t) - \frac{R_r}{1 + \sigma_r} \dot{i}_s(t) = 0 \quad (9.46)$$

This equation can now be expressed in terms of a coordinate system fixed to the rotor flux $\underline{\psi}_r(t)$ or equivalently to the current $\underline{i}_{mr}(t)$. To do this, $\underline{i}_{mr}(t)$ is first expressed in polar form with respect to stator coordinates as

$$\underline{i}_{mr}(t) = i_{mr}(t)e^{j\rho(t)} \quad (9.47)$$

Where $i_{mr}(t)$ is the instantaneous magnitude of the current space phasor $\underline{i}_{mr}(t)$ and $\rho(t)$ is its instantaneous position with respect to the stator real axis. Now equation 9.46 can therefore be written as

$$L_0 \frac{d}{dt} i_{mr}(t) e^{j\rho(t)} + \frac{R_r}{1 + \sigma_r} i_{mr}(t) e^{j\rho(t)} - j\omega L_0 i_{mr}(t) e^{j\rho(t)} - \frac{R_r}{1 + \sigma_r} \underline{i}_s(t) = 0 \quad (9.48)$$

i.e.

$$\left[L_0 \frac{d}{dt} i_{mr}(t) + \frac{R_r}{1 + \sigma_r} i_{mr}(t) + jL_0 \frac{d\rho}{dt} i_{mr}(t) - j\omega L_0 i_{mr}(t) \right] e^{j\rho(t)} = \frac{R_r}{1 + \sigma_r} \underline{i}_s(t) \quad (9.49)$$

Equation 9.49, which is still in stator coordinates, can now be transformed into rotor flux coordinates by multiplying by $e^{-j\rho(t)}$, giving

$$L_0 \frac{d}{dt} i_{mr}(t) + \frac{R_r}{1 + \sigma_r} i_{mr}(t) + j(\omega_{mr} - \omega) L_0 i_{mr}(t) = \frac{R_r}{1 + \sigma_r} \underline{i}_s(t) e^{-j\rho(t)} \quad (9.50)$$

where $\omega_{mr} = \frac{d\rho(t)}{dt}$ is the instantaneous angular speed of the rotor flux. The right hand side of the equation 9.50 contains the transformation of the stator current space phasor to the rotor flux coordinate system. If the coordinates of the stator current in this system are denoted by $i_{sd}(t)$ and $i_{sq}(t)$, then

$$\underline{i}_s(t) e^{-j\rho(t)} = i_{sd}(t) + j i_{sq}(t) \quad (9.51)$$

Equation 9.50 can now be separated into real and imaginary parts as follows:

$$\begin{aligned} L_0 \frac{d}{dt} i_{mr}(t) + \frac{R_r}{1 + \sigma_r} i_{mr}(t) &= \frac{R_r}{1 + \sigma_r} i_{sd}(t) \\ (\omega_{mr} - \omega) L_0 i_{mr}(t) &= \frac{R_r}{1 + \sigma_r} i_{sq}(t) \end{aligned} \quad (9.52)$$

Defining the rotor time constant as

$$T_r = \frac{L_r}{R_r} = \frac{L_0(1 + \sigma_r)}{R_r} \quad (9.53)$$

equation 9.52 can be rewritten as

$$T_r \frac{di_{mr}(t)}{dt} + i_{mr}(t) = i_{sd}(t) \quad (9.54)$$

$$\omega_{mr}(t) = \frac{d\rho}{dt} = \omega + \frac{i_{sq}(t)}{T_r i_{mr}(t)} \quad (9.55)$$

The above two equations now describe the dynamics of the current fed induction motor in the rotor flux oriented frame of reference. $i_{sd}(t)$ and $i_{sq}(t)$ are the inputs to the machine. $i_{mr}(t)$, $\frac{d\rho(t)}{dt}$ and ω are the outputs or the response of the machine. Of course, to make the equation complete, the torque equation should also be written in terms of field coordinates, which can be done as follows. From equation 9.25, the torque developed is given by

$$\begin{aligned} M_d(t) &= \frac{2P}{3} \frac{L_0}{2} \text{Im}[\underline{i}_s(t)(\underline{i}_r(t)e^{j\varepsilon})^*] \\ &= \frac{2P}{3} \frac{L_0}{2} \frac{1}{1 + \sigma_r} \text{Im}[\underline{i}_s(t)[\underline{i}_{mr}(t) - \underline{i}_s(t)]^*] \\ &= \frac{2P}{3} \frac{L_0}{2} \frac{1}{1 + \sigma_r} \text{Im}[\underline{i}_s(t)\underline{i}_{mr}(t)^*] \end{aligned}$$

i.e.

$$\begin{aligned} M_d(t) &= \frac{2P}{3} \frac{L_0}{2} \frac{1}{1 + \sigma_r} \text{Im}[\underline{i}_s(t)i_{mr}(t)e^{j\rho(t)}] \\ &= \frac{2P}{3} \frac{L_0}{2} \frac{1}{1 + \sigma_r} \text{Im}[i_{mr}(t)[\underline{i}_s(t)e^{j\rho(t)}]] \\ &= \frac{2P}{3} \frac{L_0}{2} \frac{1}{1 + \sigma_r} \text{Im}[i_{mr}(t)[i_{sd}(t) + ji_{sq}(t)]] \\ &= \frac{2P}{3} \frac{L_0}{2} \frac{1}{1 + \sigma_r} i_{mr}(t)i_{sq}(t) \end{aligned} \quad (9.56)$$

Therefore the complete machine equations can now be given as

$$T_r \frac{di_{mr}(t)}{dt} + i_{mr}(t) = i_{sd}(t)$$

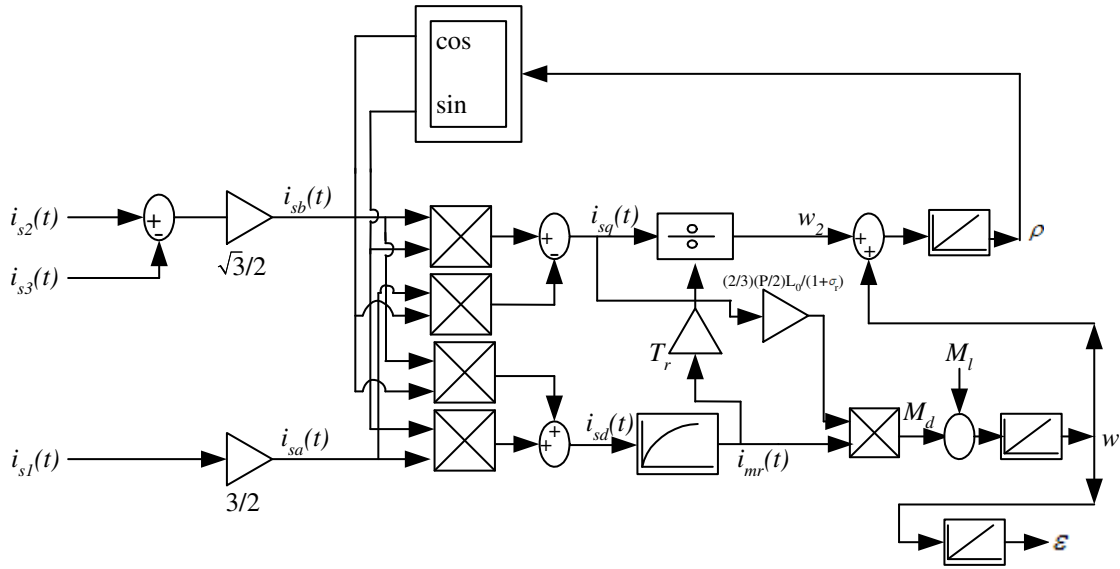


Figure 9.8: Block diagram of current fed induction motor in rotor flux coordinates.

three sections. In the first section the three phase currents in the stator windings viz. i_{s1} , i_{s2} and i_{s3} are converted into equivalent two phase stator currents i_{sa} and i_{sb} . In the second section, these two phase currents are transformed into the rotor flux oriented components i_{sd} and i_{sq} by the relationship:

$$i_{sd}(t) = i_{sa}(t)\cos\rho(t) + i_{sb}(t)\sin\rho(t) \quad (9.59)$$

$$i_{sq}(t) = i_{sb}(t)\cos\rho(t) - i_{sa}(t)\sin\rho(t) \quad (9.60)$$

ρ being the instantaneous position of the rotor flux with respect to the stator axis. The third section incorporates the dynamics described by equations 9.54, 9.55, 9.57 and 9.58.

9.6 Field Oriented Control of Induction Motor

It is clear by now that in order to achieve decoupled control of the flux and torque in an induction motor, the components i_{sd} and i_{sq} of the stator current \underline{i}_s have to be controlled. The magnitude of i_{sq} should be controlled to adjust the torque and the magnitude of i_{sd} should be controlled to adjust the rotor flux or equivalently the rotor flux magnetising current i_{mr} . The structure of an induction motor drive based on field orientation is therefore as shown in Figure 9.9.

It can be seen that the torque loop generates the command value i_{sqref} and the flux loop generates the command value i_{sdref} . The speed and position loops are closed around

into command values for the phase currents, it is clear that accurate information regarding the instantaneous position of the rotor flux, given by the angle ρ , is essential. In Figure 9.9, this is accomplished through the flux acquisition system. Provided this task can be performed accurately, field oriented control yields several significant advantages:

- it allows direct control of flux and torque, making torque limiting and field weakening possible
- with correct information regarding the angle ρ , the motor is self controlled and cannot pull out; in the event of an overload torque, the motor is stalled with maximum torque.
- decoupling between flux and torque is effective even under dynamic conditions
- since the controllers process dc quantities in the steady state, the effect of unavoidable phase shifts in the control loops is not present.

In order to realise these advantages, however, the major task of acquiring the flux signal has to be performed accurately over the entire speed range down to zero speed, especially for reversing drives. This is a formidable task and had to await the advent of microprocessors and other signal processing chips. However, with present day technology, the signal processing that is required can be effectively accomplished.

Depending on the method employed to sense the flux, field oriented control can be classified into two major categories, direct and indirect. In indirect field orientation, the air gap flux in the machine is directly measured by measuring the induced voltage in Hall sensors or flux sensing coils and integrating it. However, there are several difficulties associated with this approach. The motor has to be specially modified in order to accommodate the sensing device. Moreover, the Hall sensors are fragile. Also the integrators are subject to drift at low frequencies and this limits the lowest speed at which the technique can be used. The induced voltage in the sensing devices contain harmonics due to rotor slots. These harmonics are difficult to filter as their frequency changes with the speed of the machine. Because of these reasons the direct method is usually very difficult to employ. But it has the merit that the measurements are not dependent on machine parameter values, which change with temperature, saturation, etc.

Instead of using voltages from sensing coils, the machine terminal voltage themselves can be used. However, in this case, the stator resistance drop has to be compensated before integration. Since the resistance changes with temperature, this is also difficult to achieve accurately.

A different approach is followed in the indirect method of field orientation. This method uses the model equations of the machine with easily measurable quantities as inputs and

calculates the magnitude and position of the rotor flux. The block diagram of figure 9.8, which is based on the model of the machine in the field oriented coordinate system, can itself be used to generate the information regarding the actual values of i_{sd} , i_{sq} and i_{mr} , the torque m_d and the angle ρ that the rotor flux makes with the stator axis. Thus the total signal processing tasks to be performed to implement field orientation by the method involve two sets of coordinate transformations.

- the transformation from the actual phase quantities to field oriented coordinates in the flux acquisition system
- the reverse transformation from field coordinates to actual phase coordinates in the control system.

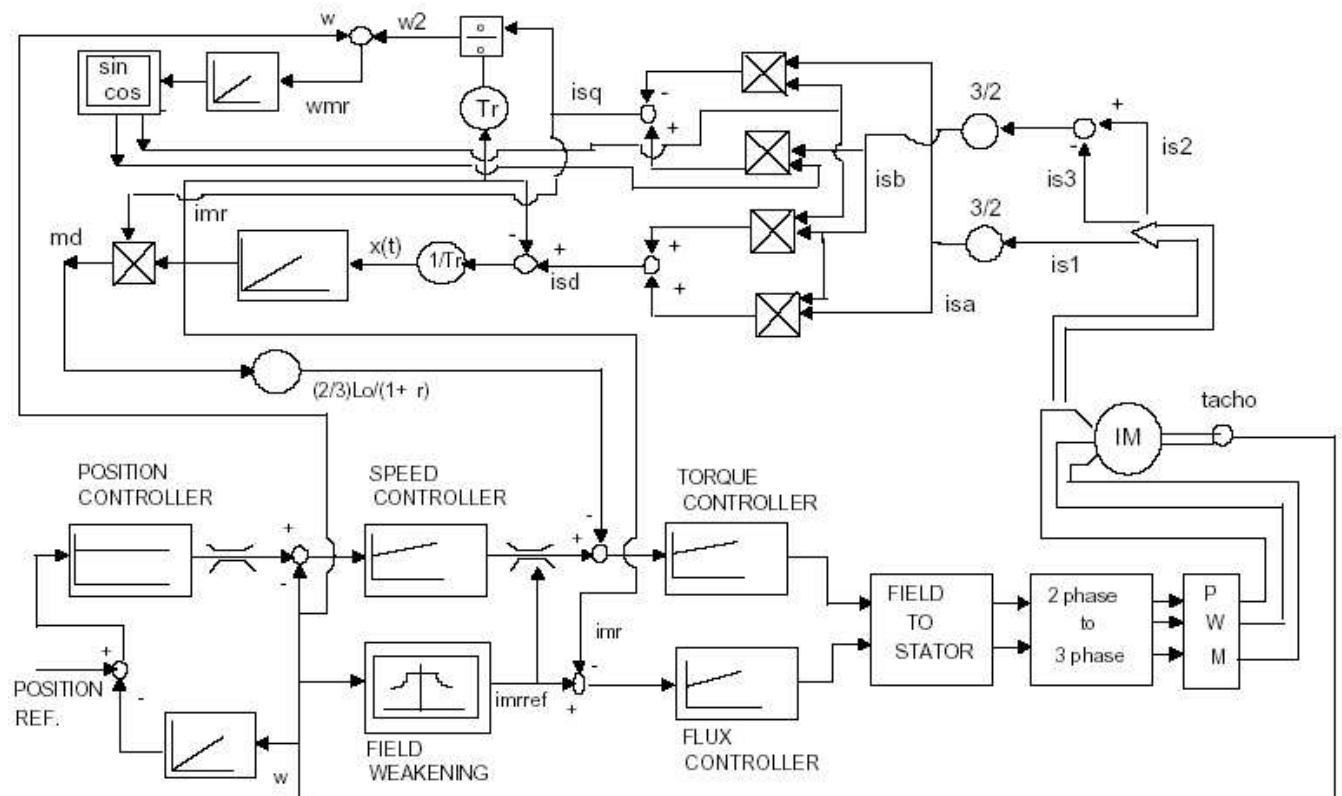


Figure 9.10:

The flux acquisition system accepts as inputs the three (two are sufficient for motors with neutral floating) stator currents and the speed ω and/or the rotor position available from tachos or position encoders used for speed and position feedback. The total drive system is therefore as shown in Figure 9.10.

Accurate orientation of the stator current space phasor by this method requires a knowledge of machine parameters for performing the computation. For example, the rotor time constant T_r should be known accurately. Since the rotor resistance varies with temperature, T_r is subject to variation. Therefore to achieve best results, indirect field orientation requires some kind of adaptation scheme to keep track of parameter variations [4, 5].

9.7 Implementation of Indirect Field Orientation

Since a lot of nonlinear elements such as multipliers, function generators, etc. are essential to perform the signal processing necessary for indirect field orientation, analog realisation becomes expensive and difficult to adjust. Therefore, a digital implementation is the only feasible solution and is a practical proposition with today's microprocessors and memories. This carries with it all the advantages of digital control by software, such as standardised hardware, flexibility, etc.

As a first step towards microprocessor based control, it is necessary to digitise the various analog signals. This requires that the necessary resolution in amplitude and the sampling rate be fixed. With respect to amplitude resolution, the use of 10 or at most 12-bit A/D converters is adequate for digitizing the analog signals from the motor such as speed and current. Only in exceptional situations is higher resolution necessary; 16-bit microprocessors such as 8086 or 8088 can provide sufficient word length. For the digital to analog conversion, 10-bit resolution is sufficient. However, the sampling rates cannot be uniform for all the control processes and have to be selected depending on the nature of the signals being processed. Basically there are three main control functions in the induction motor speed control system: a) torque control, (b) speed control and (c) flux control. In a position control application, there will be an additional position control loop. Of the three control functions, torque control requires sensing of the stator currents which may vary at frequencies of upto 100 Hz for a 50 Hz motor taking field weakening operation into account. Therefore the sampling rate is the highest for the torque control function. The speed control function should have the next lower sampling rate with the flux control function possibly having an even slower rate. For example, with a transistor PWM inverter and 8086 processor, the following sampling times have been found to be adequate.

a) Sampling rate of 1 msec for torque control; this includes the following steps:

- A/D conversion of stator currents
- Updating of flux model
- transformation to field coordinates

- torque control
- transformation of reference currents from field to stator coordinates
- outputting of stator current references

b) Sampling period of 5 msec for

- flux control including field weakening
- speed control
- position control

Where a position encoder is used for sensing speed/position, the sampling time sometimes has to be varied with the speed. Use of an absolute encoder is preferable for sensing speed and position as it removes any ambiguity regarding the initial position. However, incremental decoders are much less expensive.

Since the sampling rates are fairly high, the control loops can be treated as practically continuous time systems. Because the plant - the induction motor - has become decoupled and linearised to a considerable extent as a result of field orientation, familiar methods used in conjunction with dc drives can be used to design the controllers. The overall block diagram

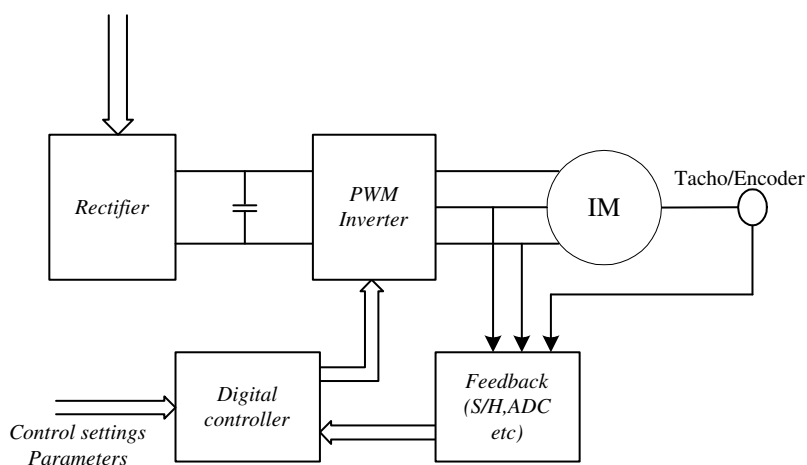


Figure 9.11:

of an induction motor drive with a microprocessor controller is as shown in Figure 9.11. A variety of processors are available with the required 16-bit word length. An essential feature that is necessary to execute field oriented control is the capability to perform multiplications and divisions. In general, by using normalized variables throughout the control system, the

need for floating point operations may be avoided and integer arithmetic will suffice. In case the speed of the processor is inadequate while executing multiply and divide instructions, the processor may be augmented by a hardware multiplier/divider. Figure 9.12 shows a possible hardware organisation of the microprocessor based controller.

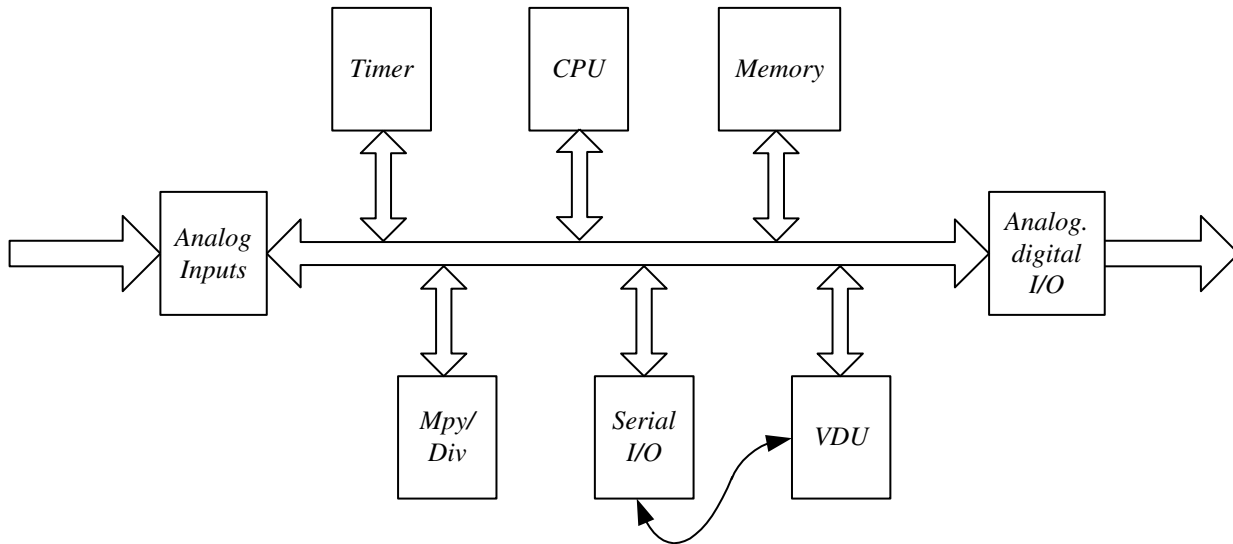


Figure 9.12:

The software should be organised in such a way that the routine for torque control gets priority over the computation for the speed loop and the flux loop. The torque control routine is invoked at regular intervals by a timer interrupt. The timing for the various routines and their priority in execution can be indicated as shown in Figure 9.13. Usually the controllers

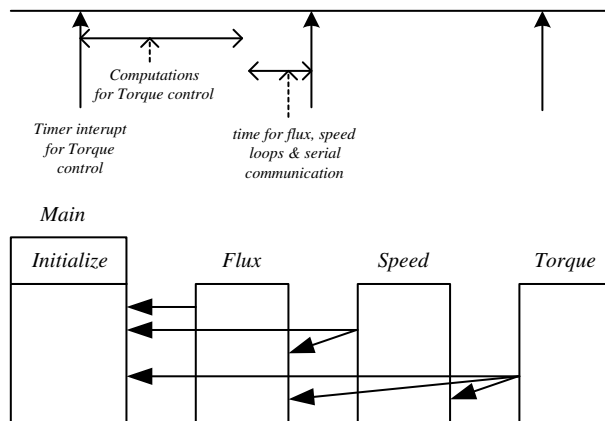


Figure 9.13:

used in the drive system are all of the PI type. Figure 9.14 shows the block diagram of a PI controller. The defining equations for the PI controller are as follows:

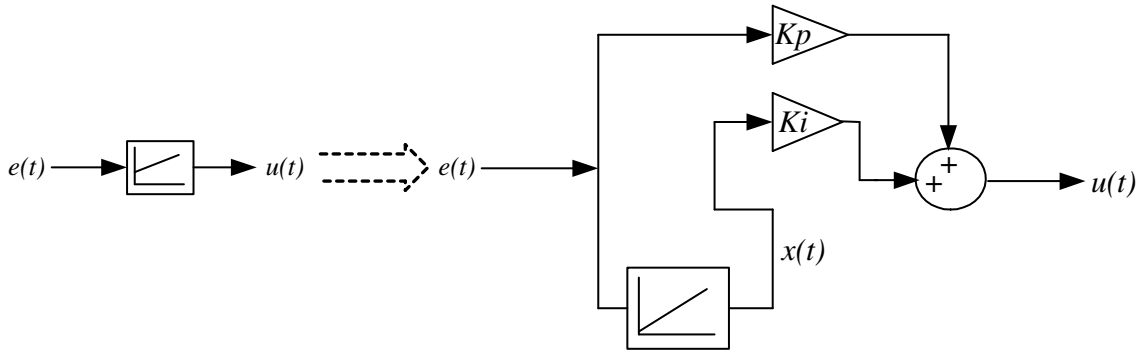


Figure 9.14:

$$u(t) = k_p e(t) + k_i \int e(t) dt \quad (9.66)$$

$$x(t) = \int_{t_0}^t e(\tau) d\tau + x(t_0) \quad (9.67)$$

The digital realisation for a microprocessor PI controller is as follows:

$$x(kT) = (T/2)[e(kT) + e[(k-1)T]] + x(k-1)T \quad (9.68)$$

$$u(kT) = k_p e(kT) + k_i x(kT) \quad (9.69)$$

using the simple trapezoidal rule for integration.

Consider the drive block diagram of Figure 9.10. Assuming that the torque, speed and flux controllers are of the PI type and also that the sampling times for the torque, speed and flux control are T_0 , T_1 and T_2 respectively ($T_0 < T_1 < T_2$), the computations to be performed in each sampling interval can be listed as shown below. The PI controller parameters are denoted by and with subscripts, k_p and k_i with subscripts m , s and t for torque, speed and flux respectively. The outputs of the unity gain integrators (Figure 9.14) in the three controllers are denoted by x_m , x_s and x_f respectively.

Note: Recent developments in fast Digital Signal Processors operating at high clock speeds upwards of 20 MHz with single cycle multiply instructions have made it much easier to organise the control loops. It is no longer essential, although it may be convenient in some ways, to execute the different loops with different times. They can all be executed once in each sampling interval. It is still possible to achieve sampling intervals of the order of $64\mu s$ comfortably.

9.8 Conclusion

The basic principle of field oriented control of a squirrel cage induction motor was developed assuming a controlled current pwm inverter. Considerations for implementation using a microprocessor based controller have been outlined. The assumption of constant current supply is usually not valid at high speeds where the inverter ceiling voltage is reached and the dc bus voltage cannot force current against the back emf of the machine. Further, in the case of high power thyristor inverters operating at switching frequencies of a few hundred hertz, it can no longer be assumed that current of any value can be instantaneously forced into the stator windings. In such cases, the inverter becomes a voltage source rather than a current source. In this case also the technique of field orientation can be applied. However, now the stator transients as represented by the stator equation 9.23 cannot be neglected [3]. Equation 9.23 has to be transformed into field coordinates and the associated interactions have to be represented in the machine block diagram. However, these are considerations for the implementation of field oriented control. The basic principle does not change. Similarly an induction motor controlled by a current source inverter (ASCI) can also be provided with vector control. In fact the principle of field orientation can be applied for the control of any rotating field machine; wound rotor induction motors, synchronous motors either with field winding or of the permanent magnet (PM) type can all be controlled using this principle to obtain high performance drives [6,7].

9.9 References

1. Blaschke, F., 'Verfahren der Feldorientierung zur Regelung der Asynchron machine', Siemens Forschung u Entwicklungs Berichte, Bd. 1, Nr. 1, pp 184-193, 1972 (in German).
2. Hasse, K., 'Zum Dynamischen Verhalten der Asynchronmaschine bei Betrieb mit Variabler Stander frequence und Standerspannung', ETZ-A, Bol. 89, H4, pp 77, 1968.
3. Leonhard , W., 'Control of Electrical Drives', Springer-Verlag, 1985.
4. Garces, L.J., 'Parameter Adaptation for the speed controlled static AC drive with a squirrel cage induction motor', IEEE Trans. Industry Applications, Vol. IA-16, No. 2, March/April 1980, pp. 173-178.
5. Krishnan, R. and Doran, F.C., 'Study of parameter sensitivity in high performance, inverter-fed induction motor drive systems', IEEE Trans. Industry Applications, Vol. IA-23, No.4, July/August 1987, pp 623-635.
6. Leonhard, W., 'Control of AC-machines with the help of microelectronics', 3rd IFAC Symposium on Control in Power Electronics and Drives, Lausanne 1983, Survey paper.
7. Bose, B.K. (Ed.), 'Adjustable speed A.C. drive systems', IEEE Press, New York, 1981.

Chapter 10

Space-Phasor Based PWM Techniques

The concept of space-phasor, which was dealt with in connection with the modelling and control of induction motors, can also be used as a basis for developing pulse width modulation (PWM) strategies for inverters. In particular, space phasor based PWM techniques for voltage source inverters are discussed in the following.

Consider a three-phase half bridge voltage source inverter, shown in Figure 10.1. Each phase to center-tap voltage, viz. V_{R0} , V_{Y0} , and V_{B0} can have only two possible values, namely $\frac{V_{dc}}{2}$ or $-\frac{V_{dc}}{2}$, depending on whether the top switch or the bottom switch is being gated. Thus each phase can be regarded as a single pole double-throw switch. The two states of each switch are denoted by $+$ and $-$ in the following, corresponding to the phase to center voltage being $\frac{V_{dc}}{2}$ and $-\frac{V_{dc}}{2}$ respectively. As there are three phases, there are eight possible switching states for the inverter at any instant of time.

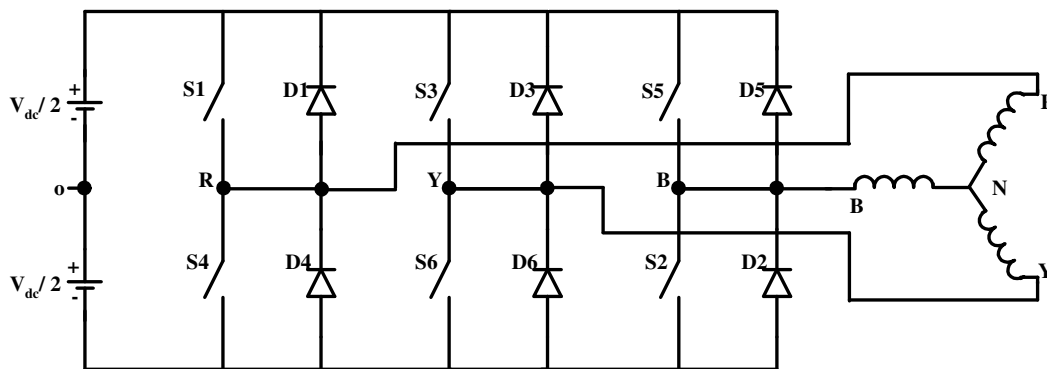


Figure 10.1: Three phase half bridge voltage source inverter.

Corresponding to each of the switching states, the motor line-to-neutral voltages can be

determined using the following equations:

$$\begin{aligned} V_{s1} &= V_{RN} = \frac{1}{3}[V_{RY} - V_{BR}] = \frac{1}{3}[2V_{R0} - V_{Y0} - V_{B0}] \\ V_{s2} &= V_{YN} = \frac{1}{3}[V_{YB} - V_{RY}] = \frac{1}{3}[2V_{Y0} - V_{B0} - V_{R0}] \\ V_{s3} &= V_{BN} = \frac{1}{3}[V_{BY} - V_{YB}] = \frac{1}{3}[2V_{B0} - V_{R0} - V_{Y0}] \end{aligned} \quad (10.1)$$

The two two-phase voltages V_{sa} and V_{sb} that occur in the definition of the space phasor can be determined as

$$v_{sa} = \frac{3}{2}v_{s1} \quad (10.2)$$

$$v_{sb} = \frac{\sqrt{3}}{2}[v_{s2} - v_{s3}] \quad (10.3)$$

The space-phasor of the machine stator voltage then obtained as

$$\bar{v}_s = v_{sa} + jv_{sb} \quad (10.4)$$

The eight switching states of the inverter and the corresponding space phasors of the machine stator voltage are shown in Figure 10.2 and 10.3 respectively.

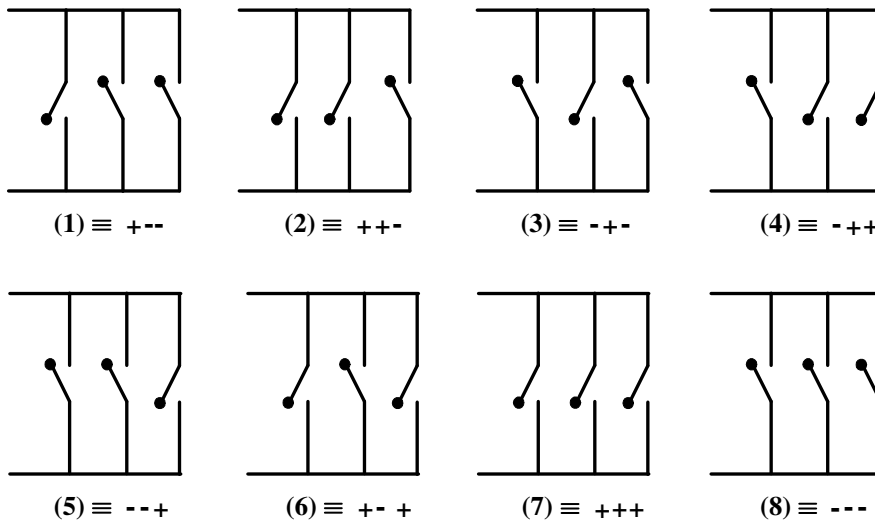


Figure 10.2: Eight switching states of the inverter.

It can be seen that at any instant of time there are only eight possible positions for the voltage space phasors. When the inverter is operated in the six step mode, the switching states go through the sequence 1-2-3-4-5-6-1-2-3. The states 7 and 8 are not used at all. The space phasor of stator voltage stays in each of the position 1 to 6 for a time interval

corresponding to 60° of the fundamental period and jumps to the next position at the end of every 60° ($\frac{1}{6}$ of the fundamental period). With the above switching sequence, at every jump in the position of the voltage space phasor, only one of the three phases of the inverter switches from top to bottom or vice versa.

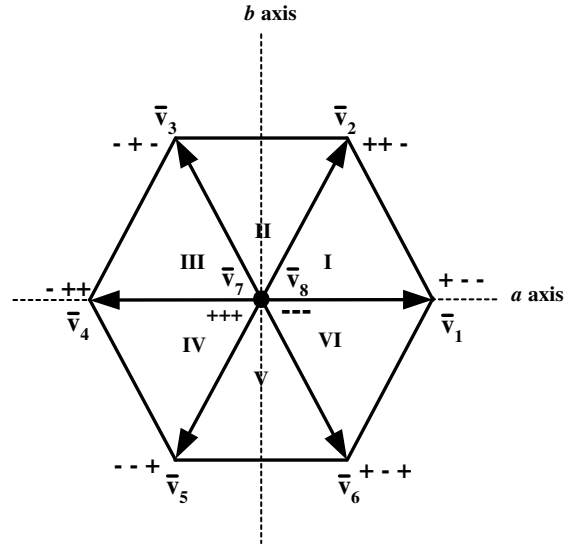


Figure 10.3: Space phasors corresponding to each switching state.

The ideal trajectory for the voltage space phasor \bar{v}_s is of course a circle described with uniform angular velocity. The objective of any PWM process is to approximate this ideal trajectory of \bar{v}_s by switching amongst the eight standard positions of \bar{v}_s . Towards this end, the continuously moving reference vector \bar{v}_s^* is sampled at a sampling frequency f_s . During the interval $T_s = \frac{1}{f_s}$ between samples, the reference \bar{v}_s^* is assumed to remain constant. It is clear that for this assumption to be valid, the sampling frequency should be fairly high compare to fundamental output frequency desired from the inverter.

Now consider that at a particular sampling instant, the reference \bar{v}_s^* is situated in sector 1 as shown in Figure 10.4. The angle α represents a position of the reference vector with respect to the beginning of the sector.

It is intuitively clear that the reference vector can be reproduced best during the period till the next sample by switching the inverter to create the vectors v_1, v_2, v_7 and v_8 in some sequence. Selecting any of the other vectors v_3 to v_6 would result in a greater deviation of the actual vector from the desired reference and would thus contribute to harmonics.

The switching pattern can be calculated as follows.

Assume that the sampling period T_s is divided into three sub intervals T_1, T_2 and T_0 . The inverter is switched so as to produce the vector V_1 for T_1 seconds and V_2 for T_2 seconds

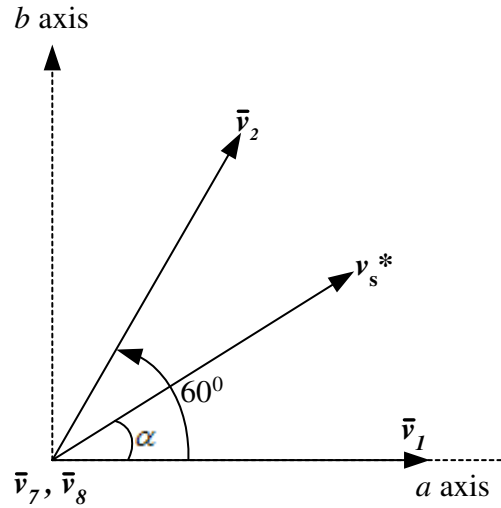


Figure 10.4: Sampled reference vector located in sector I.

and ‘zero’ (i.e. either v_7 or v_8) for T_0 seconds. The sub-intervals T_1, T_2 and T_0 have to be calculated so that the volt-seconds produced by the vectors \bar{V}_1, \bar{V}_2 and \bar{V}_7/\bar{V}_8 along the a and b axes are the same as those produced by the desired reference vector \bar{V}_s^* , i.e.

$$V_{dc}T_1 + V_{dc} \cos 60 T_2 = |\bar{v}_s^*| \cos \alpha T_s \dots a \text{ axis} \quad (10.5)$$

$$V_{dc} \sin 60 T_2 = |\bar{v}_s^*| \sin \alpha T_s \dots b \text{ axis} \quad (10.6)$$

where $|\bar{v}_s^*|$ is the amplitude or length of the reference vector.

$$a = \frac{|\bar{v}_s^*|}{V_{dc}} \quad (10.7)$$

Then equations 10.5 and 10.6 can be rewritten as

$$T_1 + T_2 \cos 60 = a T_s \cos \alpha \quad (10.8)$$

$$T_2 \sin 60 = a T_s \sin \alpha \quad (10.9)$$

Solving for T_1 and T_2

$$T_1 = T_s a \frac{\sin(60 - \alpha)}{\sin 60} \quad (10.10)$$

$$T_2 = T_s a \frac{\sin \alpha}{\sin 60} \quad (10.11)$$

$$T_0 = T_s - T_1 - T_2 \quad (10.12)$$

As the reference vector moves to other sectors, the corresponding boundary vectors of the sector should be created during the intervals T_1 and T_2 .

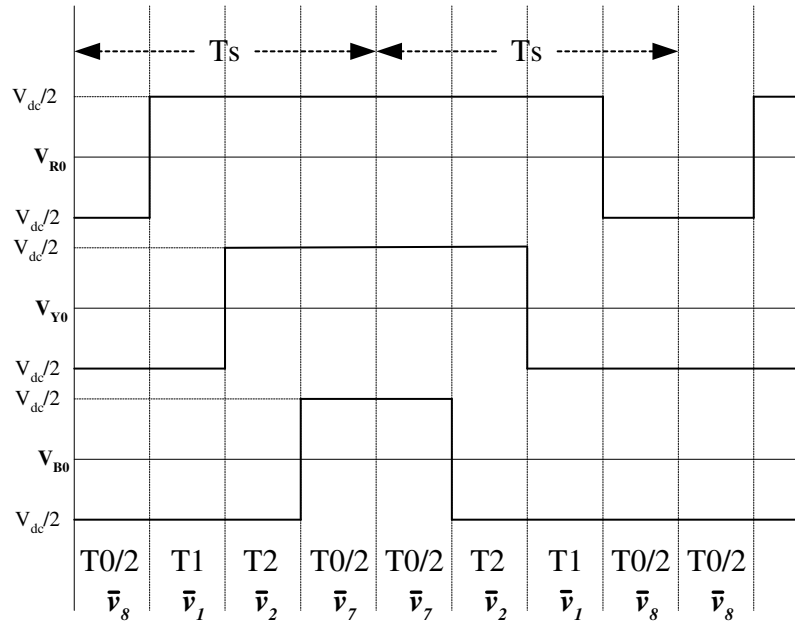


Figure 10.5: Switching sequence during each successive sampling intervals.

In order to minimize the number of switchings in the inverter, it is desirable that switching should take place in one phase of the inverter only for a transition from one state to another. This can be achieved if the following switching sequence is used:

8-1-2-7-2-1-8-1-2-7.....

Therefore the zero interval T_0 is divided into two equal halves of length $\frac{T_0}{2}$. These half intervals are placed at the beginning and end of every sampling interval T_s . If the half at the beginning is realized as v_8 , then that at the end is realized as v_7 and vice-versa. The switching sequence during successive sampling interval will then be as above.

It can be seen from the Figure 10.5 the chopping frequency f_c of each phase of the inverter is given by

$$f_c = \frac{f_s}{2} \quad (10.13)$$

It should be pointed out that during each sampling interval, the desired reference vector is approximated in an average sense, since the volt-seconds are equated. However, instantaneously, the actual vectors produced by the inverter are different from the reference vector and therefore instantaneous voltage deviations or voltage 'ripple' exists. As a result harmonic currents will flow in the machine. By following the above mentioned switching sequence, harmonics are to some extent reduced.

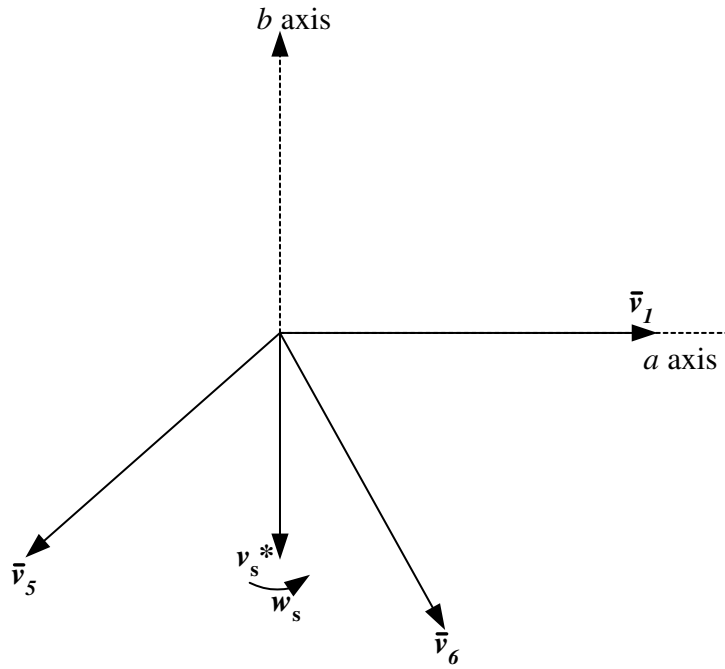


Figure 10.6: Reference time instant for calculating \underline{v}_{R0} .

10.1 Comparison with Sinusoidal PWM

In order to compare the space vector PWM with the sinusoidal PWM, the mean value of the inverter phase to dc center-tap voltages are calculated first, over one full cycle of the fundamental i.e. for one full rotation of reference vector \bar{v}_s^* . Let $t = 0$ correspond to the instant where the average value \underline{v}_{R0} of the phase to center tap voltage v_{R0} goes through its positive zero crossing. At this instant, therefore, the reference vector \bar{v}_s^* will point vertically downwards as shown in Figure 10.6. From this initial position, the reference vector rotates in the anticlockwise direction with angular velocity ω_1 . Its position at any instant t with respect to the starting position is given by the angle $\theta = \omega_1 t$. For $0^\circ \leq \theta \leq 30^\circ$, the reference vector is in sector V ; for $30^\circ \leq \theta \leq 90^\circ$, the reference vector lies in sector VI . If the variation of \underline{v}_{R0} can be determined over these 90° , then its waveform over the rest of the cycle can be drawn using symmetry.

For

$$0^\circ \leq \theta \leq 30^\circ, \quad \underline{v}_{R0} = \frac{V_{dc}}{2} \frac{1}{T_s} [-T_1 + T_2] \quad (10.14)$$

further

$$\alpha = 30^\circ + \theta \quad (10.15)$$

Using the expressions 10.10 and 10.11 for T_1 and T_2 , it can be shown that

$$\underline{v}_{R0} = V_{dc} a \sin \theta = V_{dc} a \sin \omega_1 t \quad (10.16)$$

for

$$30^\circ \leq \theta \leq 90^\circ, \quad \underline{v}_{R0} = \frac{V_{dc}}{2} \frac{1}{T_s} [T_1 + T_2] \quad (10.17)$$

However,

$$\alpha = \theta - 30^\circ$$

Again, using 10.10 and 10.11 in 10.17, it can be shown that

$$\underline{v}_{R0} = V_{dc} \frac{1}{\sqrt{3}} a \sin(30^\circ + \theta)$$

i.e.

$$\underline{v}_{R0} = V_{dc} \frac{1}{\sqrt{3}} a \sin(30^\circ + \omega_1 t) \quad (10.18)$$

Using the expressions in 10.16 and 10.18 and taking the advantage of the symmetry, the variation of \underline{v}_{R0} over one full cycle of the fundamental can be drawn. The waveforms for \underline{v}_{Y0} and \underline{v}_{B0} will also be identical except for mutual phase shift of 120° . The mean value of the line voltages \underline{v}_{RY} , \underline{v}_{YB} and \underline{v}_{BR} can also then be drawn by taking the differences. Figure 10.7 shows the variation of \underline{v}_{R0} and \underline{v}_{RY} for the period $0^\circ \leq \omega_1 t \leq 180^\circ$.

From Figure 10.7 it can be seen that the waveform of the mean value \underline{v}_{R0} of the phase to center tap voltage is not sinusoidal but contains triplen harmonics. These harmonics get cancelled in the line to line voltages and hence the waveform of \underline{v}_{RY} is perfectly sinusoidal. The machine line to neutral voltages will also be perfectly sinusoidal. Considering the waveform of \underline{v}_{RY} ,

The peak value of mean line to line voltage

$$= \frac{2}{\sqrt{3}} a V_{dc} \quad (10.19)$$

Recalling the definition of the voltage controlled ratio given by equation 10.7, the maximum value of a is given by

$$= \frac{\text{radius of the largest circle inscribed in the voltage hexagon}}{V_{dc}} \quad (10.20)$$

Therefore,

$$= \frac{V_{dc} \cos 30^\circ}{V_{dc}} = \frac{\sqrt{3}}{2} \quad (10.21)$$

Substituting in 10.19,

The maximum peak line-to-line voltage using space phasor PWM

$$= \frac{2}{\sqrt{3}} \frac{\sqrt{3}}{2} V_{dc} = V_{dc} \quad (10.22)$$

Compare this with the value for sine triangle PWM, given by

The maximum peak line-to-line voltage for sine-triangle PWM

$$= \frac{V_{dc}}{2} \sqrt{3} \quad (10.23)$$

is seen that the space vector PWM gives higher voltage output, while still remaining in

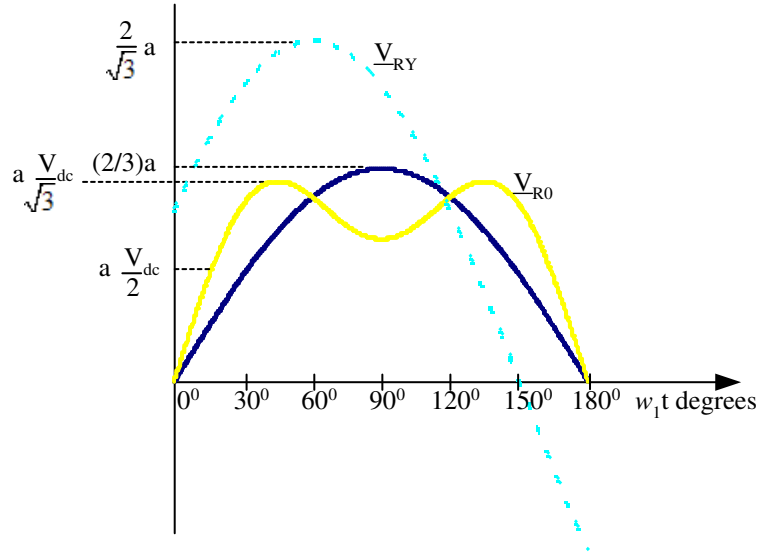


Figure 10.7: Waveform of v_{R0} and the fundamental component of v_{R0} .

modulation, by a factor of $\frac{2}{\sqrt{3}} = 1.154$, i.e. nearly 15% more output voltage without going into over modulation. This is an advantage of space vector PWM over the sine triangle technique. Space vector PWM can therefore be regarded as a carrier based PWM technique, with the difference that the reference waveform a triplen harmonics in addition to the fundamental. The method of adding a third harmonic component to the reference sine wave in sine triangle PWM as also been suggested to increase the fundamental output voltage.

It is also possible to derive the peak values of the fundamental line to neutral voltages in the two methods. For sine triangle PWM, this has a maximum value of $0.5V_{dc}$. For space vector PWM, the maximum value of the peak fundamental line to neutral voltage of the machine can be written as

$$\begin{aligned} v_{Rn1} &= \frac{2}{3}[\text{radius of the largest circle inscribed in the voltage hexagon}] \\ &= \frac{2\sqrt{3}}{3 \cdot 2} V_{dc} \\ &= 0.577 V_{dc} \end{aligned} \tag{10.24}$$

10.2 Implementation of Space-Vector PWM

Space vector PWM has the advantage that it is amenable to software implementation. In a microprocessor based drive controller, the amplitude V_s and the position α within the sector of the reference vector will both be generated as digital words by the software. It is then possible to compute equations (10.10 and 10.11) through software, perhaps by storing the functions $\sin\alpha$ and $\sin(60 - \alpha)$ in memory. On examining the switching sequence in Figure 10.5 it can be seen that the reference vector is in zero state at the beginning and end of a sampling interval. Also, the zero state at the end of one sampling interval is the same as the zero state at the beginning of the next sampling interval. Therefore, once the zero state at the end of the interval starts, the computation of T_1, T_2 and T_0 for the next interval can begin and should be completed before the end of the zero state at the beginning of the next sampling interval. The values of T_1, T_2 and $\frac{T_0}{2}$ can be loaded as terminating counts in counters clocked by a constant frequency and thus translated into pulses of appropriate width for gating the inverter switches. Some decoding will be necessary to decide the boundary states corresponding to the sector in which the reference vector is located.

Implementation by discrete hardware is also possible (3). For example, the amplitude range of $|\vec{v}_s^*|$ and the angle α can both be quantized into a finite number of discrete values. Corresponding to each value of $|\vec{v}_s^*|$ and α , the gating pulses can be stored in memory and decoded according to the sector. This approach is similar to the stored waveform technique. While the memory size required is appreciable, it is economically quite feasible with the low prices of memories.

The technique of current regulated PWM can also be implemented using the concept of space phasors (4). It is possible to optimize the switching frequency also in order to achieve either the lowest possible switching frequency for a given current ripple or to obtain the fastest possible current response.

10.3 References

- 1) Leonhard , W., 'Control of Electrical Drives', Springer-Verlag, 1985.
- 2) Van der Brock, H.W et al., 'Analysis and realization of a Pulse Width Modulator Based on Voltage Space Vector', 'IEEE Trans.Industrial Applications, Vol. IA-24, No.1, Jan-Feb. 1988, pp. 142-150.
- 3) Holtz,J et al., 'High Speed Drive System with Ultrasonic Mosfet PWM Inverter and Single-chip Microprocessor control.' 'IEEE Trans.Industrial Applications, Vol. IA-23, No.6, Nov-Dec. 1987, pp. 1010-1015.
- 4) Nabae,A et al., 'A Novel Control Scheme for Current Controlled PWM Inverter.' 'IEEE Trans.Industrial Applications, Vol. IA-22, No.4, July-August. 1986, pp. 697-701.